博士論文　(要約)

Atomic Arrangement and Segregation Behavior of Praseodymium in Zinc Oxide [0001] Tilt Grain Boundaries

（酸化亜鉛**[0001]**傾角粒界における原子配列および
プラセオジムの偏析挙動）

盧 智英

Contents

Chapter 1. Introduction ..... **- 1 -**

1.1. Zinc Oxide ..... - 2 -

1.2. Grain boundary ..... - 4 -

1.3. Structure Unit (SU) ..... - 9 -

1.4. Praseodymium (Pr) doping ..... - 11 -

1.4.1. ZnO:Pr varistors ..... - 11 -

1.5. Segregation of Pr ..... - 13 -

1.6. Objective ..... - 15 -

1.7. Reference ..... - 17 -

Chapter 2. Method ..... **- 20 -**

2.1. Bicrystal fabircation ..... - 21 -

2.2. Electron microscopy observation ..... - 23 -

2.3. Atomistic simulation and modeling of grain boundary ..... - 25 -

2.4. Reference ..... - 27 -

Chapter 3. Atomic structure of ZnO [0001] 32.2° tilt grain boundary ..... **- 28 -**

3.1. Introduction ..... - 29 -

3.2. Method ..... - 31 -

3.3. Results and discussion ..... - 32 -

3.3.1. Atomic arrangement of the grain boundary ..... - 32 -

3.3.2. Structural analysis by circuit mapping formalism ..... - 38 -

3.4. Conclusion ..... - 45 -

3.5. Reference ..... - 46 -

Chapter 4. Atomic arrangement and segregation behavior in Pr-doped ZnO grain boundaries ..-

4.1. Introduction ..... - 48 -

4.2. Method ..... - 49 -

4.3. Results and discussion ..... - 51 -

4.3.1. Atomic arrangement of Pr-doped 32.2° tilt grain boundary ..... - 53 -

4.3.2. Segregation behavior of Pr ..... - 56 -

4.3.3. Atomic arrangement of Pr-doped 30.0° tilt grain boundary ..... - 60 -

4.4. Conclusion ..... - 63 -

4.5. Reference ..... - 64 -

Chapter 5. Atomic structure, segregation behavior, and morphology in Pr-doped ZnO grain boundary ..... - 65 -

5.1. Introduction ..... - 66 -

5.2. Method ..... - 67 -

5.3. Results and discussion ..... - 68 -

5.3.1. Atomic arrangement of Pr-doped ZnO 27.8° tilt grain boundary ..... - 68 -

5.4. Conclusion ..... - 82 -

5.5. Reference ..... - 83 -

Chapter 6. Relationship between structure unit and *2θ* ..... - 85 -

6.1. Introduction ..... - 86 -

6.2. Method ..... - 88 -

6.3. Results and discussion ..... - 89 -

6.3.1. Atomic arrangement of Pr-doped ZnO 38.2° (Σ7) and 43.6° (Σ49) tilt grain boundaries. .. - 89 -

6.3.2. Atomic arrangement of Pr-doped ZnO 25.8° (Σ79) tilt grain boundary ..... - 91 -

6.3.3. Prediction of atomic structure of Pr-doped ZnO [0001] symmetric tilt grain boundaries .. - 93 -

6.4. Conclusion ..... - 102 -

6.5. References ..... - 103 -

Summary ..... - 104 -

Research Activity ..... **- 106 -**

Acknowledgements ..... **- 107 -**

Chapter 1. Introduction

The majority of solid materials that is usually found in the nature are polycrystalline. That means there are number of single crystals joined together with three dimensional networks of internal interfaces, called grain boundaries. Atomic, chemical, and electronic structures of grain boundary largely differ from those in the bulk crystal. Those would give great impacts for determination of the performance and integrity of a material. Thus, it is an important issue to reveal the detailed relations between grain boundary and the material properties.

As a model for studying such grain boundary phenomena, zinc oxide (ZnO), which is an electroceramic material where the grain boundaries control the electrical properties, such as nonlinear current-voltage characteristics, has been focused. The nonlinear current-voltage characteristic is essential for protection of electronic devices from surge voltage. A several kinds of dopant element such metal oxides have been introduced in the polycrystalline ZnO in order to enhance the voltage gradient. It is commonly believed that dopant elements inhomogeneously distributed near the zinc oxide grain boundary and cause some changes in grain boundary geometry and chemistry.

Many researchers have tried to reveal the atomic structure and segregation of dopants, but it detailed role of the dopants on the property has not been well clarified yet. The biggest problem for this is vast number of grain boundaries in nature, as well as their atomic structures. To make a breakthrough for this ambiguity, grain boundary characterization has to be done in systematical way. In this regard, ZnO grain boundaries were categorized as some simple group; tilt grain boundary in the current case, and the single tilt grain boundaries with well-defined orientation were investigated. A general introduction to the materials and the backgrounds are described first in this chapter.

1.1. Zinc Oxide

Zinc oxide is an inorganic compound with a chemical formula ZnO. ZnO has a long history as a material that had been used as an additive in numerous applications including rubbers, plastics, ceramics, glass, cements, paints, and pigments. In the field of material science, crystalline ZnO is one of the promising materials that has been studied for many decades [1],[2]. ZnO is a famous n-type semiconductor with wide band gap of 3.37 eV [1],[3]~[6]. Moreover, there have been great developments for obtaining the p-type semiconductivity from the ZnO [7]~[21]. ZnO has broad application range including light emitting diodes, transparent electrode, varistors, and sensors [21][25]. The ZnO has advantages over gallium nitride (GaN) based applications in some cases due to lower material cost, the availability of large substrate. ZnO has more stable exciton and higher binding energy (~60 meV for ZnO, ~25meV for GaN [21]~[26]) that permit excitonic recombination to dominate in ZnO at room temperature. ZnO is very robust material with a high melting temperature (T_m~2300K [27]) and high capacity to carry a large current.

The crystal structure of ZnO is typically wurtzite structure which has a hexagonal unit cell (space group $P6_3mc$) with lattice parameters a = 3.2501Å and c = 5.2071Å [28]. It is described by Zn and O planes that are alternatively stacked along the c axis. All Zn and O atoms have tetrahedral coordination with four nearest neighbors of the opposite types (**Figure 1-1**). When the ZnO is exposed to high pressure, it undergoes a phase transformation into the rock-salt structure [30],[31].

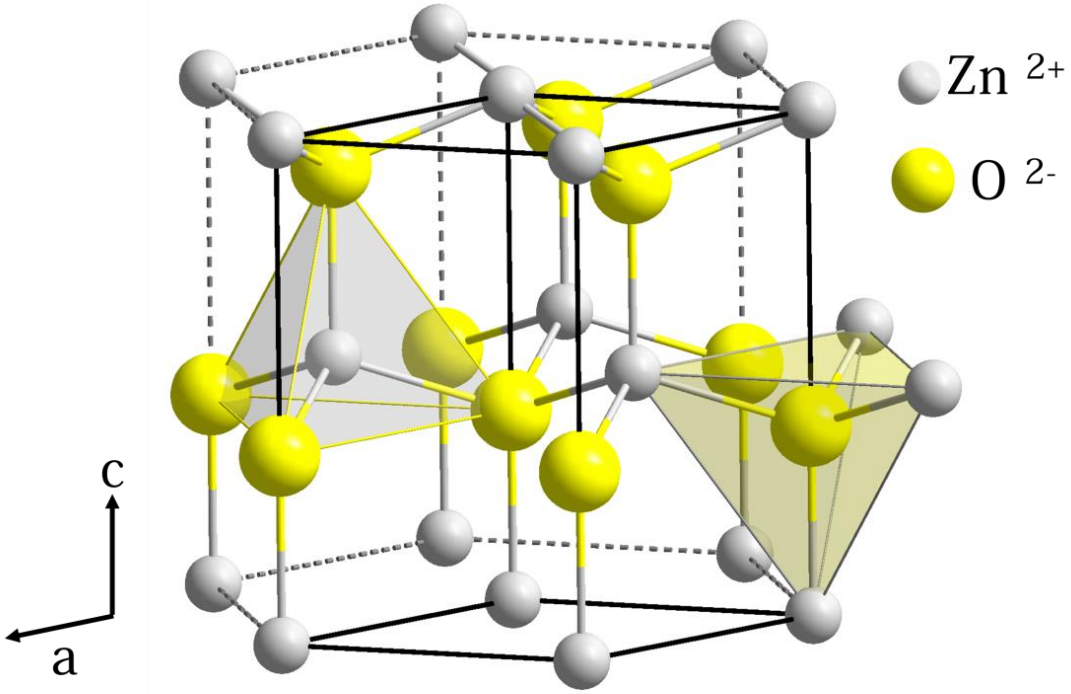

Figure 1-1. Crystal structure of ZnO (Wurtzite) with coordination polyhedra [29].

1.2. Grain boundary

Grain boundary is a planar defect, which is a homo-interface between two neighboring grains with different orientation. It has been largely demonstrated that various properties of material highly depend on the nature of the grain boundaries [32]~[38]. In general, the grain boundary can be specified by five independent parameters (five macroscopic degrees of freedom) (**Figure 1-2**) that define the crystallographic lattice misorientation and boundary plane. In addition, there are three additional microscopic parameters that define parallel / normal translation of the boundary plane. Thus, the number of distinct grain boundaries can be enormously large. The atomic structures of grain boundary are highly dependent on the misorientation between adjacent crystals. Therefore, we need to consider some special cases, such as tilt / twist boundary so that we can study the structure and properties of certain grain boundary system.

Tilt and twist boundaries are rather simple. Consider two crystals meeting at a grain boundary with the rotation product u. And let the normal product to the boundary plane n. If the u is parallel to the n, it is a twist boundary; and if the u is normal to the n, it is a tilt boundary (**Figure 1-3**). On the other hand, there is also mixed boundary that has both tilt/twist characters. The structural differences between the tilt and twist boundaries are particularly noticeable in the case of low-angle grain boundaries; these can be described in terms of edge or screw dislocations respectively. Let me more describe about tilt boundary, which are extensively investigated in the current study. Low angle tilt boundaries consist of array of isolated edge dislocation, where Burgers vector of the perfect dislocation corresponds to a translation vector in the crystal structure. The interval *d* between those dislocations of a certain set is given by Frank's formula;

$$d = |\vec{b}|/\sin\theta \tag{1-1}$$

where the $|\vec{b}|$ is the magnitude of the Burgers vector $\vec{b}$, and θ is the tilt angle. As θ increases, separation between the edge dislocations gets closer.

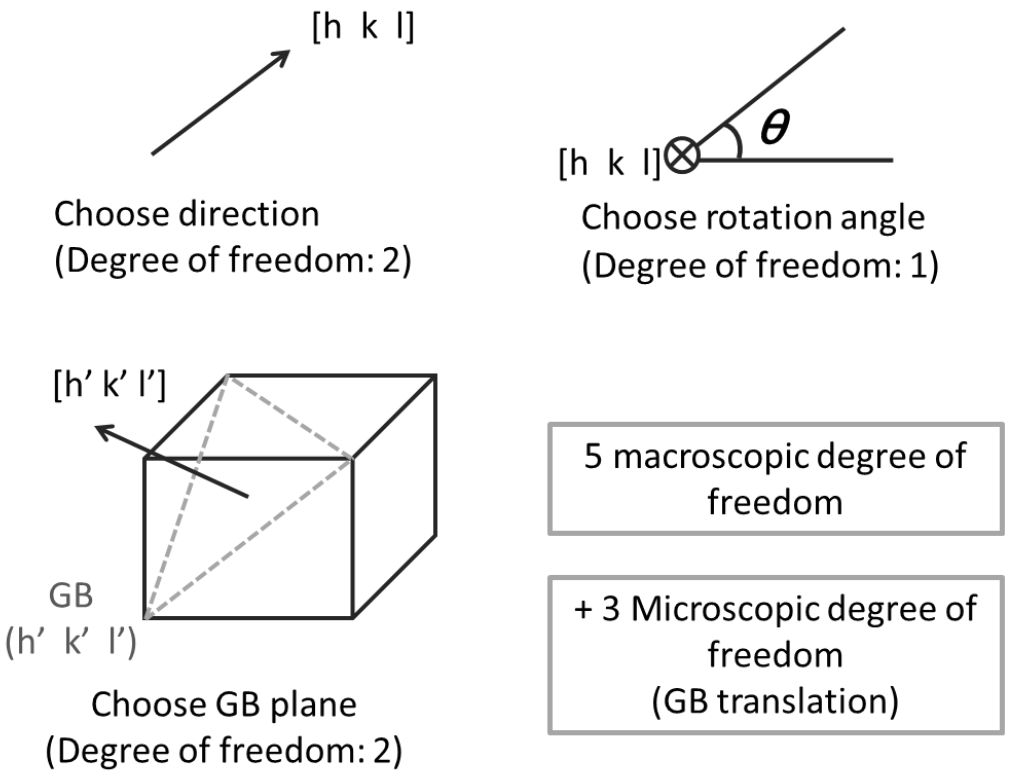

Figure 1-2. Degrees of freedom for determination of a grain boundary

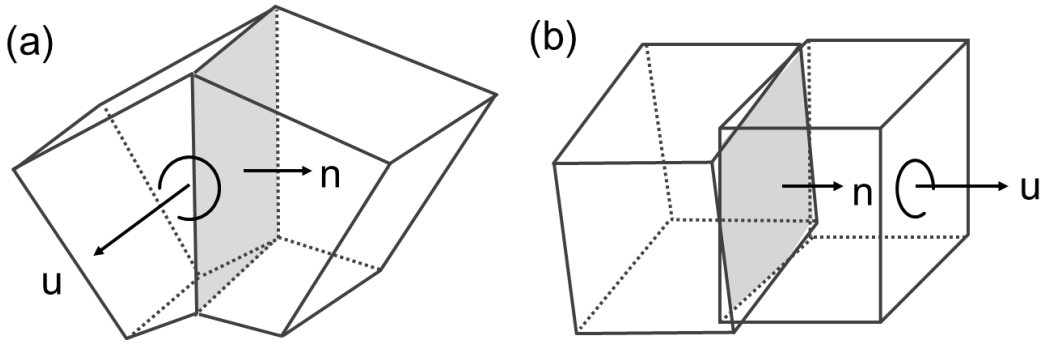

Figure 1-3. (a) Schematics of (a) tilt boundary and (b) twist boundary formed by two crystals. **u** is the rotation product and **n** is the normal product to the boundary plane.

On the other hand, as tilt angle increases, the dislocation cores are interact together and the equation (1-1) does not valid any longer. In order to characterize those high-angle grain boundaries, coincidence site lattice (CSL) theory is valuable that was first proposed in 1949 by Kronberg and Wilson [39]. Consider two overlaying finite lattices, and one lattice is rotated relative to the other one. When the rotation angle reaches at a certain value, lattice points of both lattices coincide, and they form new cell made only by those coincide lattice points, the CSL cell. The value of sigma (Σ) is defined as a volume fraction between the unit cell of CSL and a standard unit cell (1-2).

$$\Sigma = \frac{\text{Volume of CSL cell}}{\text{Volume of unit cell}} \tag{1-2}$$

Grain boundaries with the CSL relationship often called CSL boundary. The CSL boundaries may be of relatively low energy when the adjoined two crystals have a misorientation angle corresponding to a dense CSL (low Σ value). When the crystal misorientation slightly deviates from the CSL misorientation, it is proposed that a network of grain boundary dislocations is formed (displacement shift complete (DSC) dislocations) in order to compensate the deviation and produce a stable structure of the CSL boundary [40]. The CSL boundaries are often used for the detailed grain boundary analysis due to ease of observation of atomic structure with relatively short periodicity and stable arrangements. Also it provides three-dimensional periodic boundary condition that is suitable for theoretic calculations [41]~[47].

For the Wurtzite structure like ZnO, [0001] direction is the principal rotation axis for CSL-boundaries. The [0001] view of the bulk lattice in the Wurtzite ZnO has honeycomb patterns, where the Zn and O atoms are located in the corners of the hexagons. Those honeycomb patterns can form a dichromatic complex [48] as can be shown in **Figure 1-4(a)**.

Hexagonal patterns of λ and μ crystals are overlaid with the tilt angle of 32.2°, which is corresponded to the Σ13 relation. On the other hand, it is also possible to express the same dichromatic complex in different way as shown in **Figure 1-4(b).** The dichromatic complex is created by open channels in the λ and μ crystals, and expressed by grey and black dots, respectively. Due to the symmetry of the dichromatic complex, the CSL unit cell is a rhombus with an angle of 60°. Therefore, the short diagonal of the CSL unit cell is identical to an edge and only the large diagonal exhibits a different configuration.

In the case of Σ13, the short diagonal corresponds to the boundary plane of $(13\bar{4}0)$, and the large diagonal corresponds to the other one, $(25\bar{7}0)$.

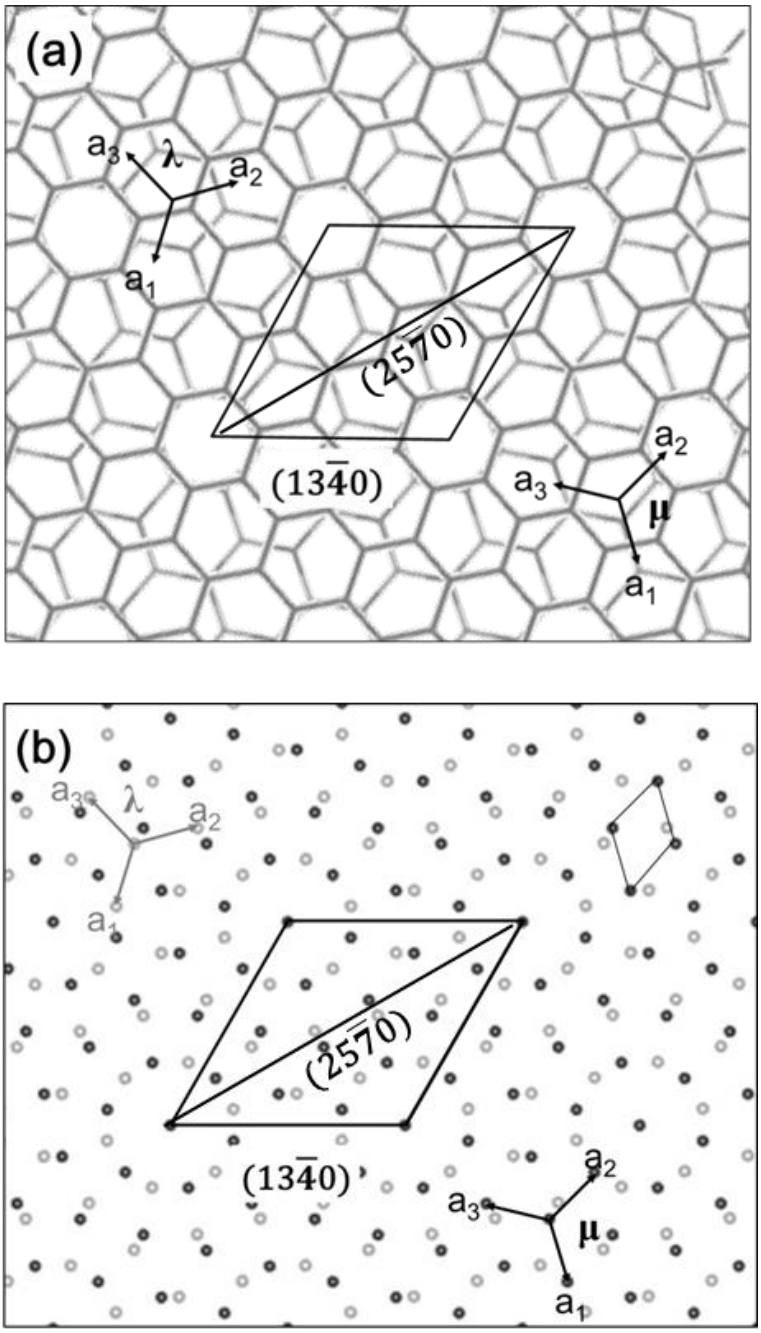

Figure 1-4. Dichromatic complex of Σ13 (32.2°/27.8°) [0001] expressed by (a) hexagonal patterns where atomic columns exists at the corner of the hexagons and (b) open channels where no atomic columns exists. (b) type is commonly used for crystallographic analysis. Large rhombus is a CSL cell made by CSL points. Area of CSL cell is thirteen times larger than that of the unit cell, which is indicated by small rombus. Short and long diagonals of the CSL cell can be the shortest Σ13 boundary planes; $(13\bar{4}0)$ and $(25\bar{7}0)$, respectively.

1.3. Structure Unit (SU)

When the separations between dislocations get close, they merge into a closed interface layer. The grain boundary cannot be explained as array of isolated dislocations any longer, and it is commonly said that transition from low-angle to high-angle grain boundary is occurred. The transition is often found at the tilt angle reaches 10~15°. The interface layer may be structurally distorted or composed of well-defined structural units (SUs) [49]. This new structural classification of grain boundary was first proposed by Sutton and Vitek (1983) [50] in rather simple symmetric tilt boundaries in cubic metal. SUs often form kite-shapes quadrilaterals in the high-resolution TEM images. Basically, the SUs should include the smallest possible number of atoms needed to identify the corresponding grain boundary structure unambiguously.

In the ZnO [0001] tilt grain boundary case, SUs were first determined in the high resolution TEM study of Σ7 ZnO grain boundary, done by Oba *et al.*(2004) [43]. The periodicity of the Σ7 ZnO grain boundary is the shortest among the [0001] tilt series, and it was represented by repeating quadrilaterals, which are made by connection of the open channels or the primitive cell edges in the [0001] view of the Wurtzite structure (**Figure 1-5**). The quadrilaterals include sublattices of both Zn^{2+} cation and O^{2-} anion in the same frame since those ions present in the same atomic column as view from [0001] view. In order to reveal the atomic configuration for the SU, they conducted atomistic calculations in conjunction with the HRTEM images. Four atomic configurations with relatively low energy were noted, as shown in **Figure 1-6**. Those atomic configurations were obtained during changing boundary plane translation. In detail, the atomic configuration of SU A-D model is composed of twelve- and four (12/4) membered ring, five- and seven (5/7) membered ring, six- and eight (6/8) membered ring, and four- and six (4/6) membered ring, respectively. Formation energy of SU A-D was reported as 1.47, 1.69, 1.54, and 1.52 J/m^2, respectively.

Here, same classification of SUs as Oba's[43] was used for grain boundary analysis for the ease of comparison of the atomistic arrangements of their Σ7 ZnO grain boundary to those of grain boundaries observed in this thesis. However, types of the SUs are slightly modified from Oba's models as will be introduced in chapter 3.

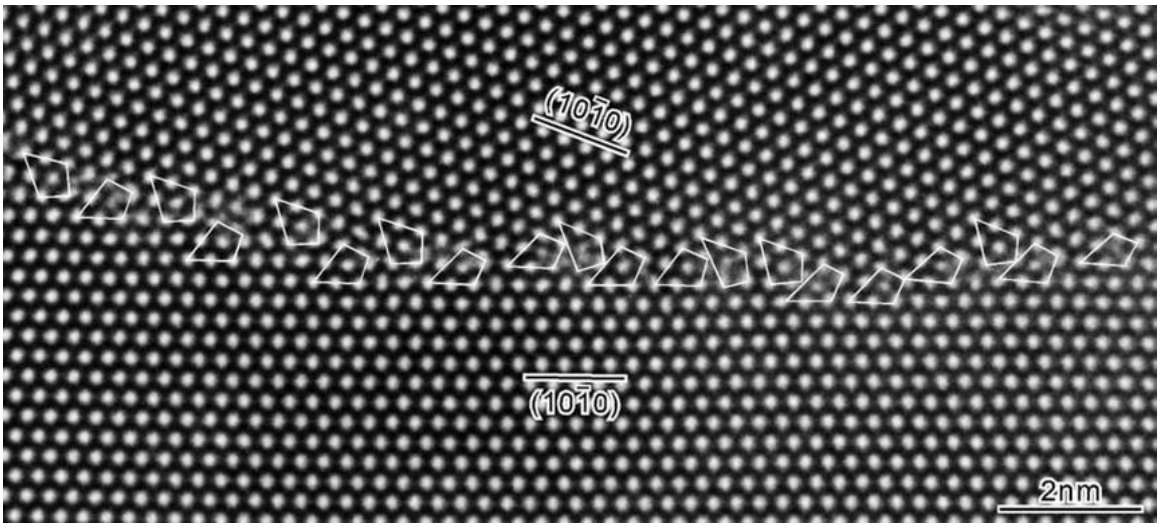

Figure 1-5. High resolution TEM image of ZnO [0001] Σ7 grain boundary, reported by Oba *et al.* [44]. The grain boundary consists of array of quadrilaterals.

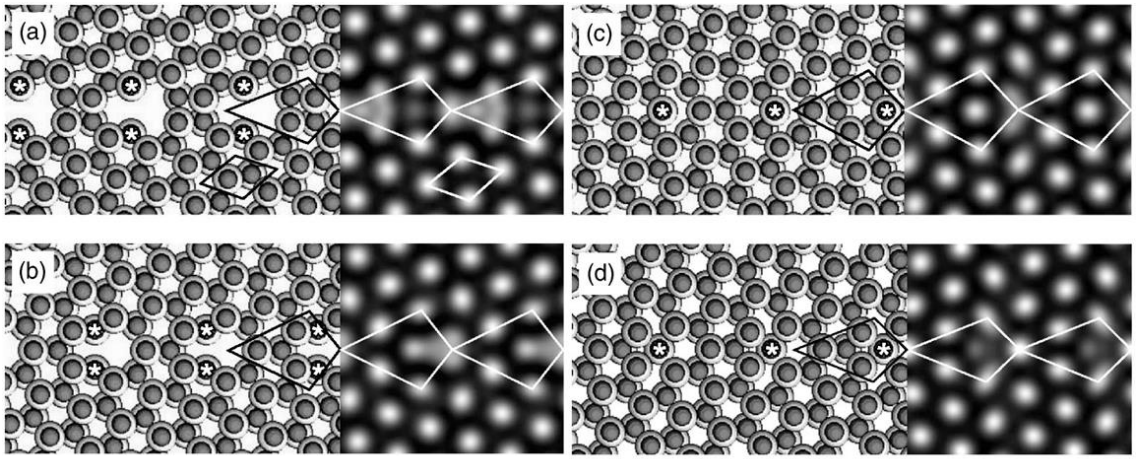

Figure 1-6. In a conjunction with HRTEM image simulation, atomic configurations of the quadrilaterals were identified by atomistic calculation (Oba *et al.*(2004) [43]) in the Σ7 grain boundary. Four kinds of SU models (A, B, C, and D) were suggested, as shown in the (a), (b), (c) and (d), respectively. The circles denote Zn and O columns. Atoms coordinated by three or five first-nearest neighbors are marked with asterisks.

1.4. Praseodymium (Pr) doping

1.4.1. ZnO:Pr varistors

ZnO is well-known varistors material. The varistors is a passive electrical component which is used for protecting electrical circuits from the surge. For low voltages, varistor normally acts as an insulator. However, when the applied voltage reaches critical voltage V_c, it starts to conduct and protect the circuits. The response of the varistor to the applied voltage thus shows non-linearity, which is called non-linear I-V characteristic (**Figure 1-7**). This characteristic is attributed to an interfacial potential barrier formed at grain boundary [51].

Typical ZnO varistors are polycrystalline ceramics with electrically active grain boundaries, where several kinds of sintering additives present. According to Gupta *et al*. (1990) [52], the additives that have been found in ZnO varistors can be classified into three categories - *varistor formers*, *performance enhancers*, and *performance highlighters*. Among them, the *varistors former* is the most important one that is necessary to add into ZnO to form varistors characteristic, and in other words, it is impossible to make a varistors without addition of the *varistors former*. So far, it has been known that the *varistors former* are mostly heavy elements with large ionic radius such as bismuth (Bi) [53],[54], vanadium (V) [55],[56], barium (Ba) [57], and praseodymium (Pr) [58],[59].

In this thesis, the Pr is chosen for dopant elements, which is being widely used in conventional varistors.

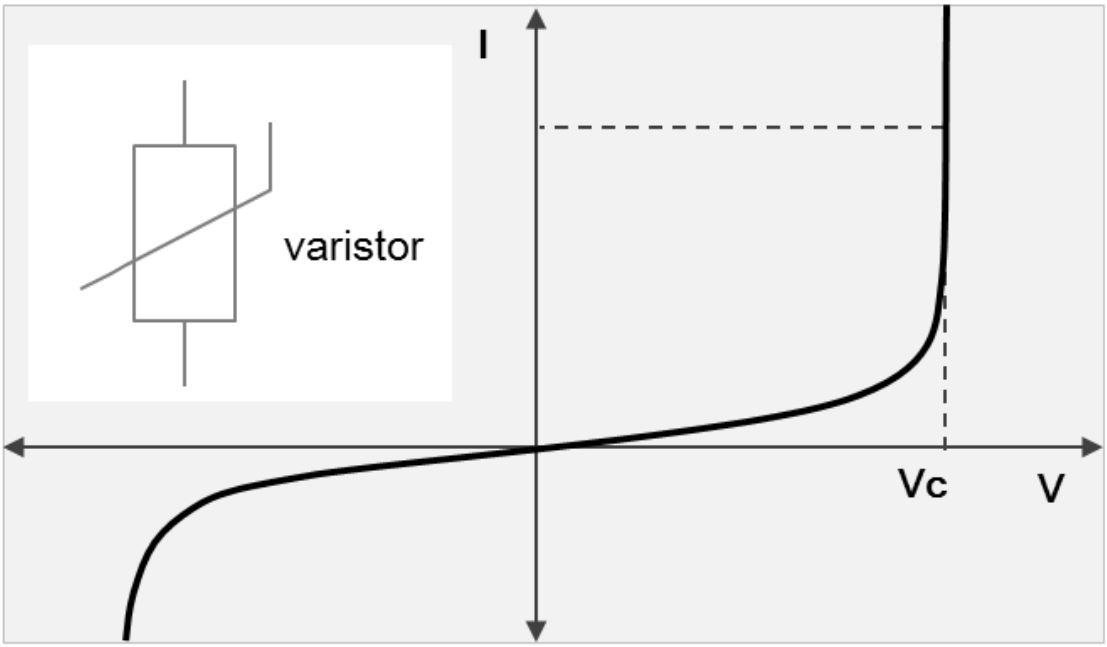

Figure 1-7. Schematic of nonlinear I-V characteristic of varistor

1.5. Segregation of Pr

Praseodymium, Pr, is a soft, silvery, and ductile metal in the lanthanide group. It is very reactive metal that often forms oxide in the nature. As most rare earth element does, Pr most readily forms Pr^{3+} ions. Pr_2O_3 is mostly used as a dopant material in the ZnO varistors. Pr_2O_3 has space group of P-3m1 (164) with the hexagonal crystal structure. Pr has larger ionic size than Zn (Pr^{3+}: 1.13 Å and Zn^{2+}: 0.74 Å [60]) and segregate at the grain boundary since the grain boundary provides more flexibility for bond relaxation and there are more possibilities to have different coordination to the Pr atoms. For the role of Pr, there were two major candidates; the Pr itself / defects cause the nonlinear I-V character or its strain effect does. However, the recent study by Sato *et al.* (2006) [61] revealed that the Pr promotes formation of the native defect such as V_{Zn} and facilitate the acceptor state at the grain boundary.

Segregation is usually concentrated around grain boundary region, as well as in other defects in material. Segregation is often connected with intrinsic grain boundary structure, which is conditioned by misorientation between adjacent crystals. Especially, dopants with large ionic radii, such as Pr, are known to segregate at the grain boundary [61]~[64]. The segregation of Pr can be observed in atomic scale by using Z (atomic number)-contrast HAADF (high angle annular dark field) STEM (scanning transmission electron microscopy) imaging [65]. The Pr atoms looks brighter than Zn atoms in the HAADT-STEM images since its atomic number is much higher (59) than that of Zn (30) (**Figure 1-8)** [61]. Pr segregated to the boundary is identified to be in the three plus state (Pr^{3+})[61].

Former investigations on Pr-doped ZnO revealed that the Pr always substitute specific Zn site within the SUs [61],[66],[67]. It is considered that those specific sites provide Pr long enough Pr-O bonds, which tend to have similar Pr-O bonds in the stable Pr_2O_3 crystal bulk [61]. Therefore, once the SU of grain boundary is determined, it may determine the segregation of Pr as well as.

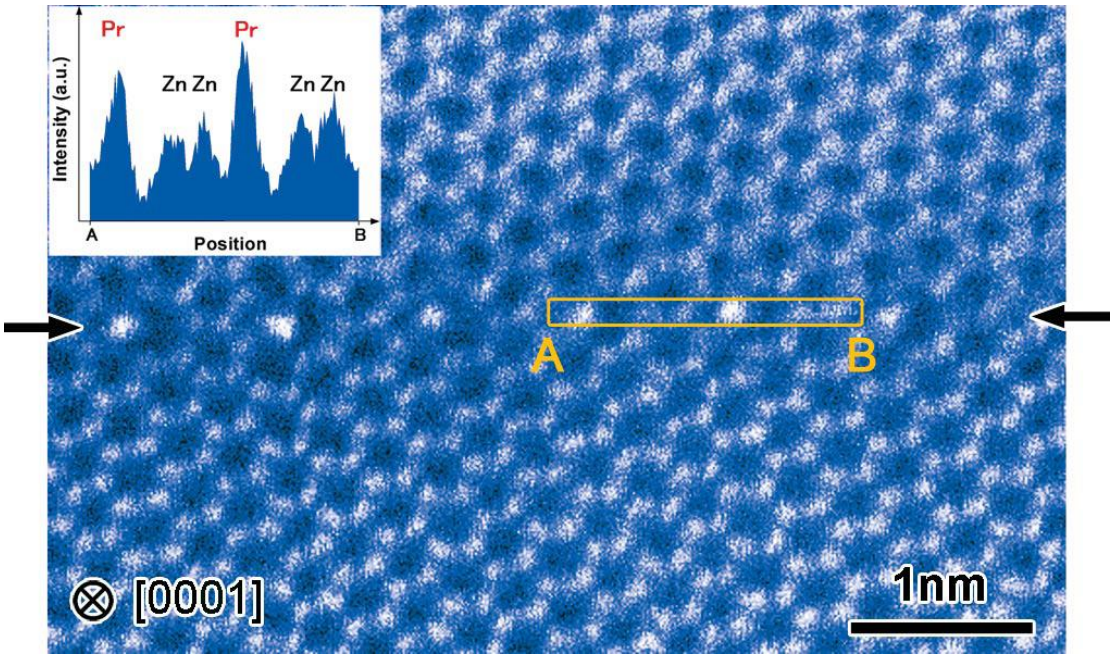

Figure 1-8. Z-contrast HAADF STEM image of Pr-doped ZnO Σ7 [0001] grain boundary by Sato *et al.* [61]. Intensity of Pr is higher than that of Zn as shown in line profile (inset).

1.6. Objective

ZnO is used in a variety of practical applications such as electronics, photonics, and optics [21]~[26]. In the most cases, the material is used in polycrystalline forms, and the properties are influenced by presence of grain boundaries as seen from a surge of relevant studies [31]~[38]. It should also be mentioned that when the additives such as dopants or defects are introduced to the material, they change the grain boundary nature and play important role on the material properties. In this regard, understanding the atomistic structures of grain boundary is a quite important issue in order to reveal the relationship between the structures - material property. In the case of ZnO, the ZnO ceramics doped with Pr exhibit highly nonlinear current-voltage (*I*-*V*) characteristics and being widely used as varistors. It is believed that Pr segregates at the grain boundary and play a central role for the nonlinear *I*-*V* characteristics. However, understanding grain boundary structure and composition are still limited because it is not easy to determine the atomistic structure of grain boundaries in polycrystalline ceramics.

In order to overcome this difficulty, well-defined single grain boundary is prepared. Particularly, ZnO [0001] symmetric tilt grain boundary is chosen that provides direct observation of Zn and O atomic columns from the both adjacent crystals. In order to obtain the grain boundary, bicrystals method is used which have common [0001] axes, and the tilt angle (2θ) made by two ($11\bar{2}0$) of the adjacent crystals. Here, 2θ ranges from 0° to 60° due to the crystal symmetry, thus controlling 2θ in this range provides a series of ZnO [0001] tilt grain boundaries. In this way, more systematic approach is possible for understanding the grain boundaries in general. Particularly, the values 2θ are determined to provide CSL grain boundary, which is useful for direct observation of atomistic structure by transmission electron microscopy and simulation within realistic computational time with sufficient accuracy. The atomic arrangement of the CSL grain boundary can be described by repeating structure unit (SU), which is a fundamental brick that contains limited number of smallest with a limited number of models. Fundamental backgrounds and analysis method used in the current thesis are described in the current chapter 1 and the chapter 2.

In this thesis, investigations on atomic structures and segregation of Pr in the ZnO grain boundaries are intensively studied. First, in chapter 3, atomistic structure of an undoped ZnO symmetric grain boundary is studied focusing on a specific grain boundary orientation, [0001] Σ13 (32.2°) tilt grain boundary. Revealing the atomistic structure of the grain boundary would give an important insight since the orientation forms very stable grain boundary arrangements.

Relation between the SU alignment and the rotation angle was discussed and the grain boundary atomic arrangement is determined in this chapter.

In chapter 4, atomistic structure and segregation behavior of Pr-doped ZnO grain boundaries are studied. It is important to determine atomistic structure and segregation tendency of Pr in the grain boundary since those are the key factors that facilitate electronic potential barrier. To study those factors, Pr-doped ZnO Σ13 (32.2°) grain boundary is investigated and compared to the other Σ13 (27.8°) grain boundary. Similarity and dissimilarity between those grain boundaries would provide an understanding the same Σ value, but different boundary planes of the CSL grain boundary. In addition, relative atomic structure and Pr segregation in 30.0° tilt grain boundary is also investigated. This would provide another opportunity to discuss the atomic structure and the segregation of Pr among the Σ13 grain boundaries and the neighboring non-low-Σ CSL grain boundary.

In the most of grain boundary studies, investigations have been limited to quite narrow boundary area, and only the representative structure is often focused on. However, grain boundary structure is not always that simple; grain boundary plane may not be completely flat, there may be secondary or more structures, steps, facets, and so on. In recent years, stability in electron microscope has been improved, enabling to observe larger area of grain boundary by a quantitative manner. In this regard, a larger area of a ZnO grain boundary is investigated to understand a variety of structures at the atomic scale in chapter 5. Pr-doped ZnO Σ13 (27.8°) grain boundary is studied that has structural multiplicity in it. Relationships among atomistic structure, Pr composition, and morphology will be discussed

Finally in chapter 6, atomic arrangements with SU description, segregation of Pr are more generalized. As will be introduced in the previous chapters, atomic arrangement and Pr segregations in a series of ZnO grain boundaries are studied. Those give an idea for understanding 2θ dependency for Pr-doped ZnO [0001] symmetric tilt grain boundaries.

1.7. Reference

[1] D. G. Thomas, J. Phys. Chem. Solids, **3**, 229 (1957)

[2] P. Wagner and R. Helbig, J. Phys. Chem. Solids, **35**, 327 (1974).

[3] H. Shibata, M. Watanabe, M. Sakai, K Oka, P. Fons, K. Iwata, A. Yamada, K. Matsubara, K. Sakurai, H. Tampo, K. Nakahara, and S. niki, Phys. Status Solidi C, **1**, 872 (2004)

[4] C. G. Van de Walle. Phys. Rev. Lett., **85**, 1012 (2000)

[5] D. C. Look, J. W. Hemsky, and J.R. Sizelove, Phys. Rev. Lett., **82**, 2552 (1999)

[6] B.K. Meyer, H. Alves, D.M. Hofmann, W. Kriegsies, D. Forster, F. Bertram, J. Christen, A. Hoffmann, M. Straßburg, M. Dworzak, U. Haboeck, and A. V. Rodina, Phys, Status Solidi B, **241,** 231 (2004)

[7] K. Minegishi, Y. Koiwai, and K. Kikuchi, Jpn. J. Appl. Phys., Part 2 **36**, L1453 (1997)

[8] M. Joseph, H. Tabata, and T. Kawai, Jpn. J. Appl. Phys., Part 2 **38**, L1205 (1999)

[9] Y. R. Ryu, S. Zhu, D. C. Look, J. M. Wrobel, H. M. Jeong, and H. W. White, J. Cryst. Growth, **216**, 330 (2000)

[10] A. Tsukazaki, A. Ohtomo, T. Onuma, M. Ohtani, T. Makino, M. Sumiya, K. Ohtani, S. F. Chichibu, S. Fuke, Y. Segawa, H. Ohno, H. Koinuma, and M. Kawasaki, Nat. Mater., **4**, 42 (2005)

[11] X-L. Guo, H. Tabata, and T. Kawai, J. Cryst. Growth **223**, 135 (2001)

[12] B. M. A. Ashrafi, I. Suemune, H. Kumano, and S. Tanaka, Jpn. J. Appl. Phys., Part 2 **41**, L1281 (2002)

[13] D. C. Look, D. C. Reynolds, C. W. Litton, R. L. Jones, D. B. Eason, and G. Cantwell, Appl. Phys. Lett., **81**, 1830 (2002)

[14] K. H. Bang, D-K. Hwang, M-C. Park, Y-D. Ko, I. Yun, and J-M. Myoung, Appl. Surf. Sci., **210**, 177 (2003)

[15] V. Singh, R. M. Mehra, A. Wakahara, and A. Yoshida, J. Appl. Phys. **93**, 396 (2003)

[16] Y. R. Ryu, T. S. Lee, and H. W. White, Appl. Phys. Lett. **83**, 87 (2003)

[17] J. Huang, Z. Ye, H. Chen, B. Zhao, and L. Wang, J. Mater. Sci. Lett. **22**, 249 (2003)

[18] X-L. Guo, H. Tabata, and T. Kawai, Opt. Mater. (Amsterdam, Neth.) **19**, 229 (2002).

[19] B. S. Li, Y. C. Liu, Z. Z. Zhi, D. Z. Shen, Y. M. Lu, J. Y. Zhang, X. W. Fan, R. X. Mu, and D. O. Henderson, J. Mater. Res., **18**, 8 (2003).

[20] Y. W. Heo, Y. W. Kwon, Y. Li, S. J. Pearton, and D. P. Norton, Appl. Phys. Lett. **84,** 3474 (2004).

[21] D.C. Look, R.L. Jones, J.R. Sizelove, N.Y. Garces, N.C. Giles, and L.E. Halliburton, Phys. Status Solidi (a) **195**, 171(2003)

[22] D.C. Look, Mater. Sci. Eng. B, **80**, 383(2001)

[23] J.E. Nause, III-Vs Review, **12,** 28 (1999)

[24] H. Ohta, K. Kawamura, M. Orita, M. Hirano, N. Sarukura, and H. Hosono, Appl. Phys. Lett., **77**, 475 (2000)

[25] M. Joseph, H. Tabata, and T. Kawai, Jpn. J. Appl. Phys., **38**, L1205 (1999)

[26] D.B. Laks, C.G. Van de Walle, G. F. Neumark and S.T. Pantelides, Appl. Phys. Lett., **63**, 1375 (1993)

[27] Landolt and Bornstein, New Series III, **22**

[28] Erich H. Kisi and Margaret M. Elcombe, Acta cryst. C, **45**, 1867 (1989)

[29] Image downloaded from Wikipedia.org (Wurzite polyhedral.png)

[30] R. Ahuja, L. Fast, O. Eriksson, J. M. Wills, B. Johansson, J. Appl. Phys., **83**, 8065 (1998)

[31] J. M. Recio, M. A. Blanco, V. Luana, R. Pandey, L. Gerward and J. S. Olsen, Phys. Rev. B, **58**, 8949 (1998)

[32] A.T. Paxton and M.W. Finnis, eds., J. Mater. Sci., **40**, 3045 (2005)

[33] T. Sakuma, L. Shepard, and Y. Ikuhara, eds., Ceram. Trans., **118**, 427 (2000)

[34] C. Elsässer, A.H. Heuer, M. Rühle, and S.M. Wiederhorn, eds., J. Am. Ceram. Soc., **86**, 533 (2003)

[35] Y. Ikuhara, J. Ceram. Soc. Jpn., **109**, S110 (2001)

[36] J.P. Buban, K. Matsunaga, J. Chen, N. Shibata, W.Y. Ching, T. Yamamoto, and Y. Ikuhara, Science, **313**, 212 (2006)

[37] Z. Zhang, W. Sigle, and M. Rühle, Phys. Rev. B, **66**, 094108-1 (2002)

[38] N.D. Browning, J.P. Buban, P.D. Nellist, D.P. Norton, M.F. Chisholm, and S.J. Pennycook, Physica C, **294**, 183 (1998)

[39] M.L. Kronberg and F.H. Wilson,Trans. Met. Soc. AIME, **185**, 501 (1949)

[40] W. Bollmann. Crystal Defects and Crystalline Interfaces, Springer. Berlin (1970)

[41] M.C. Payne, P.D. Bristowe, and J.D. Joannopoulos, Phys. Rev. Lett., **58**, 1348 (1987)

[42] K. Nakamura, T. Mizoguchi, N. Shibata, K. Matsunaga, T. Yamamoto, and Y. Ikuhara, Phys. Rev. B., **75**, 184109-1 (2007)

[43] F. Oba, H. Ohta, Y. Sato, H. Hosono, T. Yamamoto, and Y. Ikuhara, Phys. Rev. B, **70**,

125415 (2004)

[44] F. Oba, Y. Sato, T. Yamamoto, H. Ohta, H, Hosono, and Y. Ikuhara, J. Mater. Sci. **40**, 3067 (2005)

[45] W. Körner, and C. Elsässer, Phys. Rev. B, **81**, 085324 (2010)

[46] M. Kohyama, Modelling Simul. Mater. Sce. Eng., **10**, R31 (2002)

[47] F. Oba, I. Tanaka, R. S. R. Nishitani, H. Adachi, B. Slater, and D. H. Gay, Philosophical Magazine A, **80**, 1567 (2000)

[48] R. Portier, D. Gratias, and M. Fayard, Acta Crystallogr., Sect. A: Cryst. Phys., Diffr., Theor. Gen. Crystallogr. **35**, 885(1979)

[49] N. D. Browning, S.J. Pennycook. M.F. Chisholm, M.M. Mcgibbon, and A.J. Mcgibbon, Interface Science, **2**, 397 (1995)

[50] A.P. Sutton and V. Vitek, Phil. Trans. R. Soc. Lond.A, **309**, 1 (1983)

[51] G. Blatter, F. Greuter, Phys. Rev. B, **33**, 3952 (1986)

[52] T. K Gupta, J. Mater. Res., **7**, 3280 (1992)

[53] M. Matsuoka, Jpn. J. Appl. Phys., **10**, 736 (1971)

[54] J. Wong, J. Appl. Phys., **51**, 4453 (1980)

[55] J.K. Tsai and T.B. Wu, J. Appl. Phys., **76**, 4817 (1994)

[56] C.T. Kuo, C.S. Chen, and I. N Lin, J. Am. Ceram. Soc., **81**, 2942 (1998)

[57] J. Fan and R. Freer, J. Mater. Sci., **32**, 415 (1997)

[58] K. Mukae, K. Tsuda, and I. Nagasawa, Jpn. J. Appl. Phys., **16,** 1361 (1977)

[59] A. B. Alles and V.L. Burdick, J. Appl. Phys., **70**, 6883 (1997)

[60] R.D. Shannon, Acta Crystallogr. Sect. A, **32**, 751 (1976)

[61] Y. Sato, J.P. Buban, T. Mizoguchi, N. Shibata, M. Yodogawa, T. Yamamoto, and Y. Ikuhara, Phys. Rev. Lett., **97**, 106802-1 (2006)

[62] Y. Sato, F. Oba, M. Yodogawa, T. Yamamoto, and Y. Ikuhara, J. Apppl. Phys., **95**, 1258 (2004)

[63] T.R.N. Kutty and S. Exhibalavan, J. Phys. D; Appl. Phys., **29**, 809 (1996)

[64] S. Exhibalavan and T.R.N. Kutty, J. Mater. Sci.; Materials in Electrons, **7**, 137 (1996)

[65] S.J. Pennycook and D.E. Jesson, Phys. Rev. Lett., **64**, 938 (1990)

[66] Y. Sato, T. Mizoguchi, N. Shibata, T. Yamamoto, T. Hirayama, and Y. Ikuhara, Phys. Rev. B, **80**, 094114 -1 (2009)

[67] Y. Sato, J.–Y. Roh, and Y. Ikuhara, Phys. Rev. B, **87**, 140101-1 (R) (2013)

Chapter 2. Method

Understanding grain boundary structure and composition are still limited because it is not easy to determine the atomistic structure of grain boundaries in polycrystalline ceramics. To overcome the difficulty, precise experimental conditions and some special analysis techniques are required for the grain boundary investigation. The results may give us an insight for detailed understanding of the grain boundary thereby. Bicrystals method is often used that is ease of controlling boundary orientations. Several ZnO bicrystals have been fabricated in this thesis. ZnO [0001] symmetric tilt grain boundary is obtained from the bicrystals, where the tilt angle (2θ) provides CSL condition to the grain boundary. The CSL boundary is effective for experimental and theoretic analysis since it provides three-dimensional periodic boundary condition. Rapid development in electron microscope provides a unique and powerful tool for investigation on the grain boundary geometry and chemistry nowadays. Incoherent images in which atomic structure and composition across the grain boundaries can be directly interpreted. Static lattice calculation and density functional calculation were carried out for obtaining stable grain boundary structure. A combination of STEM observation and theoretic calculation will provide a powerful method for grain boundary characterization.

2.1. Bicrystal fabircation

Bicrystals were fabricated by thermal diffusion bonding of two ZnO single crystals (Shinkosha Co., Ltd.). At first, a surface of the crystals was mechanically polished to mirror-like state, and then one crystal is set on the other so that the bicrystal possess [0001] tilt grain boundary and 2θ made by $(11\bar{2}0)$ (**Figure 2-1**). Here, 2θ ranges from 0° to 60° due to the crystal symmetry. The crystal set is diffusion bonded in the furnace at 1,100 ℃ for 10 hours in air under the uniaxial load of about 1.5 MPa. The heating and cooling rates are approximately 300 ℃/h. In the case of Pr-doped ZnO grain boundary, a thin layer of Pr metal with nominal thickness of about 5 nm was deposited onto surface of one crystal prior to the bonding. The deposition was conducted by sputter coating (PECS^{TM}, Gatan, Inc.), which includes a film thickness monitor for accurate control of the thickness. Conditions of bicrystal orientations studied in this thesis are summarized in **Table 2-1**. After the bicrystals are bonded, thin specimens are prepared by conventional thinning procedures that include mechanical polishing down to about 30 μm and argon (Ar) ion beam milling for electron microscope observations (**Figure 2-2**).

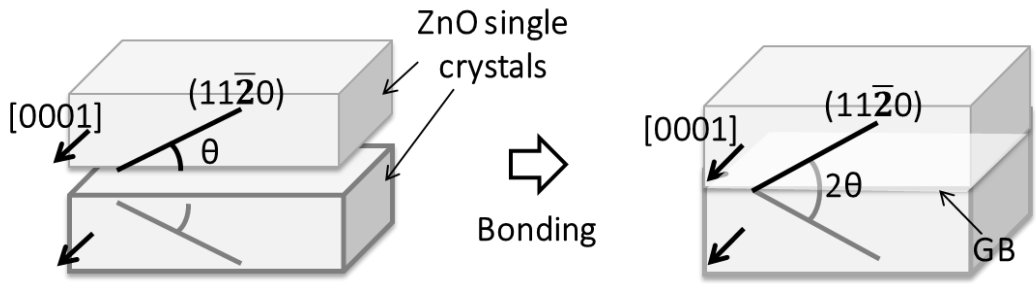

Figure 2-1. Schematic of ZnO bicrystal that forms ZnO [0001] tilt grain boundary.

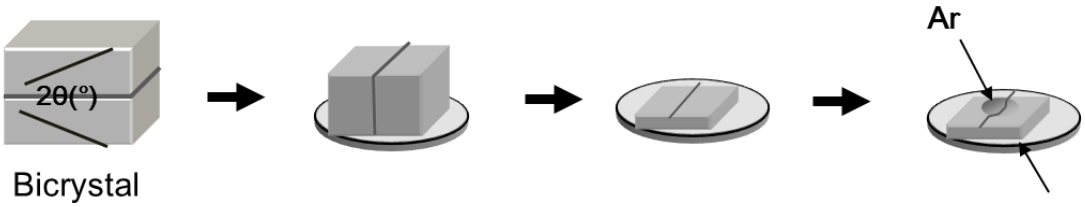

Figure 2-2. Schematic of specimen preparation. First, bicrystals obtained after diffusion bonding is resized into small enough size. Then, it is attached on the TEM mesh and mechanically polished down to ~ 30 μm. Final thinning is processed by Ar ion milling down to ~100 nm.

Table 2-1. Orientation relation of the bicrystals studied in this thesis**.**

2θ (°)	Σ value	boundary plane	doping
25.8	~79	$\{37\bar{1}\bar{1}0\}$	Pr-doped
27.8	13	$\{25\bar{7}0\}$	Pr-doped
30.0	~97	$\{38\bar{1}\bar{1}0\}$	Pr-doped
32.2	13	$\{13\bar{4}0\}$	Undoped, Pr-doped
38.2	7	$\{14\bar{5}0\}$	Pr-doped
43.6	49	$\{211\bar{1}\bar{3}0\}$	Pr-doped

2.2. Electron microscopy observation

Transmission electron microscope (TEM) and scanning TEM (STEM) were used in order to observe grain boundary structure from micrometer (μm) to sub angstrom (~Å) scale. Different imaging method such as annular dark field (ADF) and bright field (BF) were used. ADF image is formed by inelastically scattered electron collected by ADF detector, where BF image is formed by intensity of the transmitted beam collected by BF detector. Especially, high-angle ADF (HAADF) [1] detects high angle scattered electrons (**Figure 2-3**). The contrast of HAADF image is strongly dependent on the average atomic number (Z), thus, it has provided a valuable method for the current study for distinguish different elements with sufficiently different Z where Zn has atomic number of 30, and Pr has 59.

TEM observations were performed using JEM-2010 and JEM-4010 (JEOL Ltd. Tokyo, Japan) with acceleration voltage of 200keV and 400keV, respectively. STEM observations were carried out using JEM-2100F and ARM-200F under 200keV. Both STEM machines are equipped with a spherical aberration corrector for the electron probe (CEOS Gmbh, Germany).

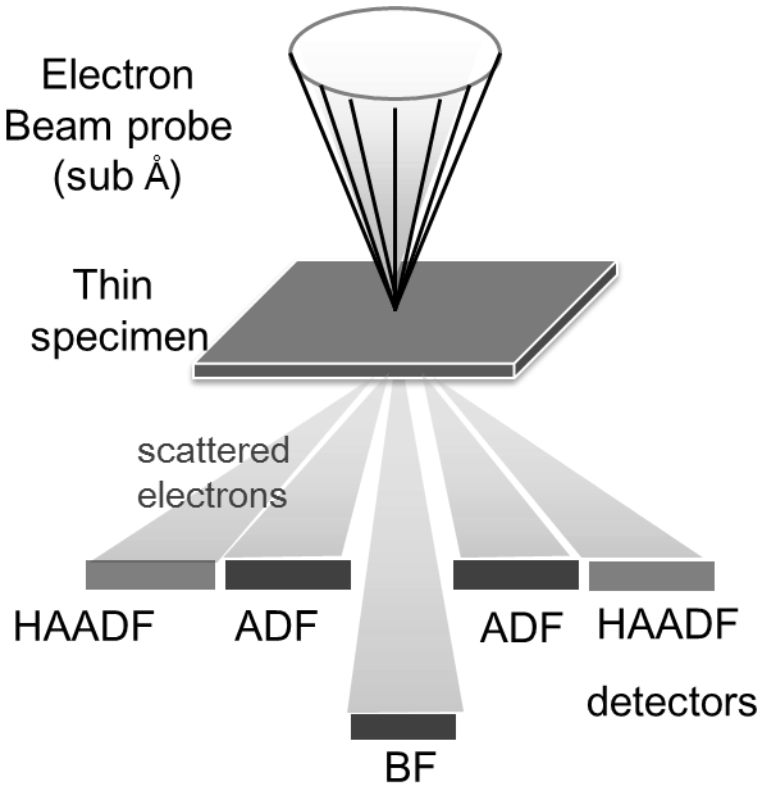

Figure 2-3. Schematic of several imaging techniques in dedicated STEM instrument. HAADF, ADF and BF detectors collect scattered electrons.

2.3. Atomistic simulation and modeling of grain boundary

Three-dimensionally periodic boundary conditions can be provided from the low-Σ CSL grain boundaries. First, the half crystal cell is made and joined with the opposite one to form supercell. It is not certain that the lowest energy of grain boundary structure is obtained from the initial supercell, but there are possibilities that one crystal is translated with respect to the other one parallel to the grain boundary. The various grain boundary structures obtained in this procedure are called translation state. For a large number of grain boundary models with the different translation state, atomic arrangements are optimized and total energy of simulation cell is estimated. However, going through all translation states is very time consuming and expensive. Static lattice methods with empirical inter-atomic potentials are used in this stage, which is much faster, but their accuracy is less reliable. The static lattice calculation was performed by the GULP code [2], where Buckingham-form two-body interatomic potential (2-1) was used. In the present study, potential parameters reported previously for ZnO was used [3] (**Table 2-2**).

$$V_{ij}(r_{ij}) = A_{ij} \exp(-\frac{r_{ij}}{\rho_{ij}}) - \frac{C_{ij}}{r_{ij}^6} \quad (2\text{-}1)$$

Table 2-2. Potential parameter [3]used in the static lattice calculation.

Interaction	A_{ij} (eV)	ρ_{ij} (Å)	C_{ij} (eV Å ^{6})
Zn^{2+} - O^{2-}	700.3	0.3372	0.000
O^{2-} - O^{2-}	22764.0	0.1490	27.879

Translation states are roughly sorted by static lattice calculation, and several models that showed lowest energies are brought to the next step that uses first-principles density functional theory (DFT) calculations. The formation energy of the grain boundary is the energy cost of distorting and breaking bonds due to the misorientation. The energy is obtained by (2-2);

$$\gamma = \frac{E_{GB} - E_{perfect}}{2A} \tag{2-2}$$

Where γ is formation energy, and E_{GB} or $E_{perfect}$ are total energies of supercells with or without grain boundary, respectively, after optimization of atomic configuration. A is the area of grain boundary plane. Since three-dimensional periodic boundary conditions are imposed for models, each grain boundary models have two grain boundaries so that the total energy was divided by 2A.

The DFT calculations were carried out with the plane-wave basis projector-augmented wave method [4] embedded in the VASP code [5]. Here, generalized gradient approximation (GGA)[6] was used for the exchange-correlation potentials. Cut-off energy for plane-wave basis sets was 400 eV for all the cases. For example, in the case of Σ13 grain boundary, Brillouin-zone integrations were performed over 2 x 1 x 4 *k*-point mesh generated by Monkhorst-Pack scheme [7], and simulation cell includes 208 atoms and two equivalent grain boundaries with the cell dimension of ~ 1.19 x 4.10 x 0.53 nm. Undoped grain boundary models were used as initial inputs for obtaining the Pr-doped case. Pr replaces several Zn sites, and the structure is optimized again. Grain boundary expansion was also considered because Pr doping may have affect to the lattice parameters.

2.4. Reference

[1] S.J. Pennycook and D.E. Jesson, Phys. Rev. Lett., **64**, 938 (1990)

[2] J.D. Gale and A.L. Rohl, Mol. Simulat., **29**, 291 (2003)

[3] G.V. Lewis and C.R.A. Catlow, J. Phys. C, **18,** 1149 (1985)

[4] P.E. Blöchl, Phys. Rev. B, **50**, 17593 (1994)

[5] G. Kresse and J. Furthmüller, Phys. Rev. B, **54**, 11169 (1996)

[6] J.P. Perdew, K. Burke, and M. Ernzerhof, Phys. Rev. Lett., **77**, 3865 (1996)

[7] H. J. Monkhorst and J. D. Pack, Phys. Rev. B, **13**, 5188 (1976)

Chapter 3. Atomic structure of ZnO [0001] 32.2° tilt grain boundary

Several ZnO [0001] tilt grain boundaries have been reported elsewhere and it was found that atomic arrangements of the grain boundaries are described by array of SUs [1]. The SUs are arranged straight or zig-zag depending on boundary planes. When the arrangements of SU were considered as a function of 2θ, SU align straight up to about 30°, while they align zig-zag for 2θ higher than 30° [1]~[4]. This implies that SU alignment would change at 2θ of about 30°. Moreover, it has been reported that ZnO [0001] tilt grain boundaries with 2θ of about 30° form in thin films [5]. These suggest the necessity to understand the grain boundary atomistic structure. Thus, ZnO Σ13 (32.2°) grain boundary was chapter. It was found that the grain boundary has two different SU alignments. Dominant structure of the grain boundary was the zig-zag SU alignment, and secondary structure was the straight SU alignment. Relation between the SU alignment and the rotation angle was discussed and the grain boundary atomic arrangement is determined in this chapter. Finally, the local configurations of the grain boundary were described in topological description that reveals edge dislocation character of the SU.

3.1. Introduction

There had been a number of reports issued on the structure and properties of ZnO [0001] tilt boundaries, either in bicrystal method or in textured films. For instance, Oba *et al*.(2004)[2] carried out high-resolution TEM observation [0001] on fiber-textured ZnO thin films grown on quartz-glass substrates by the pulsed-laser deposition. Many of undoped ZnO [0001] tilt grain boundaries were observed and it was revealed that the grain boundaries are generally described by arrangement of dislocation-like SUs (**Figure 3-1(a)**). In the previous STEM investigations on a several low-Σ CSL ZnO grain boundaries, it was also reported that the grain boundaries consist of SUs, and the atomic configurations of the SUs were revealed as SU α, and/or β [1] as shown in **Figure 3-1(b)**. The local atomic alignment in the SUs is nearly mirror symmetric on the plane indicated by the dotted lines. Grain boundaries are composed of straight SU alignment for tilt angle (2θ) from 0° to about 30°, and zig-zag alignment is likely to be formed for about 30° to 60° (**Figure 3-1(b)**) [4]. Here, the mirror planes are parallel to the boundary planes for straight and are inclined for zig-zag alignment. This implies that a structural transition from straight to zig-zag alignments occur at around 2θ of 30°. Moreover, ZnO grain boundaries with 2θ of 27°~32° are often formed in thin films when they are deposited on some particular substrates such as sapphire [5]. They suggested the grain boundaries near the orientation (2θ=27°~32°) might have low energy configuration. According to those previous results, it is important to understand atomic structure at this particular orientation, 2θ of about 30°. Also, I believe determination the atomic structure for these grain boundaries would provide an important insight.

As introduce in previous chapter, ZnO [0001] CSL tilt grain boundaries are good model systems for a detailed grain boundary analysis. Particularly, there are two low-Σ CSL grain boundaries (2θ = 27.8° and 32.2°) with 2θ around 30°. The Σ value is thirteen, where Σ represents the degree of geometrical coincidence between the adjacent crystals. Recently, atomic structure of one Σ13 (2θ = 27.8°) tilt grain boundary has been reported [3] (**Figure 3-1(b)**) that is composed by SU α, and/or β in straight arrangement. Therefore, the present chapter is carried out grain boundary investigation on the other Σ13 (2θ = 32.2°) grain boundary that has different grain boundary plane, $(13\bar{4}0)$ using SU description. Determining the grain boundary atomic structures in systematic way can model the behavior of polycrystalline ZnO based devises.

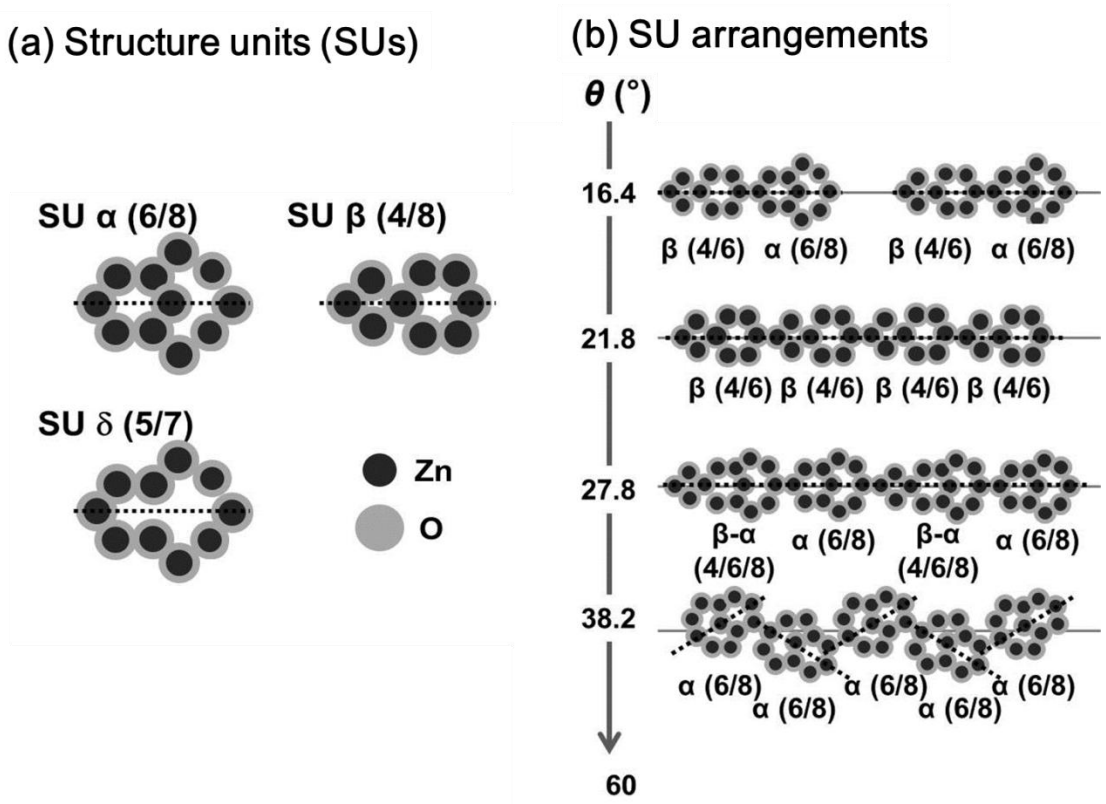

Figure 3-1. (a) SUs for ZnO [0001] tilt grain boundary [2]. SUs are characterized by the combination of six- and eight-membered rings (6/8) in SU α, four- and six-membered rings (4/6) in SU β, and five- and seven-membered rings (5/7) in SU δ. The dotted lines denote the local mirror symmetric planes. (b) SU arrangements for ZnO [0001] tilt grain boundaries with the change of 2θ. Gray lines denote the grain boundary planes. Structures for 2θ = 16.4°[1], 21.8°[2], 27.8°[3], and 38.2°[4] grain boundary have been reported in the previous reports.

3.2. Method

ZnO bicrystal was fabricated by diffusion bonding of two ZnO single crystals at 1,100 ℃ for 10 hours in air, under uniaxial stress of 1.5 MPa. The detailed fabrication procedures had been described previously. Orientation relationship of the bicrystals is shown in **Figure 3-2**. The two crystals had common [0001] and the tilt angle, which is made of $(11\bar{2}0)$ of both crystals, was intended to be about 32.2°. This leads to the boundary plane parallel to $(13\bar{4}0)$ of both crystals.

Grain boundary fabricated in the bicrystal was observed by transmission electron microscopy (TEM) and scanning TEM (STEM). Thin foils for STEM observations were prepared by conventional procedures as introduced in the chapter 2. The grain boundary structure was subsequently observed by TEM and aberration-corrected STEM (JEM-2010, JEM-4010, and ARM-200F with a spherical aberration corrector for the electron probe, JEOL Ltd. Tokyo, Japan). TEM and STEM observations with the JEM-2010 and ARM-200F were carried out at the acceleration voltage of 200 kV, and that with JEM-4010 was done at 400 kV. STEM imaging was carried out using a probe-forming aperture semiangle of 22 mrad. HAADF, BF, and annular BF (ABF) images were recorded by 68-280 mrad, 0-45 mrad, and 11-23 mrad detectors, respectively.

Stable atomic alignment of the grain boundary was simulated independently. The simulation was performed by two-step methodologies; firstly with static lattice methods with empirical inter-atomic potentials and secondly with the first-principles calculations. Cut-off energy for the plane-wave basis set was 400 eV. Brillouin-zone integrations were performed over 2 x 1 x 4 *k*-point mesh. Simulation cells included 208 atoms and two equivalent grain boundaries with the cell dimension of ~ 1.19 x 4.10 x 0.53 nm^3.

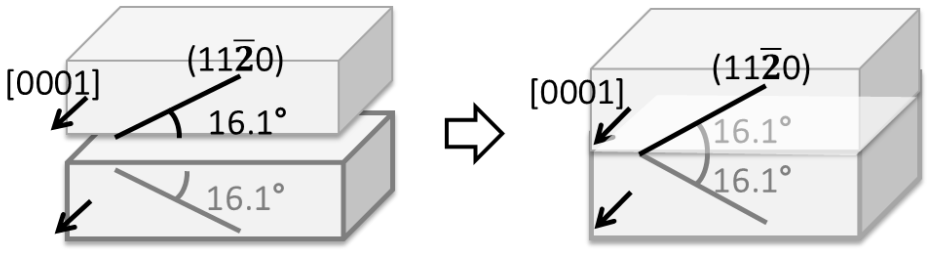

Figure 3-2. Schematic of ZnO bicrystals studied the current chapter. The 2θ is intended to be about 32.2°of the adjacent crystals in order to obtain Σ13 symmetric tilt grain boundary.

3.3. Results and discussion

3.3.1. Atomic arrangement of the grain boundary

Figure 3-3 shows the selected-area diffraction pattern (SADP) and the bright-field TEM image of the ZnO bicrystal. The tilt angle is estimated from diffraction pattern (**Figure 3-3(a)**) by measuring angle deviation between two $(11\bar{2}0)$ of the adjacent crystals. In the current bicrystals, tilt angle was estimated to be ~32.5°, which is close to that of the ideal Σ13 (32.2°).

Moreover, two crystals are well bonded without any secondary phases and the boundary plane is flat in macroscopic level (**Figure 3-3(b)**). It is therefore confirmed that the desired specimen was successfully obtained.

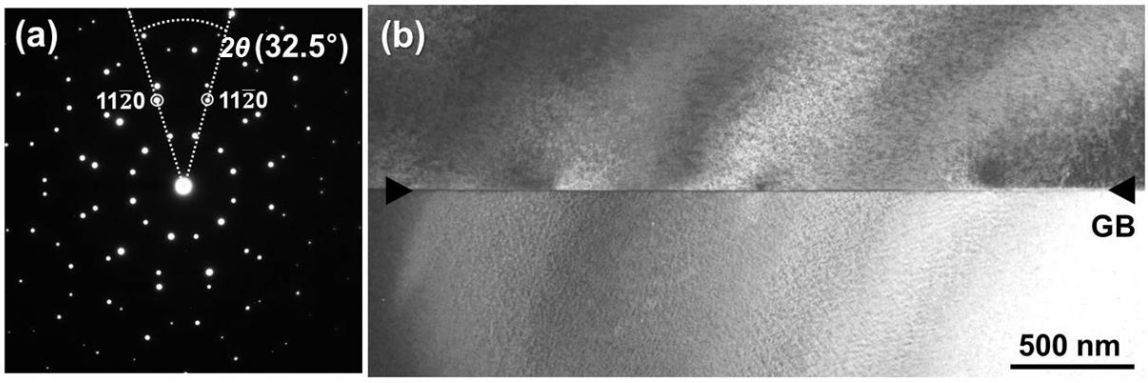

Figure 3-3. (a) Selected-area diffraction pattern taken from the grain boundary region of ZnO bicrystal. Dotted lines indicate the actual tilt angle (~32.5º) made by two $(11\bar{2}0)$ of the adjacent crystals. (b) Bright-field TEM image of the bicrystal, where the black arrows indicate the location of grain boundary.

Atomic structure of grain boundary is further observed by STEM (**Figure 3-4**).It is confirmed that the boundary plane is flat and parallel to $(13\bar{4}0)$ of the adjacent crystals. In HAADF images, Zn-O columns appear as bright spots. Atom locations in bulk are observed as hexagonal patterns, and the grain boundary atomic configuration is also directly observed. Close inspection reveals that the structure is periodic as indicated by vertical lines (**Figure 3-4(a)**). The atomic configuration can be described by the set of circles. It should be noted that this structure was observed in the majority of the grain boundary area. The circle sets are composed of six- and eight-membered rings, which are characteristics of the SU α. This SU model is same as one that was observed in the previous studies [1]~[8]. Considering the direction of local mirror planes in SU (dotted lines in the inset) as introduced above, it can be stated that the SUs align zig-zag.

The grain boundary structure was also observed by ABF STEM for further confirmation (**Figure 3-4(b)**). On the contrary to HAADF image, Zn-O columns are observed as dark spots. The grain boundary atomic configuration again consists of combination of six- and eight-membered rings. It was also confirmed that SUs align zig-zag. On the other hand, a stable atomic alignment obtained from the first-principles calculation is shown in **Figure 3-4(c)**. Within the structural period indicated by vertical lines, eight- six-, eight- and six-membered rings are connected from the left to the right. This can be also described as zig-zag alignment of SUs α. This atomic configuration agrees well with the result of STEM images. It is therefore considered that major structure of the grain boundary is zig-zag alignment of SU α. In addition to the SU model description as shown here, circuit mapping analysis [5],[9]~[11] was also conducted as will be explained later.

Secondary structure was also observed in this grain boundary. In HAADF STEM image in **Figure 3-5(a)**, the grain boundary structure differs from the previous case (**Figure 3-4(a)**). The structural period is again composed of the six-, eight-, six-, and eight-membered rings that are characteristic of SU α. However, the direction of the local mirror planes (dotted lines in the inset) in the SU is parallel to the boundary plane and the eight-membered rings are rotated by about 150° as compared to the previous case. There are two SUs α in a period, and the second SU is shifted up by monolayer height. The same tendency was also observed for the BF image in **Figure 3-5(b)**. Another stable structure obtained from the first-principles calculations (**Figure 3-5(c)**) reproduces this feature. It is therefore concluded that the secondary structure can be understood as straight alignment of SUs α where the second SU is shifted up by monolayer height.

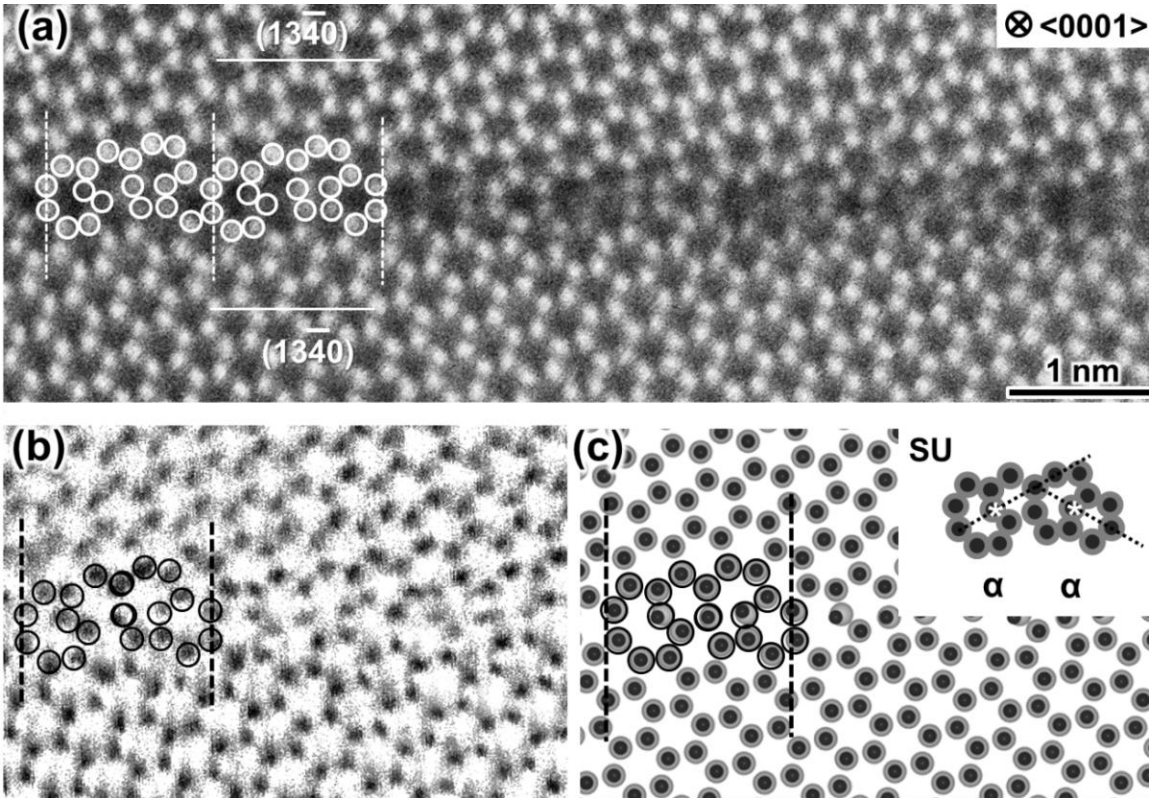

Figure 3-4. (a) HAADF and (b) ABF STEM images for the major structure of the ZnO Σ13 tilt grain boundary. (c) A stable atomic configuration obtained by the first-principles calculation. Vertical lines show a structural period and set of circles denote the SUs α (highlighted in the inset), and dotted lines in the inset indicate the local mirror plane of the SU. Here, the grain boundary structure is visualized using the VESTA [12].

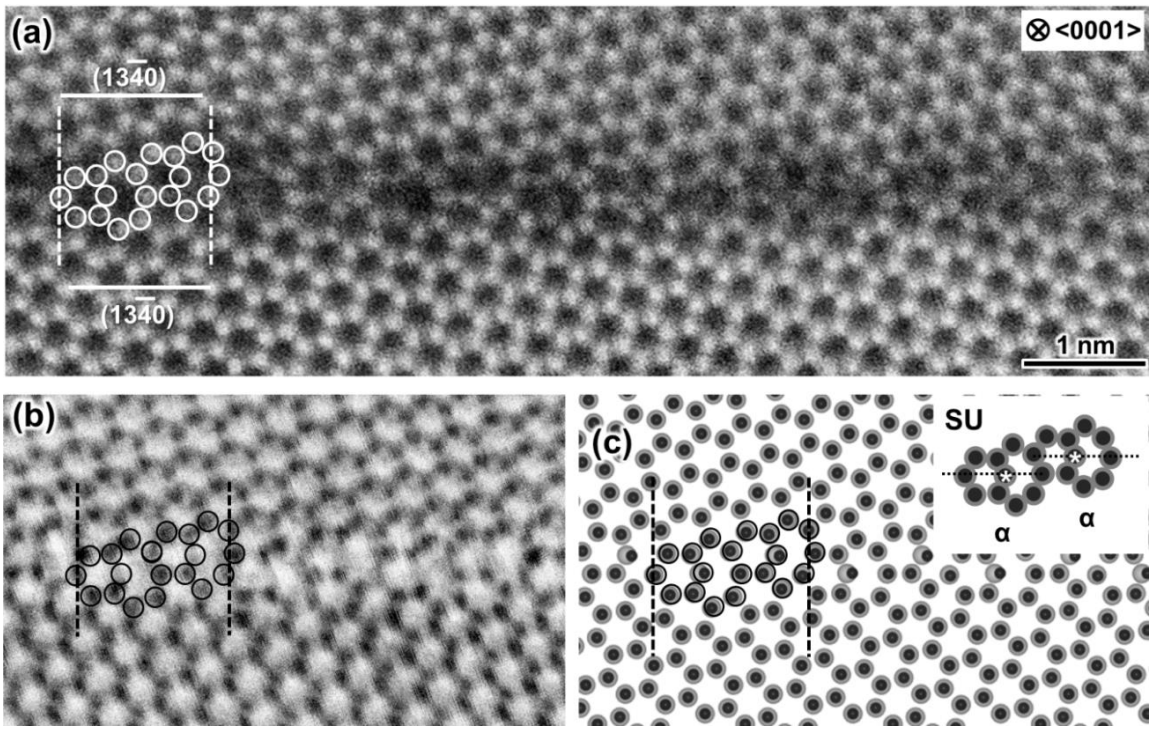

Figure 3-5. (a) HAADF and (b) BF STEM images for the secondary structure of the ZnO Σ13 tilt grain boundary. (c) A stable structure obtained from the first-principles calculation. Vertical lines show the structural period, and set of circles denotes the SUs α. Dotted lines in the inset indicate the local mirror plane of the SU.

Here, let me briefly remind the previous studies, reported atomic structure of ZnO [0001] tilt grain boundaries with 2θ near 30°. For 2θ smaller than or close to 30°, Σ13 ($25\bar{7}0$) (2θ = 27.8°) grain boundary [3] and 2θ = 30.2° grain boundary [5] have the straight SU alignment. On the other hand, the zig-zag alignment has been reported for the 2θ = 31.5° and 32.2° grain boundaries [9][13]. These results suggest that transition from straight to zig-zag alignment may occur for 2θ in between 30.2° and 31.5°. The result of the present study that the dominant structure of 2θ = 32.5° grain boundary is the zig-zag alignment is also consistent with this trend. On the other hand, it would be also possible that the zig-zag and the straight SU alignments may coexist, as is suggested by the presence of secondary structure in this study. For a better understanding, areas exhibiting straight and the zig-zag segments should be more extensively studied.

On the other hand, the detailed atomic configuration of the SU is discussed. Some of previous studies have designated the structure as the SU δ (five – seven membered ring) [9][13] instead of the SU α (six- eight membered ring). Therefore, for considering the relative stabilities, grain boundary models with the SU δ [9][13] and the SU α were simulated (**Figure 3-6(a)-(d)**) and their boundary energies were calculated (**Table 3-1**). It was found that the SU α tends to show lower energies than the SU δ. The grain boundary energies from first principle calculations were 1.18 J/m^2 for the zig-zag alignment of SU α, 1.08 J/m^2 for straight SU α, 1.26 J/m^2 for zig-zag SU δ, and 1.19 J/m^2 for straight SU δ, respectively. The energies obtained by the GULP code were slightly larger: 1.81 J/m^2 (zig-zag SU α), 1.65 J/m^2 (straight SU α), 2.06 J/m^2 (zig-zag SU δ), and 1.97 J/m^2 (straight SU δ), respectively. These values are similar to those reported by Ruterana *et al.* for the same grain boundary obtained with similar method [5]. A reason for the lower energies of SU α over δ may be that Zn-Zn or O-O bonds for the five-membered rings in the SU δ are not favored which results in the formation of energetically unfavorable dangling bonds. This would be in contrast to the GaN cases where Ga-Ga and N-N bonds are formed because of the covalent nature [11][14].

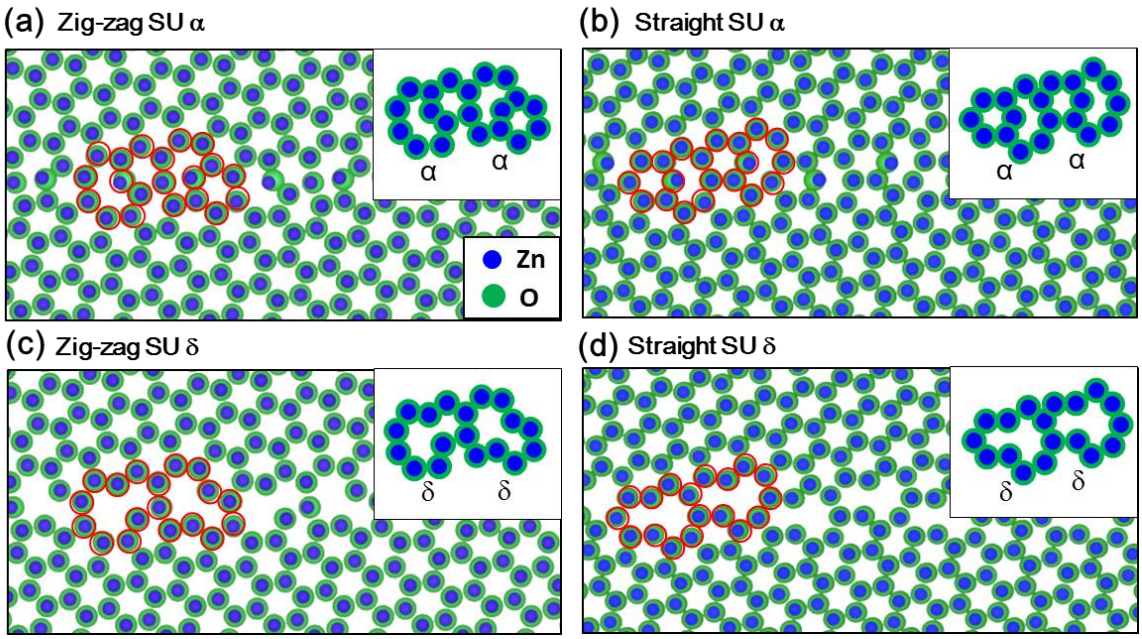

Figure 3-6. Zig-zag and straight alignments of SUs α (six- eight membered ring) and δ (five – seven membered ring); (a) zig-zag and (b) straight alignment with the SUs α, and (c) zig-zag and (d) straight alignment with the SUs δ.

Table 3-1. Calculated formation energies for the different SU alignments (a)-(d), as shown in **Figure 3-6**.

remark	SU alignment	Energy (J/m^2)
(a)	zig-zag α	1.18
(b)	straight α	1.08
(c)	zig-zag δ	1.26
(d)	straight δ	1.19

3.3.2. Structural analysis by circuit mapping formalism

So far, atomic structure of grain boundary was characterized by the SU model based on CSL formalism. Although this is the most often used methodology to analyze grain boundary structure in general, it has also been demonstrated that circuit mapping [5],[8]~[11] successfully describes the atomic arrangements of ZnO and GaN grain boundaries. It is a crystallographic analysis carried out using dichromatic complex. Mapping of a circuit can characterize the grain boundary structure and allows us to completely determine the nature of grain boundary including various steps.

In this formalism, the configuration of a grain boundary is described by a periodic network of primary dislocations, which characterize the corresponding Σ. Then, any deviation from the coincidence (Σ) is compensated by the introduction of secondary dislocations which often have a step character. When a conventional circuit is made around one period of the grain boundary and then mapped inside one of the crystals, it presents a closure failure corresponding to the dislocation content of the grain boundary period. However if the circuit is mapped within the dichromatic complex of the grain boundary, any additional defects which leads to the deviation of the boundary from coincidence constitute any measured closure failure.

First, the primary dislocation of the grain boundary local configuration was determined. The major structure that corresponds to the zig-zag SU alignment is analyzed (**Figure 3-7(a)**). The SXF circuit around one period can be express by half circuit SX on the upper crystal and the rest half circuit XF on the lower crystal which are corresponded to translation vector of SX= $-3\vec{a}_1 - 4\vec{a}_3$ and XF = $-4\vec{a}_2 - 3\vec{a}_1$, respectively. Same circuit possessing the same translation vector is drawn in bulk area. The circuit S-X-F exhibits closure failure, indicating primary dislocation with the Burgers vector $\boldsymbol{b} == -\boldsymbol{a}_1 + \boldsymbol{a}_3 = [10\bar{1}0]$, thus, $|\boldsymbol{b}| = \sqrt{3}\boldsymbol{a}$. Note that $\boldsymbol{a}$ is elemental lattice vectors of the Wurtzite [0001] lattices with $\vec{\boldsymbol{a}} = \frac{1}{3}\langle 11\bar{2}0\rangle$. Same circuit mapping can be shifted on the Σ13 dichromatic pattern (**Figure 3-7(b)**). Burgers vector was resulted to be identical. Next, the primary dislocation of the secondary structure (straight SU alignment) is analyzed. Same mapping operation has been carried out ((**Figure 3-8(a),(b)**)) and the Burgers vector of was revealed to be $\boldsymbol{b} = -2\vec{\boldsymbol{a}}_1 = \frac{2}{3}[11\bar{2}0]$, and $|\boldsymbol{b}| = 2\boldsymbol{a}$. These results agree with the previous reports by Ruterana *et al*. for the $\{13\bar{4}0\}$ 32.2° grain boundary [5].

Zig-zag pair of two SUs consists one period in the major structure. As revealed beforehand, a period give rise to primary dislocation of $\sqrt{3}\boldsymbol{a}$. Thus, each SU is given elemental dislocation of $\boldsymbol{a} = \frac{1}{3}[11\bar{2}0]$. In the same way, the secondary structure is analyzed, and a single SU was also given $\boldsymbol{a} = \frac{1}{3}[11\bar{2}0]$. Thus, the Σ13 $(13\bar{4}0)$ grain boundary can be described by arrangements of dislocation-like SU, which has edge dislocation core.

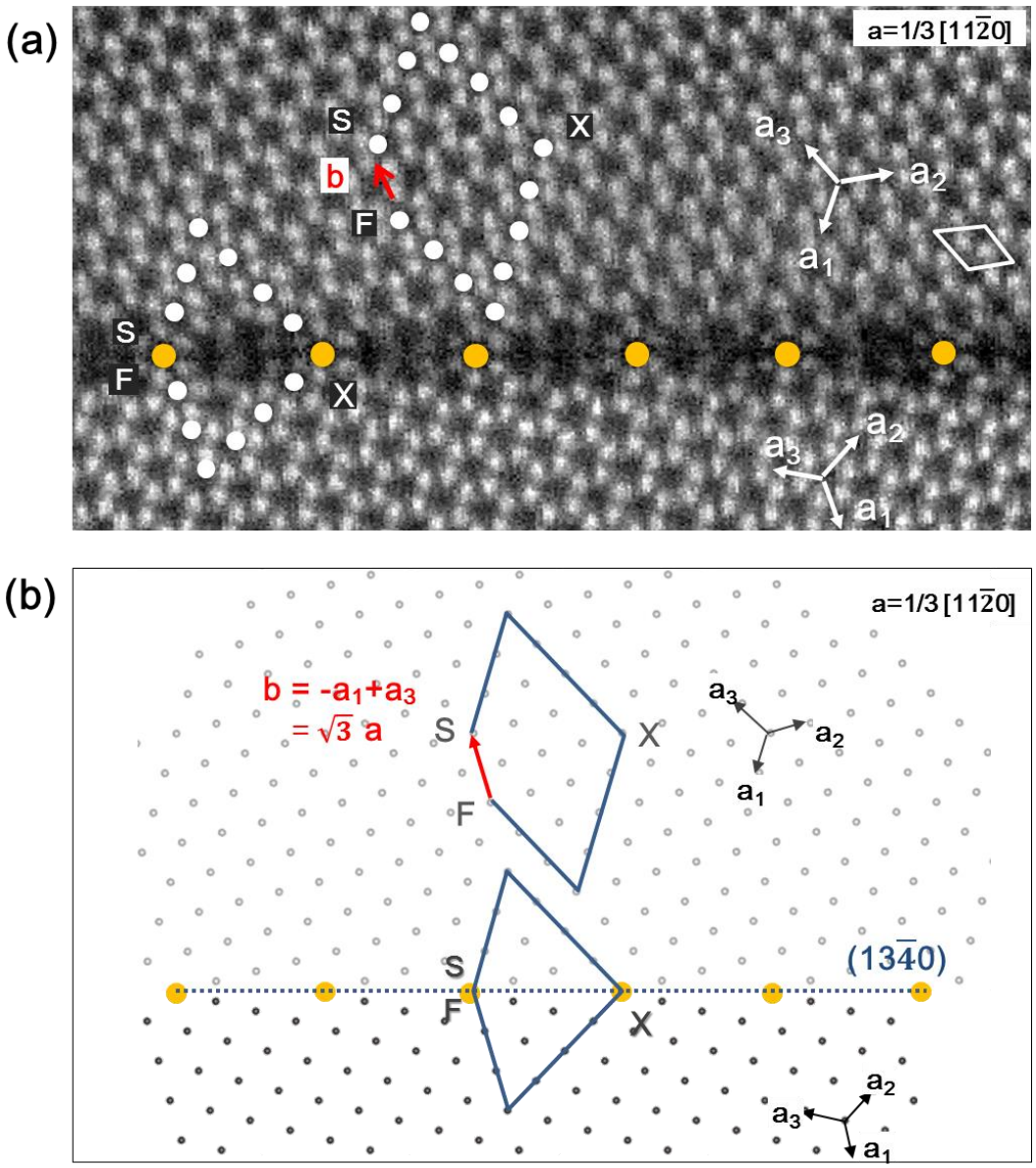

Figure 3-7. (a) HAADF-STEM image with the circuit mapping for one period of the major structure (zig-zag SU alignment). Burgers circuits SXF at the grain boundary region with the shortest period and closure failures in bulk are shown. (b) Same circuit is mapped on the dichromatic complex showing identical burgers vector for the period, $|\boldsymbol{b}| = \sqrt{3}\boldsymbol{a}$, where $\boldsymbol{a}$ is the elemental lattice vectors of the Wurtzite [0001] lattices, $\vec{\boldsymbol{a}} = \frac{1}{3}\langle 11\bar{2}0\rangle$.

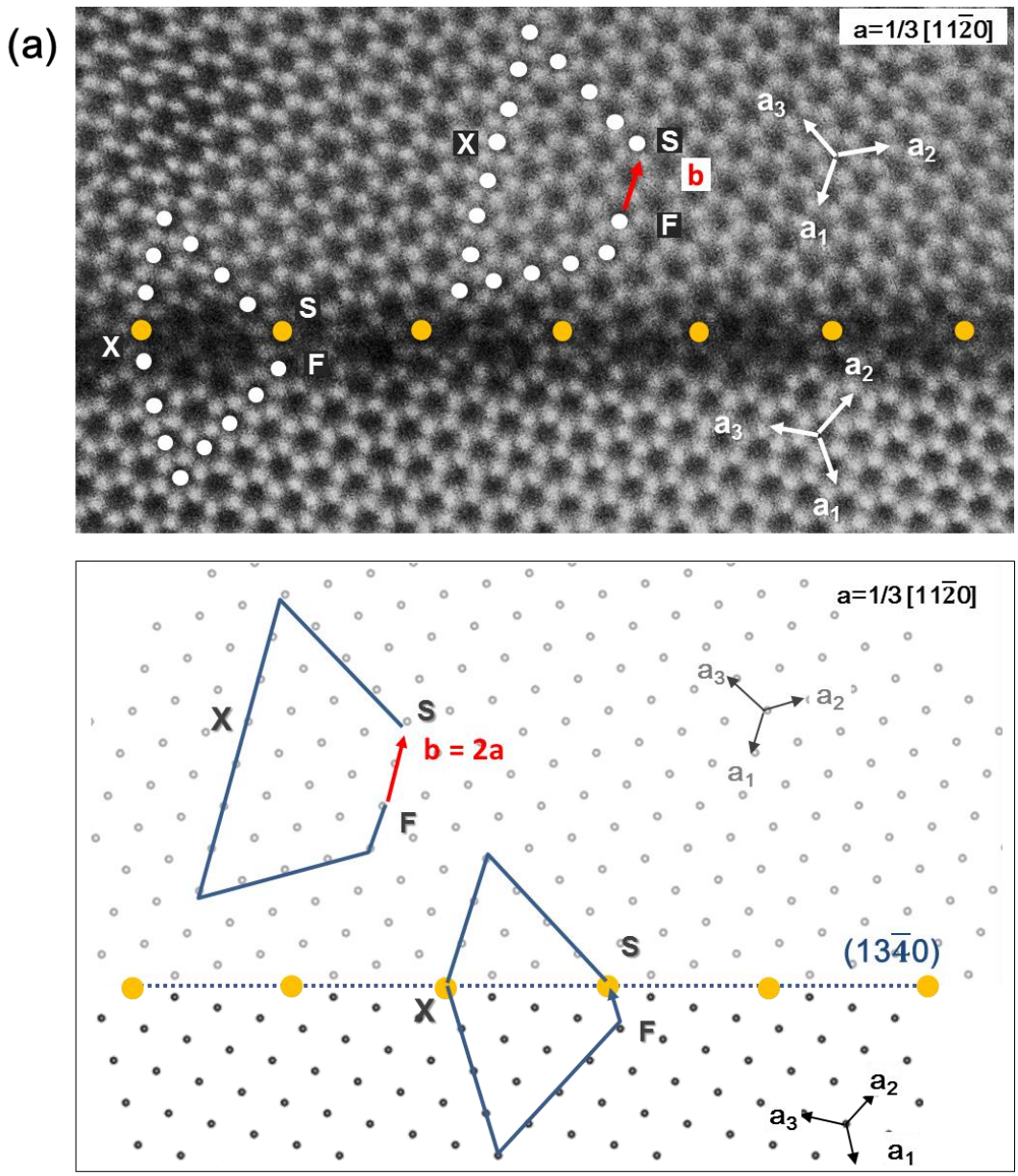

Figure 3-8. (a) HAADF-STEM image with the circuit mapping for one period of the secondary structure (straight SU alignment). Burgers circuits SXF at the grain boundary region with the shortest period and closure failures in bulk are shown. (b) Same circuit is mapped on the dichromatic complex showing identical Burgers vector of the period, $|\boldsymbol{b}| = 2\boldsymbol{a}$.

Circuit mapping formalism can be applied for analyzing any secondary dislocation in the grain boundary. **Figure 3-9** shows a HRTEM image of the area with a step, which is probably formed due to small deviation from CSL. It should be noted here that bright dots in HRTEM image represent the locations of open channels in contrast to the ADF STEM images. Here, a circuit $S_1X_1F_1$ has been drawn to surround a step. Half circuit of upper crystal (λ) can be expressed as S_1X_1= -5$\vec{a}_2$ - 6$\vec{a}_3$, and that of lower crystal (μ) can be expressed as X_1F_1= -6$\vec{a}_1$ - 4$\vec{a}_2$. Mapping $S_1X_1F_1$ into the dichromatic complex (**Figure 3-10(a)**) reveals the Burgers vector ***b*** of secondary dislocation is generated by translation vectors. The Burgers vector can be understood as the difference of 2t(λ) and $t(\mu) + t'(\mu)$, where t(λ) and t(μ) represent the smallest translation vectors for the upper crystal (λ) and the lower one (μ), and t'(μ) is rotated by 120° with respect to t(μ). It should be also noted that the Burgers vector corresponds to the smallest vector of the DSC (displacement shift complete) lattice (**Figure 3-10(b)**) which is revealed to be b = 1/39[$\bar{2}7\bar{5}0$]

The step structure can be characterized as in (**Figure 3-10(c)**). The step height is estimated by $h(\lambda) = n \cdot 2t(\lambda)$ and $h(\mu) = n \cdot t''(\mu)$ for respective crystals, where *n* is the unit vector normal to the boundary plane and $t''(\mu) = t(\mu) + t'(\mu)$. Using this, $h(\lambda)$ and $h(\mu)$ were estimated to be $2 \cdot d(\bar{4}130)$, where $d(\bar{4}130)$ represents the interplanar spacing of $(\bar{4}130)$. Therefore, the circuit mapping formalism successfully interpreted the grain boundary dislocations: it allows not only determining the primary dislocation content in the local configuration (SU), but it also the nature of the additional defect such as step which explains its measured *2θ.*

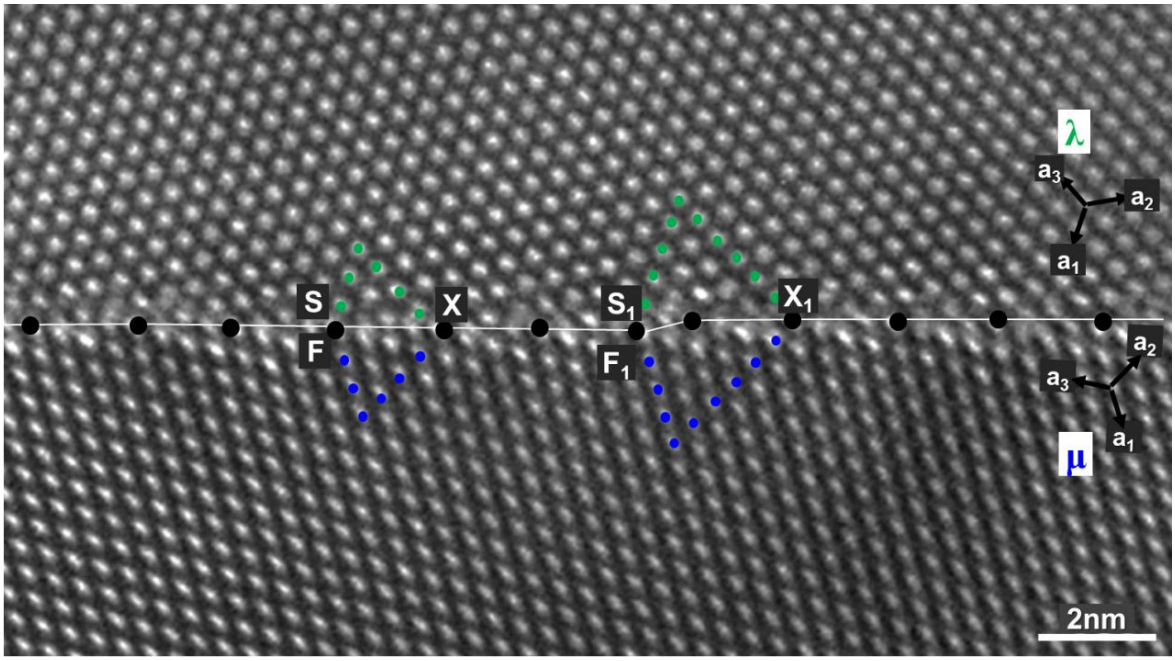

Figure 3-9. High-resolution TEM image with the circuits for the interfacial area. SXF circuit includes a periodic arrangement, while step element is included in the $S_1X_1F_1$ circuit.

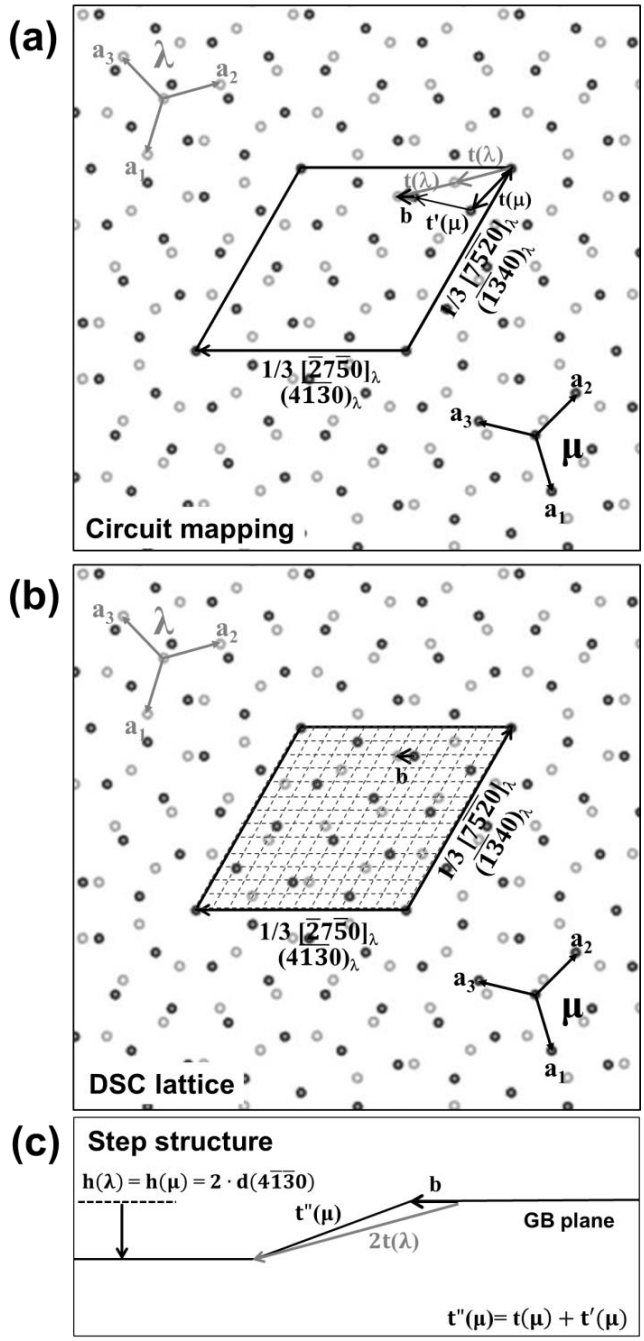

Figure 3-10. Dichromatic complex for the Σ13 orientation relationship. One hexagonal crystal (λ) with gray circles and the other (μ) with black ones. CSL cell is drawn by a quadrilateral. (a) The complex for obtaining the Burgers vector of secondary dislocation by circuit mapping. Burgers vector (**b**) of the secondary dislocation and smallest translation vectors t(λ), t(μ), and t'(μ) for the crystal lattices are shown by arrows. (b) The same pattern with DSC lattice indicated by the dotted lines. (c) Schematic illustration of the step in **Figure 3-9.**

3.4. Conclusion

In this chapter, undoped Σ13 (32.2°) tilt grain boundary has been fabricated from bicrystals. STEM observation and first principles calculations were carried out in order to determine stable atomic structure.

I. The grain boundary was described by SU, which has six- and eight membered ring that comprises SU α.

II. SU γ in the boundary forms two kinds of the alignments; one is zig-zag and the other is straight. It suggests transition of the SU alignment occurs for 2θ smaller than 32.2°, and the two different alignments may coexist in the grain boundary.

III. Circuit mapping characterized local boundary configurations as well as the secondary defects, step component. Atomic arrangement of the grain boundary can be described by dislocation-like SUs, which have $\frac{1}{3}<11\bar{2}0>$ edge dislocation core. Step has been characterized as secondary dislocation with the Burgers vector of **b** = 1/39[$\bar{2}7\bar{5}0$], which would be due to the tilt angle deviation from the exact CSL relation.

3.5. Reference

[1] Y. Sato, T. Mizoguchi, F. Oba, Y. Ikuhara, and T. Yamamoto, Phys. Rev. B, **72**, 064109-1 (2005)

[2] F. Oba, H. Ohta, Y. Sato, H. Hosono, T. Yamamoto, and Y. Ikuhara, Phys. Rev. B. **70**, 125415-1 (2004)

[3] Y. Sato, J. –Y. Roh, and Y. Ikuhara, Phys. Rev. B, **87**, 140101-1 (R) (2013)

[4] F. Oba, Y. Sato, T. Yamamoto, H. Ohta, H. Hosono, and Y. Ikuhara, J. Mater. Sci., **40**, 3067 (2005)

[5] P. Ruterana, M. Abouzaid, A. Bere, and J. Chen, J. Appl. Phys., **103**, 033501-1 (2008)

[6] Y. Sato, T. Mizoguchi, N. Shibata, T. Yamamoto, T. Hirayama, and Y. Ikuhara, Phys. Rev. B, **80**, 094114 -1 (2009)

[7] Y. Sato, T. Yamamoto, and Y. Ikuhara, J. Am. Ceram. Soc., **90**, 337 (2007)

[8] J.-Y. Roh , Y. Sato, and Y. Ikuhara, J. Am. Ceram. Soc., **97**, 617 (2013)

[9] A. Kiselev, F. Sarrazit, E. Stepantsov, E. Olsson, T. Claeson, V. Bondarenko, R. Pond and N. Kiselev, Phil. Mag. A, **76,** 633 (1997)

[10] F. Sarrazit, R. Pond, and N. Kiselev, Phil. Mag. Lett., **77**, 191 (1998)

[11] V. Potin, P. Ruterana, G. Nouet, R.C. Pond, and H. Morkoç, Phys. Rev. B, **61**, 5587 (2000)

[12] K. Momma and F. Izumi, J. Appl. Cryst., **44**, 1272 (2011)

[13] J. M. Carlsson, B. Hellsing, H.S. Domingos, and P.D. Bristowe, J. Phys.: Condens. Matt., **13**, 9937 (2001)

[14] A. Béré and A. Serra, Phys. Rev. B, **65**, 205323 (2002)

Chapter 4. Atomic arrangement and segregation behavior in Pr-doped ZnO grain boundaries

Knowing that the dopants at grain boundary may significantly affect to the material's properties, the atomic-scale dopant behavior has been widely studied. In some cases [1]~[5], the location of dopant could be explained by using SU models because the dopant atoms tend to be relaxed by being segregated at certain sites within the SUs, which sufficiently produce the optimum atomic environment. Thus, it implies that once the SU of the grain boundary is determined, the location of dopant will be fixed. In order to further investigate this point, atomic structure of the Pr-doped ZnO [0001] 30.0° and 32.2° tilt grain boundaries were investigated in this chapter. The same kind of SU was commonly observed for these grain boundaries, which is also the same as that for the 27.8° tilt grain boundary [6], On the other hand, the locations of Pr were not all the same for the different grain boundaries. This demonstrates that site selectivity of Pr dopant can be varied at different grain boundaries even with the identical SUs. It is suggested that the variation of strain distribution is a cause of change in the location of Pr. Since Pr has larger ionic size than Zn, it would preferentially substitute the Zn sites with locally largest space.

4.1. Introduction

It is well known that the presence of dopant elements near grain boundary may influence performances of polycrystalline materials. Therefore, we should understand the dopant behavior such as the distribution, the atomic-scale location, the electronic structure, and so on, so that we can obtain optimized material performances. In this chapter, atomistic structure and segregation behavior in Pr-doped ZnO grain boundary are studied. This system is practically important because Pr-doped ZnO ceramics have long been used for varistor devices owing to the nonlinear current-voltage characteristics, where Pr at the grain boundaries plays central role for the electrical functions [7]~[9]. Atomistic structure of dopant-introduced grain boundary also can be described by arrangement of SUs. In the recent years, the atomic structure and the location of Pr in ZnO [0001] 2θ = 27.8° (Σ13) [6] CSL symmetric tilt grain boundary were reported. The boundary plane was described by SU γ with periodic zig-zag arrangement. It was suggested that the Pr always locates the same specific sites in the SU γ which is also corresponding findings from other material systems [1]~[3].

In this chapter, the atomic structures and Pr-segregation of Pr-doped ZnO [0001] 30.0° and 32.2° symmetric tilt grain boundaries were studied. The 32.2° of tilt angle also provides the other boundary plane of the Σ13 orientation in the 6-fold ZnO hexagonal system. Comparison the atomic structures and the Pr locations in the 32.2° tilt grain boundary to the previous 27.8° tilt case [6] would give us an insight for understanding the same Σ value, but different boundary planes of the CSL grain boundary. On the other hand, it is quite meaningful to determine the atomic structure of a non-low-Σ CSL grain boundary for not limiting the discussion to low-Σ CSL grain boundaries. The 30.0° tilt grain boundary is chosen as such a case since its 2θ is between those of Σ13 (27.8°/32.2°) grain boundaries. This would provide another opportunity to discuss the atomic structure and the segregation of Pr among the Σ13 grain boundaries and the neighboring non-low-Σ CSL grain boundary. Therefore, the objective of this chapter is twofold: The first one is to compare the atomic structures and the location of Pr in the Σ13 grain boundaries and to found the effect of different boundary planes. And the second one is to extend our understanding to the relationship among low- and non-low-Σ CSL grain boundaries.

4.2. Method

ZnO bicrystal fabrications, TEM/STEM observations, and theoretical calculations were conducted in similar ways to those in the previous chapter. In order to dope Pr into ZnO grain boundaries, 5nm of Pr is deposited on surface of ZnO crystal using sputter coating (PECS^{TM}, Gatan, Inc.), which includes a film thickness monitor for accurate control of the thickness before bonding two single crystals. Pr-doped ZnO [0001] tilt grain boundaries with 2θ = 30.0°, and 32.2° were fabricated (**Figure 4-1**). Orientation of initial surfaces was $(13\bar{4}0)//(25\bar{7}0)$ for the 30.0° grain boundary and Σ13 $\{13\bar{4}0\}$ for the 32.2° tilt grain boundary, respectively. Therefore, 32.2° tilt grain boundary was a symmetric tilt grain boundary from the initial state, while 30.0° tilt grain boundary was an asymmetric tilt grain boundary before the bonding.

Grain boundary structures were observed using conventional transmission electron microscope (TEM, JEM-2010HC, JEOL Ltd. Tokyo, Japan), and aberration-corrected scanning TEM (STEM, ARM-200F, JEOL Ltd. Tokyo, Japan). TEM and STEM images were acquired with the acceleration voltage of 200 kV. A probe-forming aperture semiangle of 22 mrad. and a detection angle ranging from 68 to 280 mrad. were used to record high-angle annular dark-field (HAADF) [10] STEM images. The HAADF STEM imaging is useful for observing heavier ions such as Pr because the image intensity depends on atomic number (Z) where Z of Pr is 59, and Zn is 30.
For obtaining the calculated structure of the Pr-doped grain boundary, some Zn ions are replaced by Pr ions and the atomic positions were again optimized.

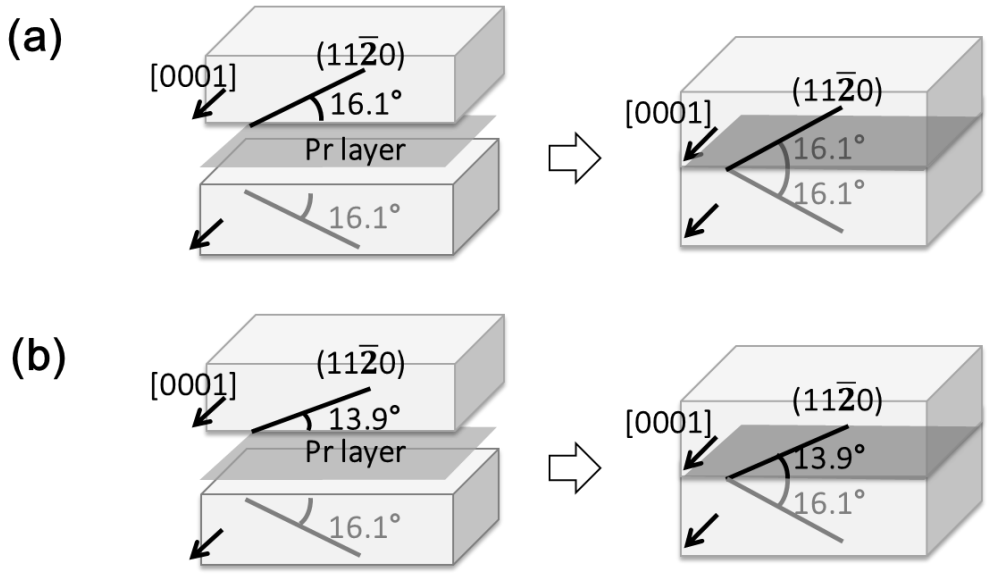

Figure 4-1. Orientation relationships of the bicrystals; (a) Pr-doped 32.2° symmetric tilt grain boundary and (b) Pr-doped 30.0° asymmetric tilt grain boundary.

4.3. Results and discussion

Bright-field TEM images of both the bicrystals are shown in **Figure 4-2(a),(b)**. It has been confirmed that the two crystals are well bonded. Precipitation of Pr oxide was observed in part, suggesting that Pr is saturated at the grain boundary as was discussed in our previous study [11]. For the first bicrystal with the 32.2° tilt grain boundary (**Figure 4-2(a)**), the boundary plane is flat and parallel to $(13\bar{4}0)$ of the adjacent crystals. Diffraction pattern taken from the grain boundary shows the actual 2θ is measured to be about 32.5° (**Figure 4-2(c)**), which is close to the ideal value of 32.2°. Therefore, orientation relationship of two crystals and boundary plane orientation were maintained during the bonding.

On the other hand, the grain boundary is facetted in part for the second bicrystal (**Figure 4-2(b)**). The actual 2θ was measured to be ~ 29.7° from the diffraction pattern (**Figure 4-2(d)**), which is also close to the intended value of 30.0°. The majority of grain boundary area is flat with the local boundary plane parallel to $(38\bar{1}\bar{1}0)$ of the adjacent crystals which is the boundary plane of Σ97(29.4°). Rest of the area exhibits the local grain boundary facets. It is considered that the initial boundary plane of $(13\bar{4}0)//(25\bar{7}0)$ before the bonding is less stable than symmetric $(38\bar{1}\bar{1}0)//(38\bar{1}\bar{1}0)$ and grain boundary facets. The latter ones were obtained during the bonding process. In this chapter, the analysis is focused on the major $\{38\bar{1}\bar{1}0\}$ symmetric tilt grain boundary segment.

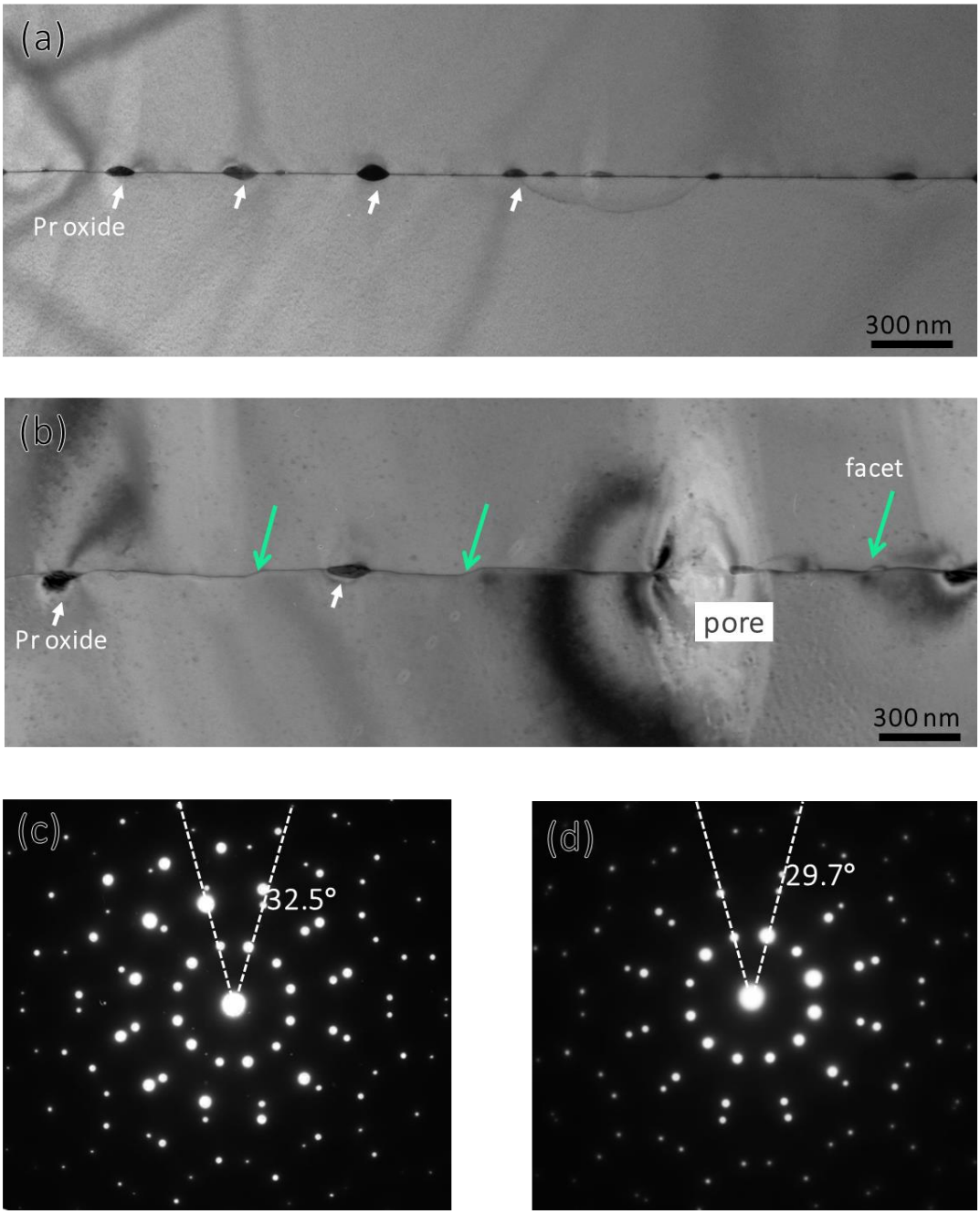

Figure 4-2. Bright-field TEM images of the Pr-doped ZnO (a) 32.2° and (b) 30.0° tilt grain boundaries. The arrows indicate the precipitations of Pr oxides and the facets in (b). Diffraction patterns taken from the boundary regions are shown inset, where the actual tilt angles are measured.

4.3.1. Atomic arrangement of Pr-doped 32.2° tilt grain boundary

Pr-doped 32.2° tilt grain boundary is first characterized. **Figure 4-3(a)** shows atomic-scale HAADF-STEM image of the 32.2° grain boundary. The boundary plane is flat in atomic scale and parallel to $(13\bar{4}0)$ of the adjacent crystals. As indicated by solid circles in the image, the grain boundary structure consists of repeating SU. Pr is visible with brighter columns in the image due to z-contrast imaging. The Pr is located at three specific atomic sites within one SU and forms triangle-like pattern.

In order to confirm stability of the grain boundary structure, atomic arrangement of the STEM image is compared with that of obtained by the first-principles calculations. As shown in **Figure 4-4(a)**, the grain boundary structure before replacing Zn with Pr, that is, the undoped case, is made beforehand. The grain boundary structure includes the SU γ which have twelve- and four-membered rings, and the SUs γ are linked with a six-membered ring that is quite similar to the bulk configuration. Thus, set of a SU γ composes a repeating period with bulk configuration (**Figure 4-4(b)**). This atomic configuration somewhat resembles that observed in the STEM image, and the columns #1, #3', and #6 as shown by the arrows roughly correspond to the location of Pr. Therefore, further structural optimization was performed after replacing Zn at these columns (#1, #3', and #6) are by Pr. The SU γ is distorted by the structural optimization; twelve-membered ring is reconstructed into six- and eight-membered rings since atomic distance between #3 and #3' became more closer due to Pr relaxation. The structure becomes even closer to that in the STEM image and the locations of Pr also agree well (**Figure 4-4(c)**).

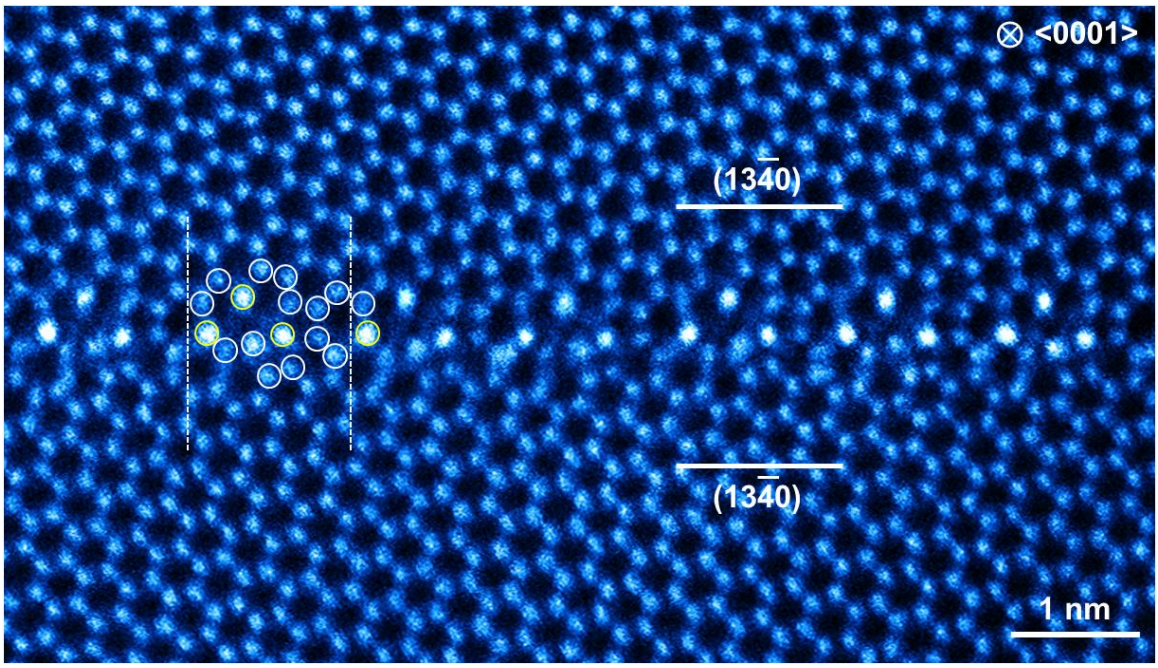

Figure 4-3 (a) HAADF-STEM image of the Pr-doped ZnO [0001] 32.2° tilt grain boundary. The boundary plane is flat in atomic scale and parallel to (13$\bar{4}$0) of the adjacent crystals. Solid circles indicate structure period that consists of SU (six- eight- and four-membered ring) and a bulk configuration (six-membered ring). Pr is visible with brighter columns in the image due to z-contrast imaging. The Pr is located at three specific atomic sites within one SU and forms triangle-like pattern.

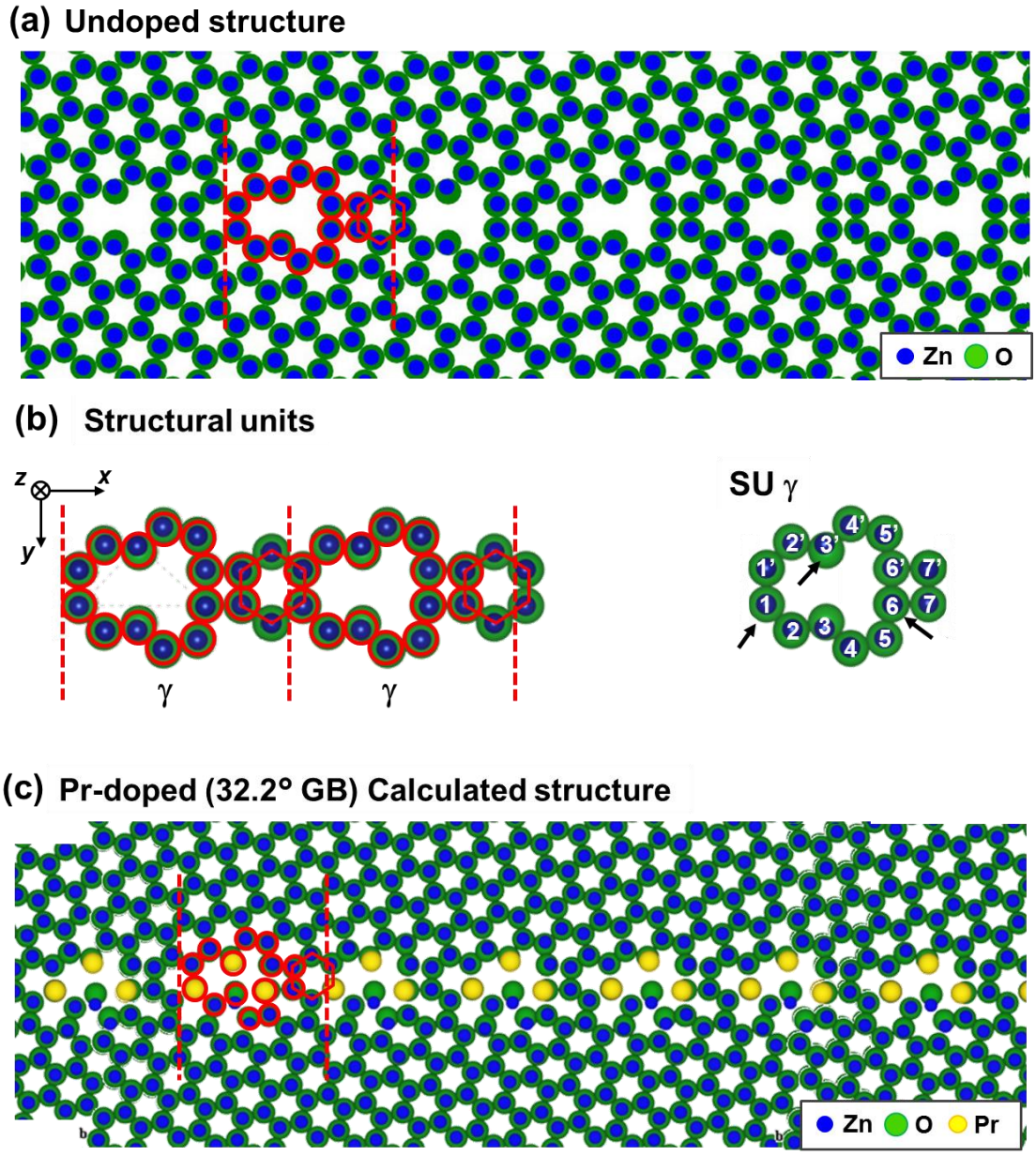

Figure 4-4 (a) A stable atomic arrangement of the undoped grain boundary obtained by the first-principles calculations. (b) The SU is formed in the grain boundary. The repeating structural period is shown on the left, and the SU γ numbered at each column is on the right. The arrows roughly correspond to the location of Pr. Since the grain boundary has the glide symmetry, the columns correlated with the symmetry operation are identified by the same numbers but differentiating by the apostrophe. The SU γ is connected by the bulk-like six-membered ring, indicated by the hexagon. (c) Stable atomic arrangement of the Pr-doped grain boundary obtained by the first-principles calculations. Set of the circles denotes the SU γ, hexagon shows a bulk configuration, and the dotted lines indicate a repeating period.

4.3.2. Segregation behavior of Pr

In order to compare the atomic structure and segregation of Pr, atomic structure of Pr-doped ZnO 27.8° tilt grain boundary is again referred (**Figure 4-5**) [6]. In the HAADF-STEM image of 27.8° tilt grain boundary, it is described by periodic arrangement of SU γ, which is also found in the current 32.2° tilt grain boundary (**Figure 4-3**). SU γ aligns zig-zag in the 27.8° case while the 32.2° case has the straight one. Pr forms triangle-like patterns within the SU γ that is similar to the 32.2° tilt grain boundary.

Pr segregation sites are compared from those Σ13 (27.8°/32.2°) grain boundaries (**Figure 4-6(a),(b)**) in more detail**.** Pr occupies the columns #2, #3' and #6 in the 27.8° tilt grain boundary, while #1, #3' and #6 in the 32.2° tilt grain boundary. This demonstrates that the location of Pr can vary with boundary planes even for the identical SUs. Zn-O bond length maps (**Figure 4-6(c),(d)**) are investigated in order to reveal the reason for this tendency.

The bond length map is obtained from undoped grain boundary models, obtained from first principles calculations. Bond lengths of four bonds of each atomic column in the boundary are estimated. Those values are averaged and compared to that of atomic column in bulk area. Difference of the averaged bond length is expressed with color distribution. Red and blue indicate longer and shorter bonds while whit indicates no difference from bulk. Therefore, Red and blue colors correspond to local tension and compression states, respectively. Here, the maps are used to discuss the local strain distribution. By the way, atomic configuration of SU γ has large open space inside of it, and there are less coordinated atomic columns (#3 and #3' in the SU γ) with dangling bonds. In order to take into account of effect of this space, Zn and O atoms at these columns were allowed to form one additional Zn-O bond between the #3 and #3' across the SU γ.

As a result, the strain is asymmetrically distributed with respect to the boundary plane in the 27.8° tilt grain boundary because the structure itself is not mirror symmetric. The columns #2, #3' and #6 possess the locally longest bond length, which agrees with the actual location of Pr [6]. On the other hand, the strain distributes symmetrically on the boundary plane in the 32.2° tilt grain boundary. This is because the grain boundary has glide symmetry on the boundary plane. Pr actually occupies three columns (#1, #3', and #6) out of six (#1, #1', #3, #3', #6, and #6') with the local highest tension.

It is speculated that once Pr occupies one site, the neighboring ions are pushed out because Pr has larger ionic radius than Zn (Pr^{3+}: 1.13 Å and Zn^{2+}: 0.74 Å [12]. For example, when Pr occupies the column #1, the neighbor column (#1') would be pushed out, reducing the local

tensile strain. The same thing may hold for the #3 and #6', which may be a reason why all the six columns are not occupied by Pr.

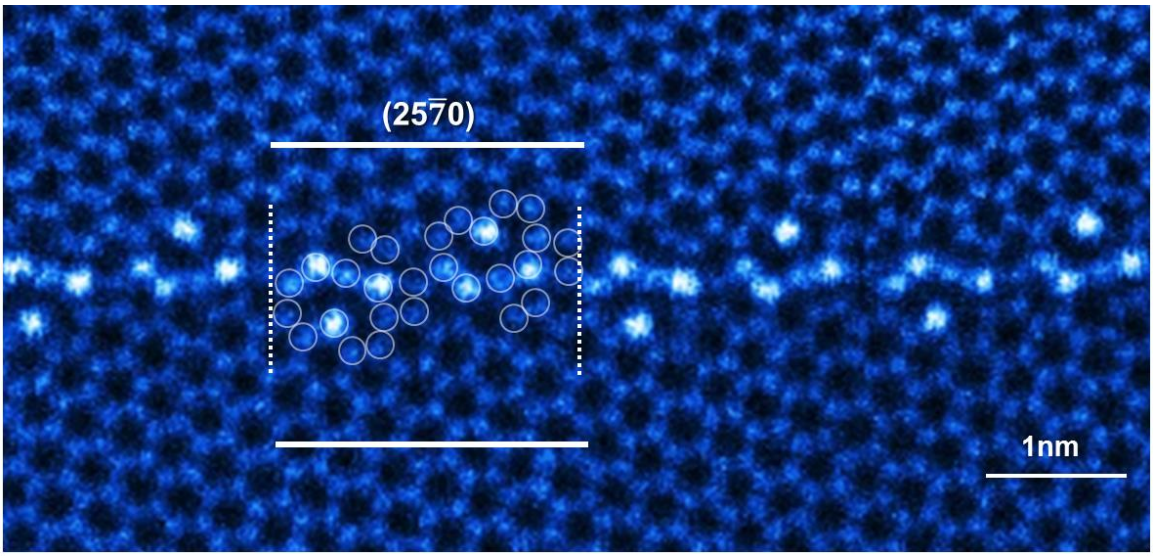

Figure 4-5. HAADF-STEM image of the Pr-doped ZnO [0001] 27.8° tilt grain boundary [6]. Boundary plane is parallel to (25$\bar{7}$0) of adjacent crystals. Structural period is indicated by solid circles that is composed of zig-zag arranged SU γ. Pr locates at specific sites within the SU γ and forms triangle patterns.

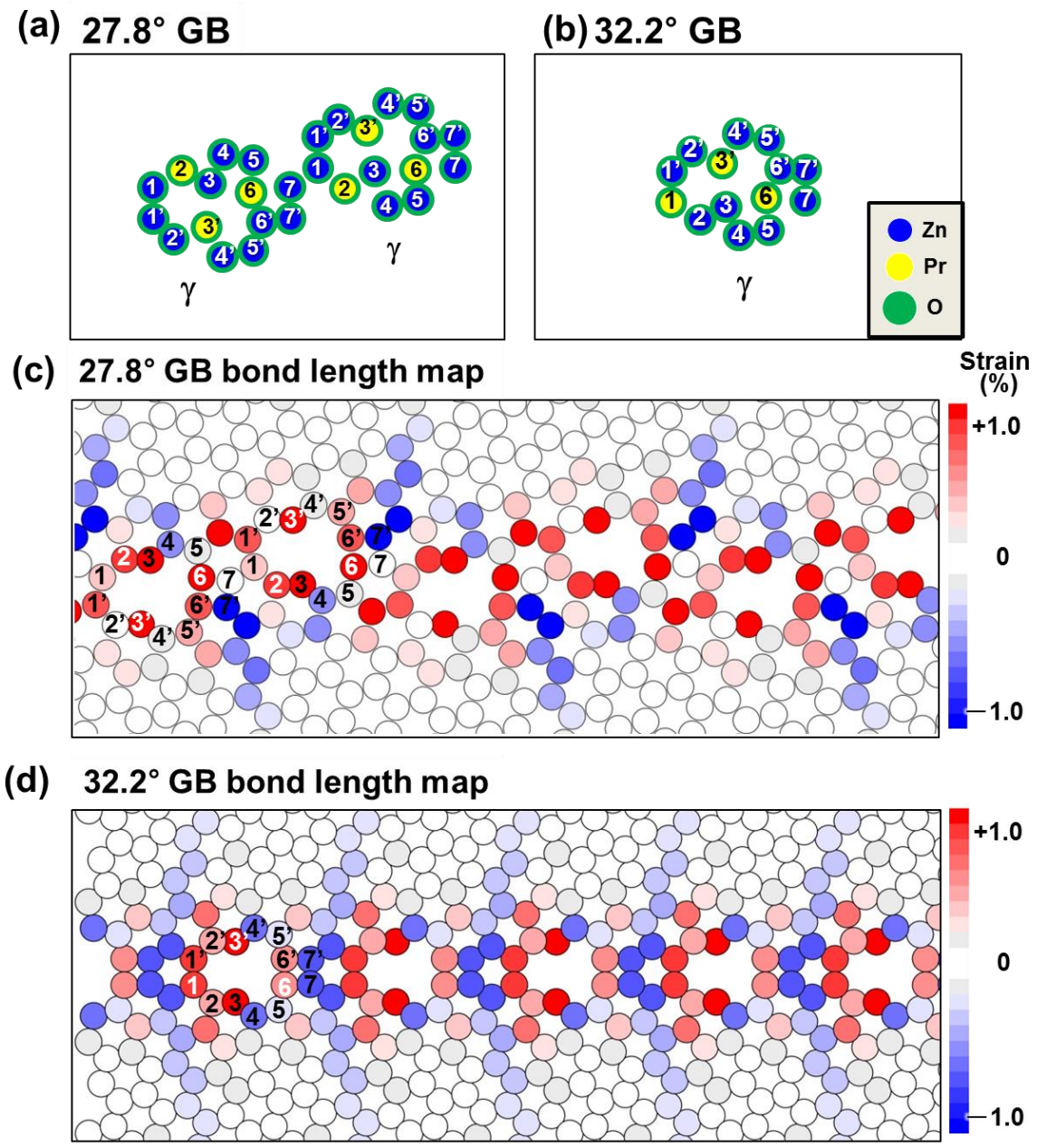

Figure 4-6. SUs of Pr-doped ZnO grain boundaries with (a) 2θ=27.8° and (b) 2θ=32.2° tilt grain boundaries. Each column is identified by the number. Since the grain boundary has the glide symmetry, the columns correlated with the symmetry operation are identified by the same numbers but differentiating by the apostrophe. Zn-O bond-length maps of (c) 27.8° and (d) 32.2° tilt grain boundaries. Structures for the undoped cases (before Pr introduction) were used for obtaining these maps. Circles indicate the atomic column, and color of the circles indicates the difference of the averaged bond length from that in ZnO bulk crystal. Red and blue represent longer and shorter bond length, respectively.

Occupation of Pr at the columns #1, #3', and #6 in the 32.2° tilt grain boundary results in triangle-like configuration of Pr (**Figure 4-3**). Observation of extensive grain boundary area reveals that this is the dominant segregation behavior and the triangular configurations all go up. This implies that there is an interaction among segregated Pr ions. Otherwise, direction of the triangles would be disordered. This point is discussed a little more. Here, the two cases where the triangles all go up ("polar-like" configuration in **Figure 4-7(a)**), and up and down alternatively ("Zig-zag" configuration in **Figure 4-7(b)**) are considered. This comparison reveals that there is a difference in the inter-atomic distances between #1'- #6 (**Figure 4-7(a)**) and #1 - #6 (**Figure 4-7(b)**). From [0001] view, inter-atomic distance between #1'-#6 looks closer than that of #1 - #6. However, the actual distance between #1 - #6 is measured to be closer (5.78 Å between #1'-#6, and 5.50Å between #1 - #5) from the boundary model. This is because Zn ions at #1 and #6 are on the same (0001) plane but those at the #1' are at different plane with the 3/8*c* height above or below. Therefore, taking the all-up configuration would reduce interaction among Pr ions.

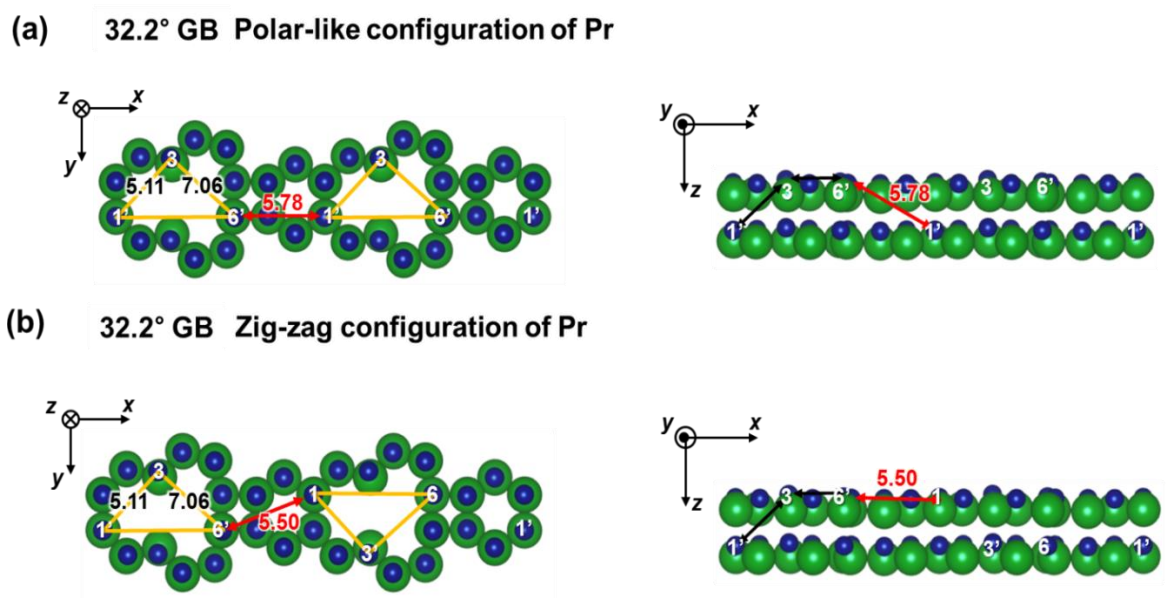

Figure 4-7. Inter-site distances for Pr with (a) the all up and (b) the up-down triangle configurations. Top views on the left and the side views on the right. The inter-site distances are shown in Å .

4.3.3. Atomic arrangement of Pr-doped 30.0° tilt grain boundary

The second bicrystals with the Pr-doped 30.0° (non-low-Σ) tilt grain boundary is observed using STEM. The grain boundary is atomically flat and the structure is nearly periodic (**Figure 4-8(a)**). As shown in the maginified HAADF-STEM image (**Figure 4-8(b)**), three SUs γ and a six-membered ring compose the repeating unit. The SUs possess at least three sites for Pr segregations forming the triangular configurations that go down, up, and up from the left to the right (**Figure 4-8(c)**). This SU configuration can be explained by the combination of 27.8°-like and the 32.2°-like SUs with the one-to-one ratio. That is, the first two SUs are of 27.8°-like segment (**Figure 4-5** [6]), and a six-membered ring and the third SU are of 32.2°-like segment (**Figure 4-3**). This would be because the 2θ of 30.0° is in between 27.8° and 32.2°.

On the other hand, locations of Pr in the SUs are not always clear in **Figure 4-8(b)**. That is, "brighter" columns with Pr and "less bright" columns without Pr are not clearly distinguished. Line profiles of column intensity can be a good way for solve this matter, however, Pr columns are not in the one-dimensional boundary plane but in the two-dimensional boundary area. Thus, the image intensities of the each column are quantitatively measured using *ImageJ* software[13] and the find peaks plug-in [14]. 433 columns are identified in **Figure 4-8(b),** and the image is reconstructed by quantified intensities, as shown in **Figure 4-9(a)**. A histogram is drawn with the number of columns respect to their column intensities (**Figure 4-9(b)**. The histogram shows nearly symmetric peak but shows a tail on the right side, while another histogram taken from the bulk part does not show such a tail (inset) (**Figure 4-9(b)**). This indicates that the tail is due to the presence of extra bright columns, that is, Pr at the grain boundary. Therefore, maximum intensity in the bulk part is used as the border to distinguish the columns with and without Pr. It is found that 31 columns in **Figure 4-8(b)** have the intensities exceeding this border value. From the brightest column, 31 columns were identified as Pr columns. Location of Pr is shown in the **Figure 4-9(c)**. In the rightmost period, Pr locates at the #2, #3', and #6 in first two SUs and #1, #3', and #6 in the third one. This can be understood as the SU characteristic for the 27.8° and the 32.2° grain boundaries. However, in the middle period, Pr additionally occupies the #1 in first two SUs, and also additionally occupies the #3 in the third SU. Further variation can be found in the leftmost period. Pr locates at #1 instead of #2 in the first SU and additionally locates at #1 in the second SU. Thus, it is again demonstrated the variable location of Pr. It is also speculated that mixed configuration of the 27.8°-like and 32.2°-like segments alters the strain distribution and subsequently the preferred location for Pr.

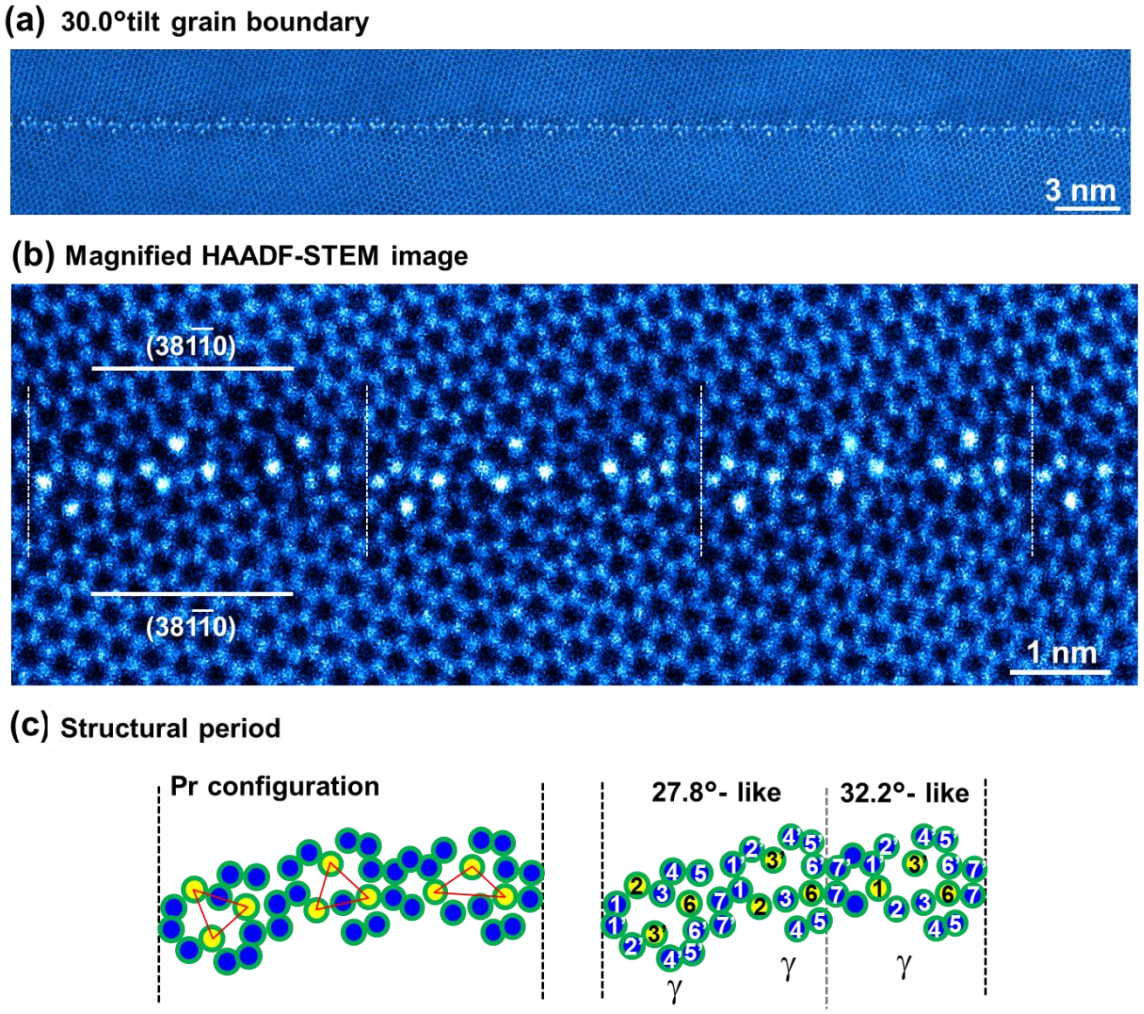

Figure 4-8. (a) HAADF-STEM image of the Pr-doped 30.0° ZnO symmetric tilt grain boundary, and (b) the magnified image. (c) SUs in repeating period of the grain boundary, which is deduced from the image in (b). Note that the left and the right halves of the period can be characterized as 27.8°–like [6] and 32.2°–like SU segment, respectively

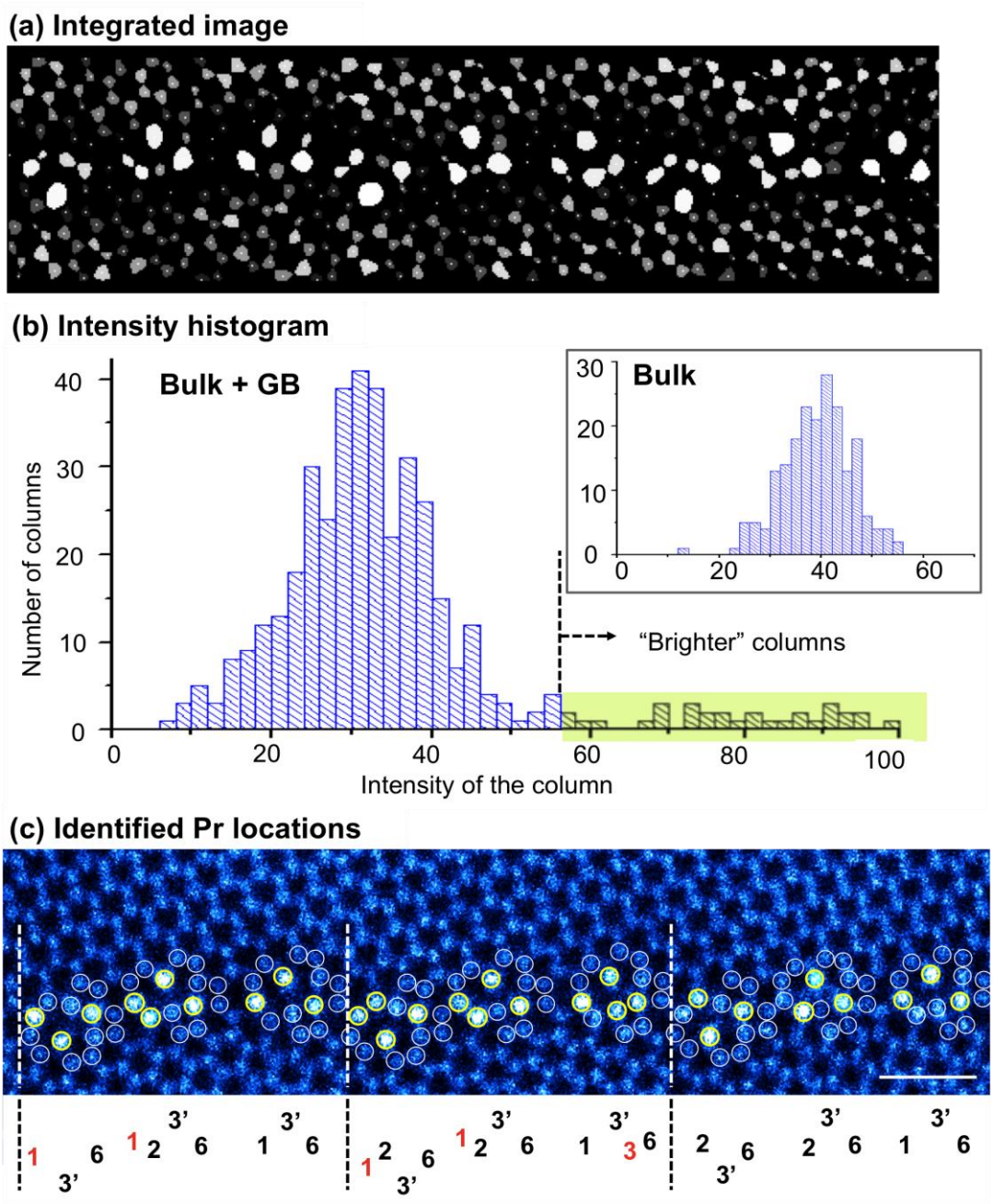

Figure 4-9. (a) Identification of atomic columns with their quantified intensity. 433 columns are identified and their intensities are quantified. Columns with higher intensity are shown by white colors. (b) Histograms of the column intensity in the image in **Figure 4-8(b)** and from bulk region (inset). Maximum intensity for the bulk region is indicated by the vertical dotted line. The columns with higher intensities than this are categorized into the columns with Pr. (c) Identification of the columns with Pr by yellow circles and number of the sites below. Locations of Pr that is not common for all repeating periods are indicated by red characters.

4.4. Conclusion

Pr-doped ZnO Σ13 (27.8°/32.2°) and 30.0° tilt grain boundaries were studied. Their atomic arrangements and segregation behavior of Pr were investigated using HAADF-STEM and bond-length mapping.

I. ZnO Σ13 (27.8°/32.2°) and 30.0° tilt grain boundaries are commonly composed of same type of SU, γ. However, the alignments of SUs are slightly different from each grain boundary.
II. Those grain boundaries have different relative location of Pr in the SU. It is considered that Pr seeks Zn sites of locally highest tension and that variation of strain distribution in the different grain boundaries would be a reason for differentiating the Pr segregation sites.
III. The atomic structure and the segregation behavior in the 30.0° tilt grain boundary case can be described as the mixed configuration of those in the 27.8° and 32.2° tilt grain boundaries. The result suggests a way to understand the SU alignment of non-low Σ CSL boundary.

4.5. Reference

[1] J.P. Buban, K. Matsunaga, J. Chen, N. Shibata, W.Y. Ching, T. Yamamoto, and Y. Ikuhara, *Science*, **313**, 212 (2006)

[2] N. Shibata, S.D. Findlay, S. Azuma, T. Mizoguchi, T. Yamamoto, and Y. Ikuhara, *Nature Mater.*, **8**, 654 (2009)

[3] Z. Wang, M. Saito, K.P. McKenna, L. Gu, S. Tsukimoto, A.L. Shluger, and Y. Ikuhara *Nature*, **479**, 380 (2011)

[4] Y. Sato, J. P. Buban, T. Mizoguchi, N. Shibata, M. Yodogawa, T. Yamamoto, and Y. Ikuhara, *Phys. Rev. Lett*., **97**, 106802-1-4 (2006)

[5] Y. Sato, T. Mizoguchi, N. Shibata, T. Yamamoto, T. Hirayama, and Y. Ikuhara, *Phys. Rev. B*, **80**, 094114 -1-7 (2009)

[6] Y. Sato, J.–Y. Roh, and Y. Ikuhara, *Phys. Rev. B*, **87**, 140101-1 (R) (2013)

[7] D.R. Clarke, *J. Am. Ceram. Soc.*, **82**, 485 (1999).

[8] K. Mukae, K. Tsuda, and I. Nagasawa, *Jpn. J. Appl. Phys.*, **16**, 1361 (1977).

[9] Y. Sato, J.P. Buban, T. Mizoguchi, N. Shibata, M. Yodogawa, T. Yamamoto, and Y. Ikuhara, *Phys. Rev. Lett*., **97**, 106802-1 (2006)

[10] S.J. Pennycook and D.E. Jesson, *Phys. Rev. Lett.*, **64**, 938 (1990).

[11] Y. Sato, F. Oba, M. Yodogawa, T. Yamamoto, and Y. Ikuhara, J. Appl. Phys., **95**, 1258 (2004)

[12] R.D. Shannon, Acta Crystallogr. Sect. A, **32**, 751 (1976)

[13] C. A. Schneider, W. S. Rasband, and K. W. Eliceiri, Nature Methods, **9**, 671 (2012).

[14] A. Herbert, ImageJ Find Peaks plug-in, University of Sussex, UK (http://www.sussex.ac.uk/gdsc/intranet/microscopy/imagej/findpeaks)

Chapter 5. Atomic structure, segregation behavior, and morphology in Pr-doped ZnO grain boundary

It is well known that grain boundary may largely affect to the various properties of a material. And those are mostly determined by local atomic structures including dislocations, defects, or segregated dopant elements. On the other hand, grain boundary atomic scale investigations have so far mostly focused on the major structures that describes the most of boundary area. However, the boundary area where we commonly look at using microscope is very small, and there could be multiple types of atomistic structure and different morphology such as facet in further boundary area. As a case study to characterize these, we have carried out extensive scanning transmission electron microscopy observations for a ZnO [0001] 27.8° tilt grain boundary doped with Pr in this paper. In addition to the major structure [1] that covers most of the $(25\bar{7}0)$ boundary area, additional structures were found; one is the secondary structure that forms in rest of the $(25\bar{7}0)$ boundary accompanied with facets formation, and the other one is step that is between the major and the secondary structures. Pr concentration is lower in the secondary structure than in the major one. Comparison to the 30.0° tilt grain boundary suggested that the secondary structure is locally preferred at the facet corners where Pr concentration is lowered. Step may lead to the structure transformation from the major structure to the secondary one by shifting boundary plane upward or downward.

5.1. Introduction

Various properties of polycrystalline material are influenced by grain boundary structures [2]~[8], thus, understanding the grain boundary nature over wide area is essential. So far, many researchers have been characterized grain boundaries using (S)TEM. However, atomic-scale analysis has been limited in small grain boundary area due to experimental difficulties. Most of the studies were simplified focusing on the major type of structure, which is believed to be the most stable and periodic. On the other hand, grain boundary actually includes not only the major atomistic structure but also metastable ones. Furthermore, the boundary plane is not completely flat in large area but could be stepped, or facetted parallel to lower energy plane [9],[10]. In recent years, stability in electron microscopy observations has been largely improved. This allows us to investigate grain boundary atomistic structure in larger area by a quantitative manner [11][12]~[13].

In this regard, wide area of the Pr-doped ZnO grain boundary area investigated in the present chapter. So far, a several STEM studies were reported on the ZnO grain boundaries doped with Pr were reported [1],[14],[15]. Comparison of atomic structures among those grain boundaries, it is founded that the Pr doping as well as increase of the tilt angle up to 27.8° for the [0001] symmetric tilt grain boundary cooperatively induce the structural transition. In detail, atomistic structures of the 16.4° and the 21.8° tilt grain boundaries were described as SUs α and/or β [14],[15], while that of the 27.8° tilt grain boundary is characterized using SU γ [1]. In addition, undoped and Pr-doped 27.8° tilt grain boundary had different atomic structures while the other cases have not. It implies that segregation of Pr induced structural transformation in the ZnO [0001] tilt grain boundaries, in conjunction with 2θ increase.

Thus, Pr-doped ZnO 27.8° tilt grain boundary has a unique structure, and its atomistic structure in the larger area should be investigated because multiple types of structure may coexist. Also, if there are multiple structures in the grain boundary, their relative stabilities need to be discussed. Accordingly, extensive atomic-scale observation for a larger area of the Pr-doped ZnO [0001] Σ13 (27.8°) grain boundary is carried out in this chapter. In addition, the detailed atomic structure is compared to that of Pr-doped 30° tilt grain boundary whose boundary condition is very close to that of 27.8° tilt grain boundary.

5.2. Method

ZnO bicrystal specimen used in previous study [1] is again investigated (**Figure 5-1**). The bicrystal was fabricated by bonding two ZnO single crystals after precisely control the crystal orientation. In the beginning, the $(25\bar{7}0)$ surface of the crystals was polished to the mirror state. Then, a thin layer of Pr metal with nominal thickness of 5 nm was deposited on the surface of one crystal. One crystal was set on the other so that the bicrystal possess [0001] 27.8° tilt grain boundary. The crystal set is heat treated at 1,100 ℃ for 10 hours in air under the uniaxial load of about 1.5 MPa for bonding. The heating and cooling rates were 300 ℃/h.

Thin foils for STEM observation were prepared by conventional methods that include mechanical polishing and Ar-ion beam milling processes. STEM observations were carried out using JEM-2100F (JEOL Ltd.) with a spherical-aberration corrector for the electron probe (CEOS Gmbh). 36 images were continuously taken along the grain boundary where each image covers about 30nm grain boundary length. Thus, atomic structure in almost 900nm length of the grain boundary is studied. The probe forming aperture semiangle was 22 mrad. BF and ADF STEM images were acquired with the detection angle ranges of about 0 ~ 13 mrad. and about 100 ~ 230 mrad., respectively. In order to measure the Pr composition, energy dispersive spectroscopy (EDS) analysis was performed using the EDS system and software attached to the JEM-2100F microscope. Electron was scanned over 2 x 1 nm^2 boxes. using the EDS system and software attached to the JEM-2100F microscope.

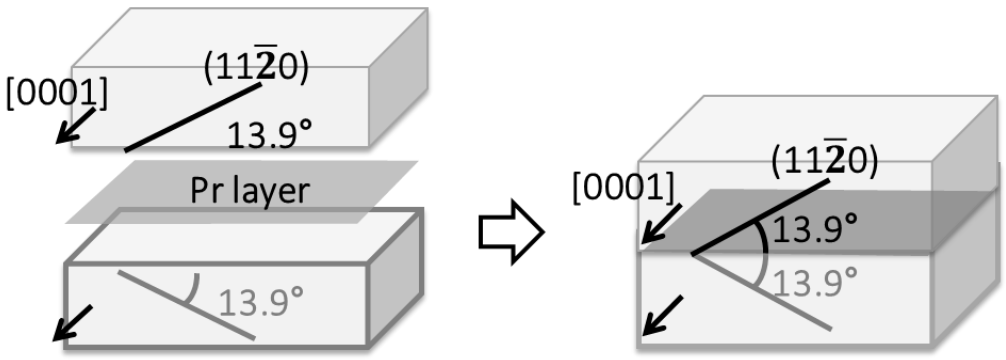

Figure 5-1. Schematic of ZnO bicrystals studied the current chapter. The 2θ is intended to be 27.8°of the adjacent crystals in order to obtain Σ13 grain boundary.

5.3. Results and discussion

5.3.1. Atomic arrangement of Pr-doped ZnO 27.8° tilt grain boundary

It has been confirmed that the two crystals are directly bonded at the grain boundary (**Figure 5-2(a)**). The boundary plane is almost flat, however it is locally facetted. The tilt angle was identified to be about 27.8° from selected area diffraction pattern, which is quite close to the ideal value for Σ13 orientation relation in the CSL theory.

The grain boundary has been further characterized at higher magnification (**Figure 5-2(b)**). Since contrast of ADF STEM image depends on the atomic number (*Z*) of the constituting elements, Pr (*Z* = 59) looks brighter than Zn (*Z* = 30) does, and therefore the brightest spots indicate the presence of Pr. Grain boundary segments can be recognized by the boundary plane orientation and the Pr segregation pattern. Continuous Pr segregation pattern with the brightest contrast is observed as shown (I) (**Figure 5-2(b)**) at the flat $(25\bar{7}0)$ boundary area. Quantitative analysis over ~635nm of grain boundary has carried out and this segment (I) covered roughly 77 % of the $(25\bar{7}0)$ boundary area. Thus, it is designated as major structure hereafter.

Another segment (II) (**Figure 5-2(b)**) is found in the rest of the $(25\bar{7}0)$ boundary area, which will be called secondary structure. Pr segregation pattern with less bright contrast is seen.. Also, there are facets ((II) in **Figure 5-2(b)**) that are almost parallel to $(10\bar{1}0)$ and $(11\bar{2}0)$ of the adjacent crystals. The formation of the facet is considered to be due to low energy for the specific facet inclination. Interesting tendency was found that the secondary structure mostly forms near facets.

Detailed atomistic structure of major and the secondary structures can be shown in **Figure 5-3**. The major structure is described by the repetition of SUs γ (**Figure 5-3(a)**) as it was reported [1]. On the other hand, the secondary structure is described as the SU alignment of β-α α (**Figure 5-3(b)**) which is similar to that of the undoped case [1]. Since contrast for Pr-containing columns seems less bright as compared with the major structure case, occupancy of Pr in these columns would be lower. Relative location of Pr within the SUs α and β is similar to those in the 16.4° and the 21.8° tilt grain boundary cases [14][15].

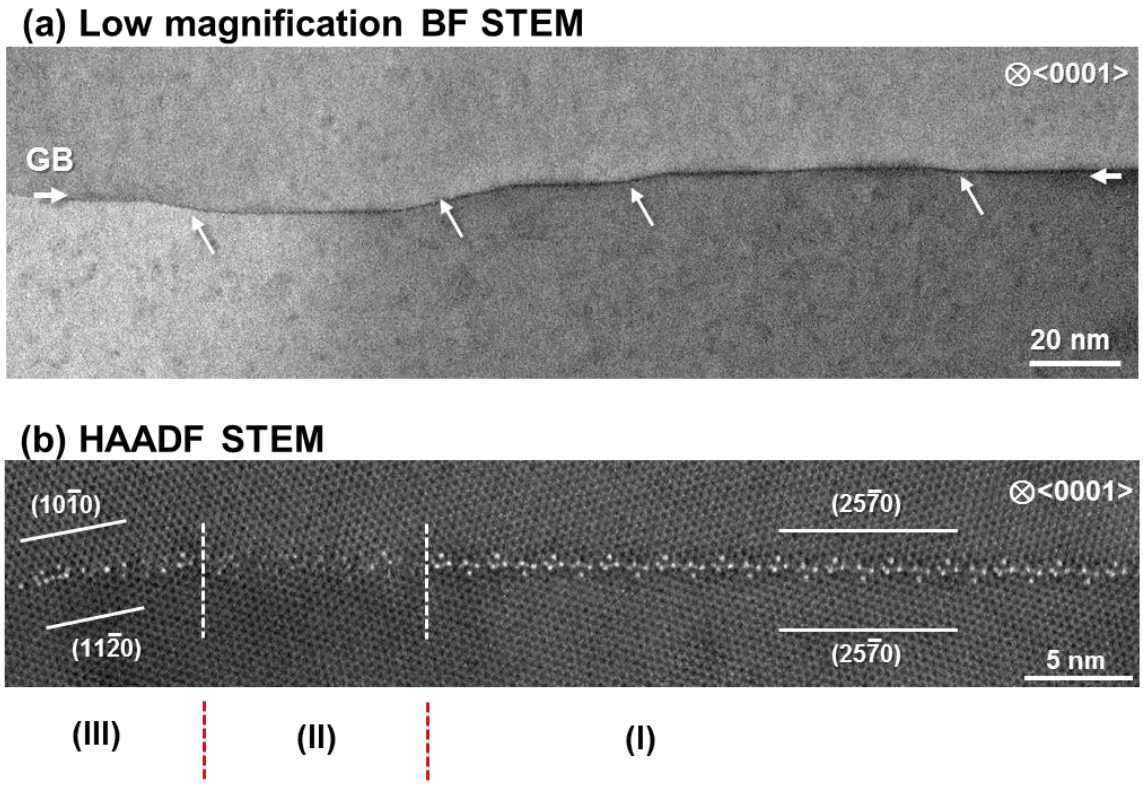

Figure 5-2. (a) Low-magnification BF STEM image of the Pr-doped 27.8° tilt grain boundary. Arrows indicate locally facetted region. (b) Higher-magnification ADF STEM image of the grain boundary. There are three different segments in the image; (I) major structure in the (25$\bar{7}$0) grain boundary; (II) secondary structure in the (25$\bar{7}$0) grain boundary; and (III) facet that is almost parallel to (10$\bar{1}$0) and (11$\bar{2}$0) of adjacent crystals.

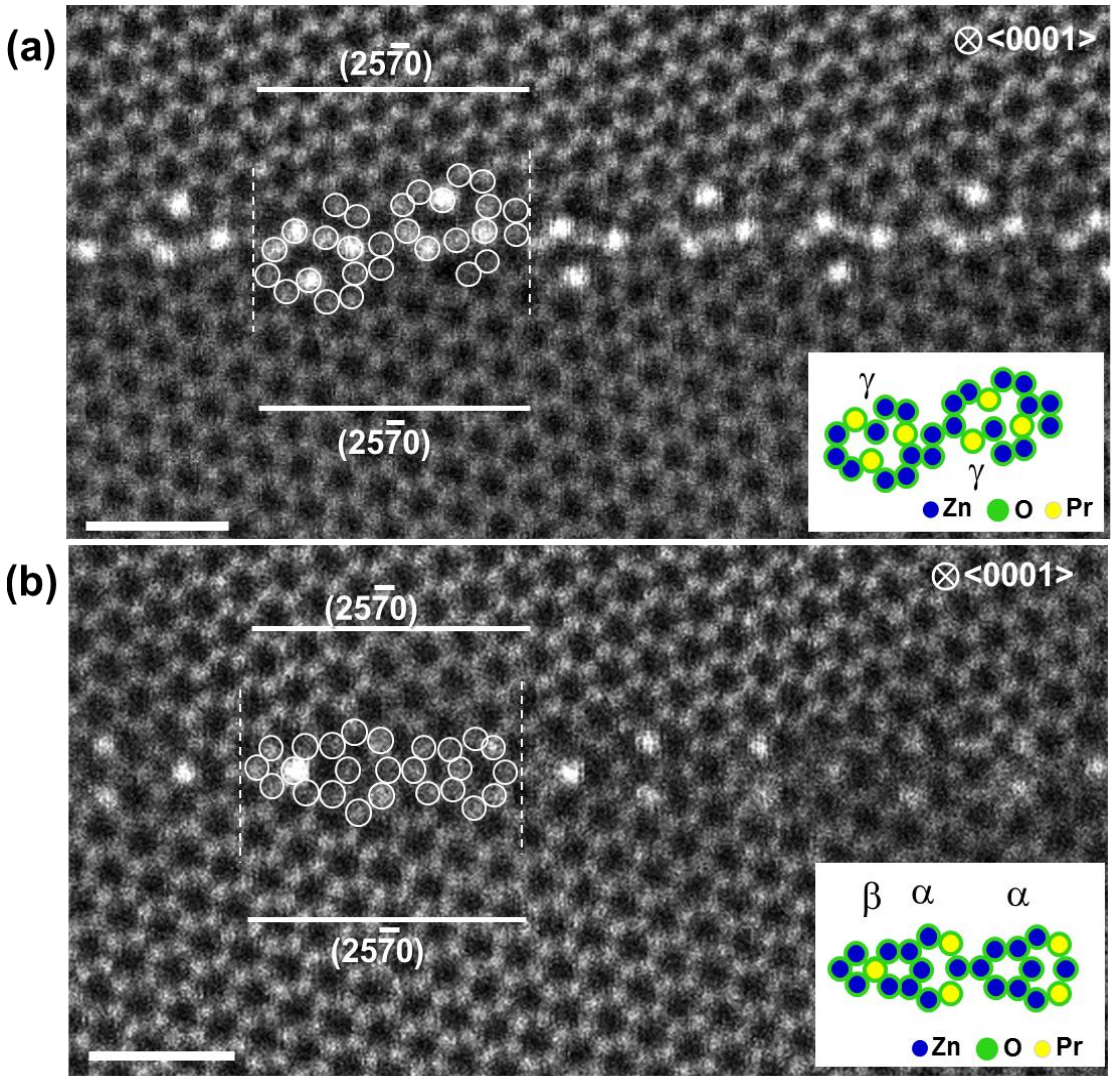

Figure 5-3. HAADF-STEM images of (a) major and (b) secondary structures in the in the symmetric boundary region. Boundary plane is parallel to (25$\bar{7}$0) of the adjacent crystals. Set of circles indicates the alignment of SUs in a boundary period, which is shown by dotted lines. The respective SUs of structures is highlighted in the inset that is containing SU models, α, β, and γ.

In addition to SU descriptions, grain boundary structures have been analyzed by using circuit mapping formalism [17]~[20] in order to understand their dislocation like character. Interface structure including any kinds of defects can be characterized as dislocation like feature with this formalism, which has been already demonstrated in undoped ZnO case, in chapter 3.

First, primary dislocation of the major and the secondary structure is determined. For doing that, circuits (S_1-X-F_1 in the major structure, and S_2-X-F_2 in the secondary one) are drawn around a grain boundary period, and then circuits with identical components are mapped into grain interior (**Figure 5-4**). Then, closure failures of the circuits, where vectors from the finishing to the starting points (F_1-S_1 in the major structure, and F_2-S_2 in the secondary one) correspond to dislocation content of the boundary periods. Here, both of the structures exhibit the failures with $-3a_1 = [1\bar{2}10]_\lambda$, which is the content of primary dislocations for these structures. Here, a_1 is one of the translation vector in the Wurtzite [0001] lattices.

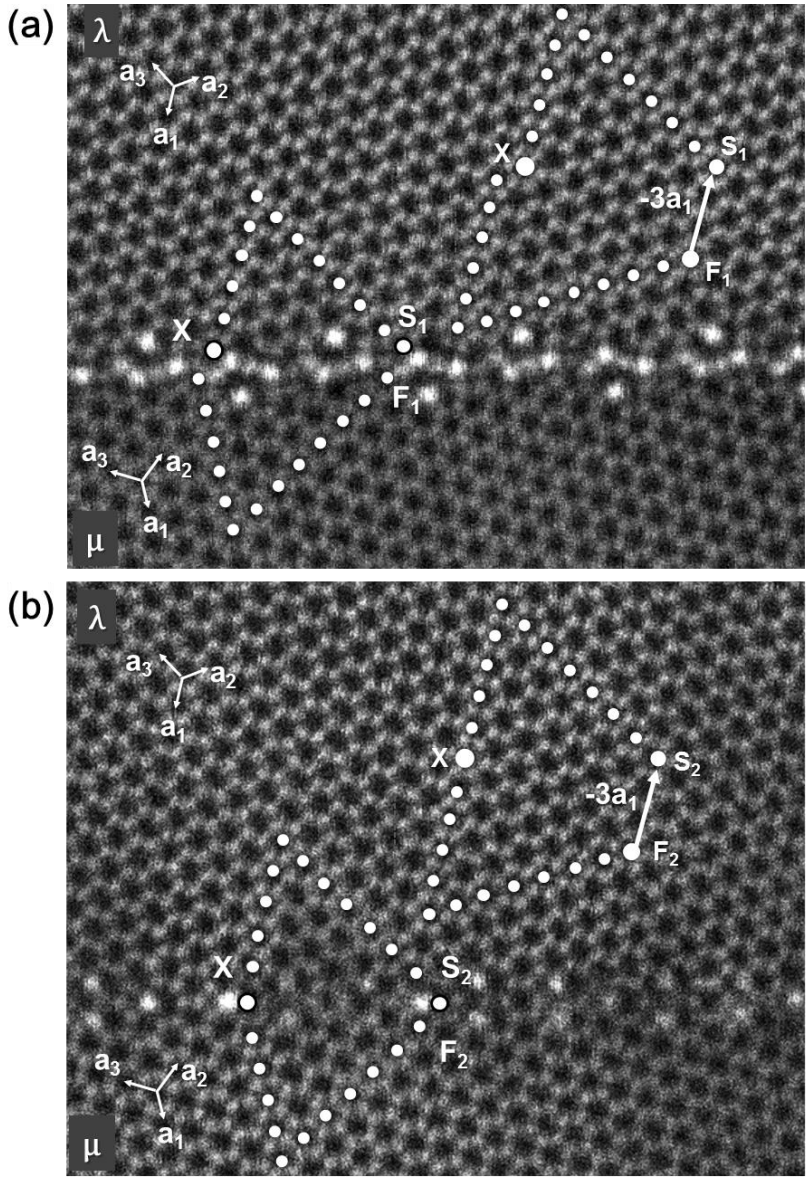

Figure 5-4. Circuit mapping analysis for (a) major and (b) secondary structures. ***a*** is the elemental lattice vectors for the upper (λ) and the lower (μ) crystals. Circuits (S_1-X-F_1 and S_2-X-F_2) for a boundary period are drawn in the grain boundary and bulk regions. Mapping on the bulk region reveals primary dislocation of both the major and the secondary structure as $\boldsymbol{b} = -3\boldsymbol{a}_1 = [1\bar{2}10]_\lambda$, $|\boldsymbol{b}| = 3\boldsymbol{a}$.

Vitek *et al*. [21] reported that structure transformation in the grain boundary can be regarded as produced by gliding a partial DSC dislocation. This might be come from presence of vacancies, segregated impurities and possibly other defects may lead local transformation of the boundary structure into another energetically more favorable configuration. Thus, there should be step in between the major structure and the secondary structure that leads to the displacement of the boundary plane upwards or downward. It is experimentally found that there is a step in between major and the secondary structures (**Figure 5-5(a)**). In order to understand the step character, circuit mapping formalism is again used. In order to analyze the step, a circuit (S_3XF_3) to surround a step is drawn on the image. Next, a circuit with identical translation component is mapped into a dichromatic complex for the Σ13 CSL (**Figure 5-5(b)**). Then, the circuit exhibits closure failure as indicated by arrow in **Figure 5-5(b)**, which is the secondary dislocation character.

The Burgers vector ***b*** of this secondary dislocation can be understood as the difference between the translation vectors for the upper (t(λ)) and the lower (t(μ)) crystals, which can be known by mapping circuits S_3-X and X-F_3 on the dichromatic complex (**Figure 5-6(b)**). The translation vectors can be estimated to be $t(\lambda) = -2\boldsymbol{a}_2 = 2/3[\bar{1}2\bar{1}0]_\lambda$, $t(\mu) = \boldsymbol{a}_3 - \boldsymbol{a}_2 = 1/3[0\bar{3}30]_\mu = [0\bar{1}10]_\mu$. When the t(μ) is re-expressed on the t(λ), the burgers vector can be revealed as $\boldsymbol{b} = 1/39[5\bar{7}20]_\lambda$. It should be also noted that the Burgers vector is identical to that expected for displacement shift complete (DSC) dislocation (**Figure 5-6(c)**).

Step height can be also estimated by h(λ) = -n•c(μ) and h(μ) = -n•c(λ), where n is the unit vector normal to the boundary plane. These heights are quantified in units of *d*(*hkil*), which is the interplanar spacing of the lattice planes parallel to the boundary. As a result, h(λ) and h(μ) were estimated to be -4, and $-3d(25\bar{7}0)$. Thus, the results demonstrate the major and the metastable structures are at the different grain boundary height with the step element in between. Detailed results of the circuit mapping analysis are summarized in **Table 5-1**.

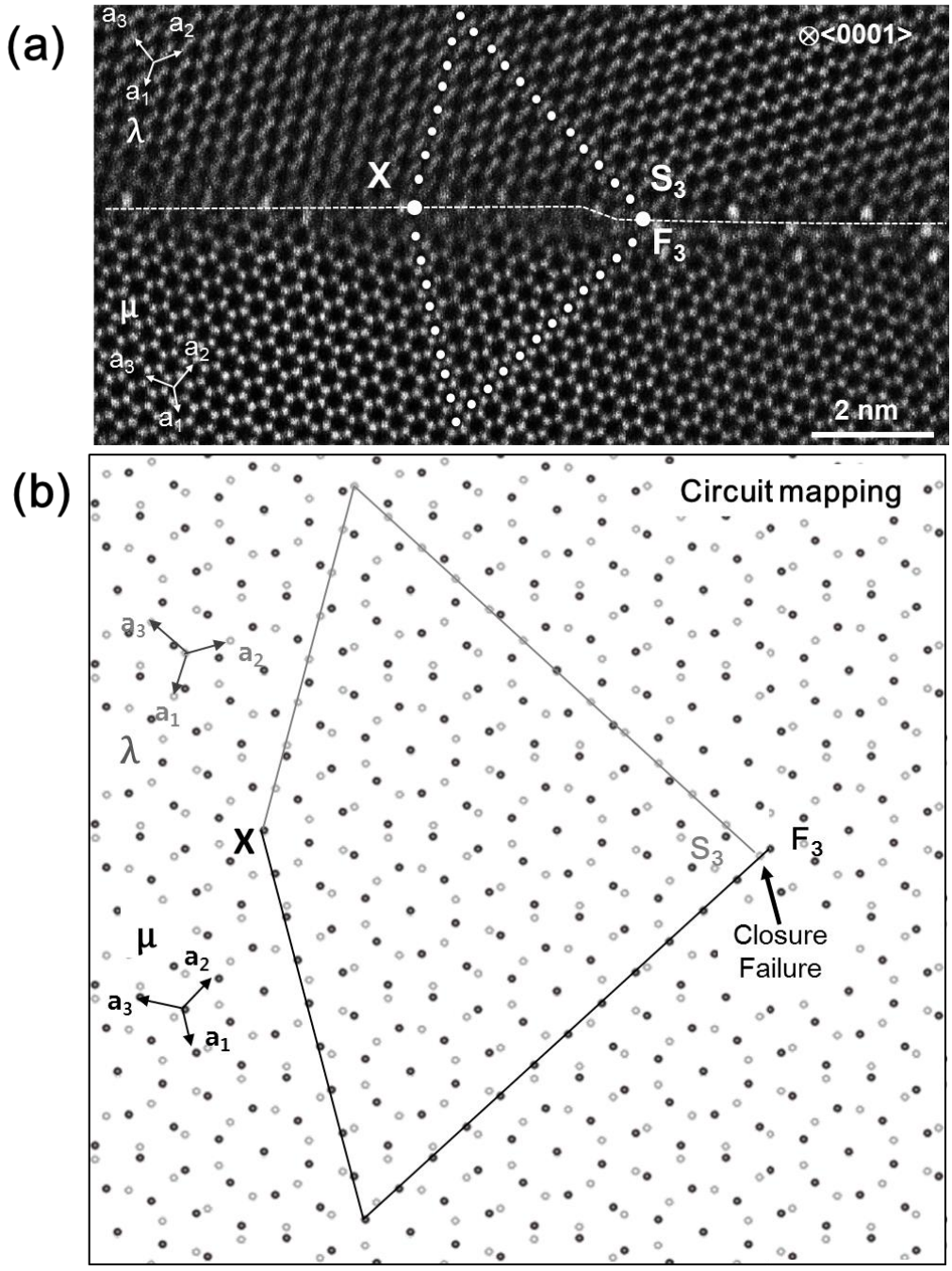

Figure 5-5. HAADF-STEM image including the secondary structure, step, and the major structure from left to right side of the boundary area. Boundary plane is indicated by a dotted line. Circuit S_3XF_3 (described by connecting half circuit S_3X for λ crystal $=12\boldsymbol{a}_3+8\boldsymbol{a}_1$, and the opposite circuit XF_3 for μ crystal $=9\boldsymbol{a}_1+12\boldsymbol{a}_2$) is drawn including the step structure. (a) Same circuit (S_3XF_3), directly mapped on the dichromatic complex. Arrow indicates closure failure of the circuit.

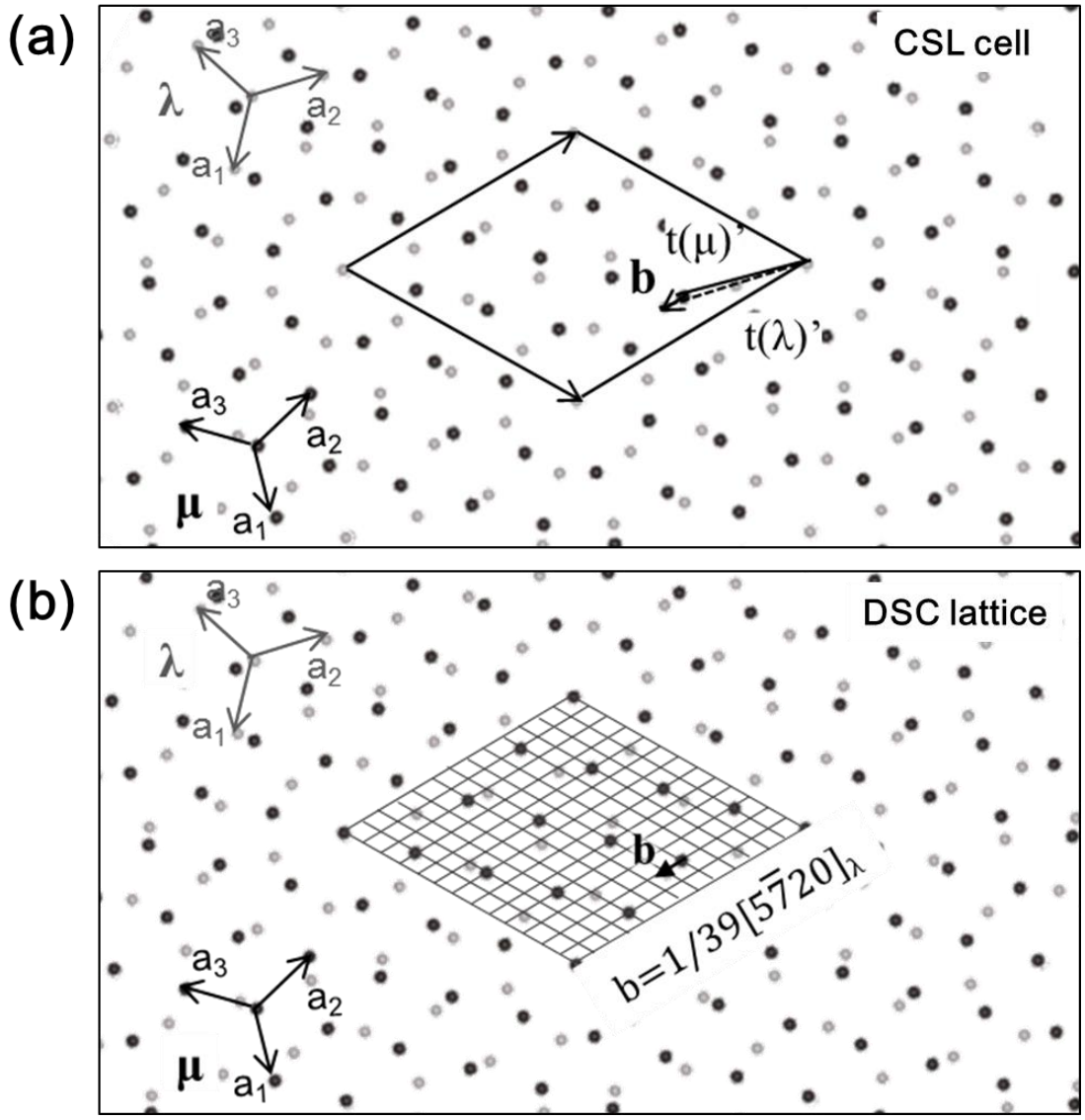

Figure 5-7. (a) Dichromatic complex with a CSL lattice. Translation vectors of circuit are shown by t(λ) and t(μ), and **b** indicates the Burgers vector of the secondary dislocation included in the circuit S_3XF_3. (b) The same pattern with DSC lattice.

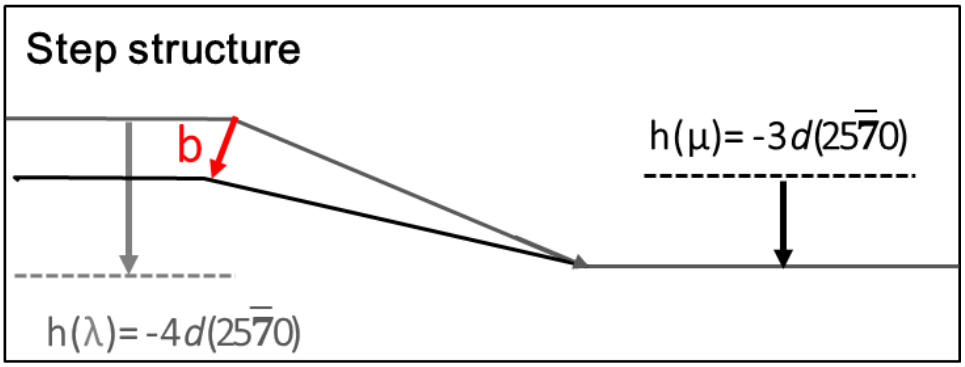

Figure 5-7. Schematic illustration of the step structure, shown in **Figure 5-6.** h(λ) and h(μ) represent the step height for the upper and the lower crystals that correspond to four and three inter planner spacing of (25$\bar{7}$0) boundary, respectively.

Table 5-1. Details for the circuit mapping analysis of a step in the **Figure 5-6.** c(λ) and c(μ) denote the vectors S_3-X in the upper and X-F_3 in the lower crystals, and c(λ, μ) denotes the vector S_3-F_3. h(λ) and h(μ) denote the step height, n is the unit vector normal to the boundary plane, b is the Burgers vector of secondary dislocation, and P_{13} [22] refers a 4x4 matrix that re-expresses the vectors in the lower crystal (μ) into those in the upper crystal (λ).

Upper crystal (λ)	Lower crystal (μ)	Secondary dislocation
c(λ) = 1/3[4$\bar{\mathbf{2}}\mathbf{0}$160]$_λ$	c(μ) = [25$\bar{7}$0]$_μ$	
h(λ) = -**n**•c(λ) = -4 •*d*(25$\bar{7}$0)	h(μ) = **n**•c(μ) = -3•*d*(25$\bar{7}$0)	**b** = - c(λ, μ) = c(λ) - P_{13}c(μ) = 1/39[5$\bar{7}$20]$_λ$
t(λ) = -2a_2 = 2/3[$\bar{\mathbf{1}}$2$\bar{\mathbf{1}}$0]$_λ$	t(μ) = a_3 - a_2= 1/3[0$\bar{3}$30]$_μ$ = [0$\bar{1}$10]$_μ$	t(λ) - P_{13} t(μ) = 1/39[5$\bar{7}$20]$_λ$

$$\mathbf{P}_{13}=\frac{1}{13}\begin{bmatrix}12 & \bar{3} & 4 & 0\\ 4 & 12 & \bar{3} & 0\\ \bar{3} & 4 & 12 & 0\\ 0 & 0 & 0 & 13\end{bmatrix}$$

5.3.2. Analysis of grain boundary facets

A different type of atomic configuration is found in facets (Figure 5-9(a)). There are wide open spaces in the middle, and there are several four-membered rings. Most of Pr are present at the corner of the four-membered rings that face the open spaces (inset). It should be noted here that $\{10\bar{1}0\}$ and $\{11\bar{2}0\}$ of the adjacent crystals are not actually parallel but 2.2° of misfit angle deviates. And the secondary structure is locally formed at the facet corner. In order to understand the effect of the angle deviation to formation of secondary structure, facet structure in the 30° tilt grain boundary is investigated. The major structure of the 30° tilt grain boundary is already reported in the Chaper.4.3.3; however, facet structure has not been discussed.

Figure 5-9(b) shows the detailed facet structure found in the 30° tilt grain boundary. The boundary plane is parallel to $\{10\bar{1}0\}//\{11\bar{2}0\}$, and the area of facet is more larger than 27.8° tilt grain boundary. Atomic configuration in the facet shown in **Figure.5-9(b)** also forms open spaces in the middle, with several four-membered rings outside. Most of Pr present at the corner of the four-membered rings that face the open spaces. However, there is one big difference between the 27.8° tilt and 30.0° tilt grain boundaries. That is the presence of the secondary structure. No secondary structure was found in the 30.0° tilt grain boundaries, but there is only SU γ, which is the major structure for this boundary (Chaper.4.3.3).

Here, let me suggests the formation of secondary structure in 27.8° tilt boundary. The boundary tends to facetted along $\{10\bar{1}0\}$ and $\{11\bar{2}0\}$. Considering the crystals geometry, there may be compressive or tensile strain near the facet structure due to lattice mismatch. Thus, it is considered that the facetted structure attracts the segregation of Pr into its large open space so that release the residual strain. Thus, it is suggested that formation of secondary structure would be preferred when the segregation of Pr is locally depleted.

EDS spectra were measured (**Figure 5-10**) in order to compare the Pr concentration in major and secondary structures, and facet. Zn-K, Zn-L, O-K, and Pr-L lines are detected in all the cases. Eleven spectra were used to quantify the Pr concentration for each case (**Table 5-2**). Average Pr concentration and standard error in cation % were estimated to be 9.5 (± 0.3), 5.1 (± 0.2), and 7.1 (± 0.3) in major and secondary structures and facet, indicating that the secondary structure has relatively low Pr concentration.

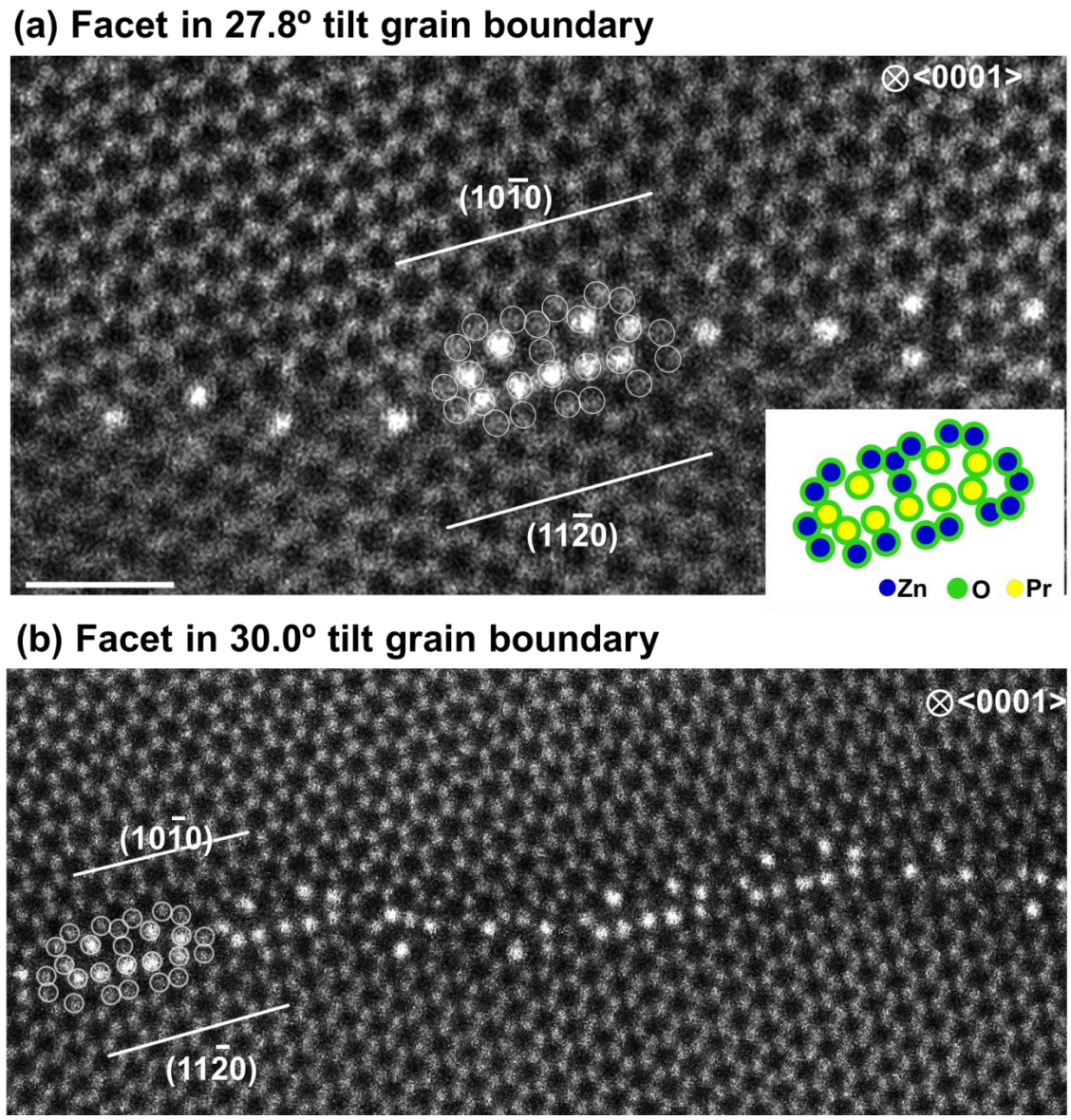

Figure 5-9. HAADF-STEM images of facets in (a) Pr-doped ZnO 27.8° tilt grain boundary and (b) 30.0° tilt grain boundary. The facets have similar atomic configuration for both grain boundaries; as well as Pr segregation sites. Secondary structure (SU a (and/or) b) is formed at the facet corner in 27.8° tilt grain boundary, however, it is not applicable to 30.0° tilt grain boundary.

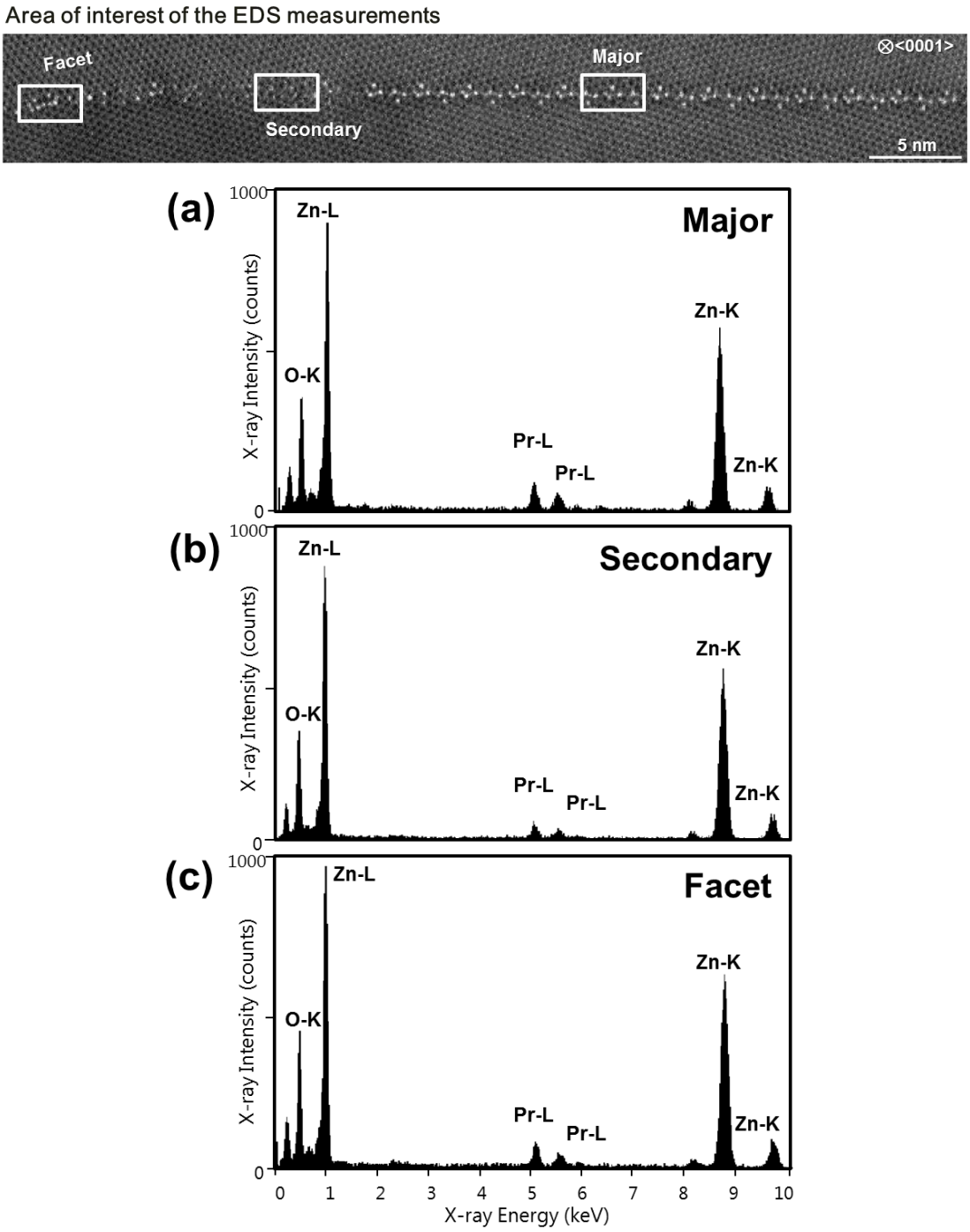

Figure 5-10. EDS spectra taken from (a) major and (b) secondary structures and (c) facet in order to compare the Pr concentration in major and secondary structures, and facet. Zn-K, Zn-L, O-K, and Pr-L lines are detected in all the cases. Electron beam was scanned over a 1 nm (in grain boundary normal direction) x 2 nm (in grain boundary parallel direction) square box during the measurements. Peaks at ~ 8.05 keV are artifacts from the TEM specimen holder.

Table 5-2. Average Pr concentration and standard error in cation % in (a) the major, (b) the se condary structure and (c) facet.

Remark	**Structure**	**Pr (at%)**
(a)	Major	9.5 (± 0.3)
(b)	Secondary	5.1 (± 0.2)
(c)	Facet	7.1 (± 0.3)

Relationship among atomistic structure, Pr concentration, and morphology of the 27.8° tilt grain boundary is schematically shown in **Figure 5-11.** Grain boundary is mostly composed of the flat $(25\bar{7}0)$ boundary area and partly of facets that are almost parallel to $\{10\bar{1}0\}$ and $\{11\bar{2}0\}$ of the adjacent crystals. Major structure with SU γ appears in the most of $(25\bar{7}0)$ boundary area while the secondary structure with SUs α and β appears in the rest of the area, mostly near facets. There is a step in between the major and the secondary structures. The step is characterized as secondary dislocation with the Burgers vector of $1/39[5\bar{7}20]$, and the height of the step is estimated. Formation of step rearranges the boundary plane hence the major structure transforms into the secondary one, or, vice versa.

There is strain field near facets to enhance Pr segregation. And the secondary structure is locally preferred near the facet, where Pr concentration is lowered. Thus, it is considered that segregation at the grain boundary affects to the local atomic arrangements.

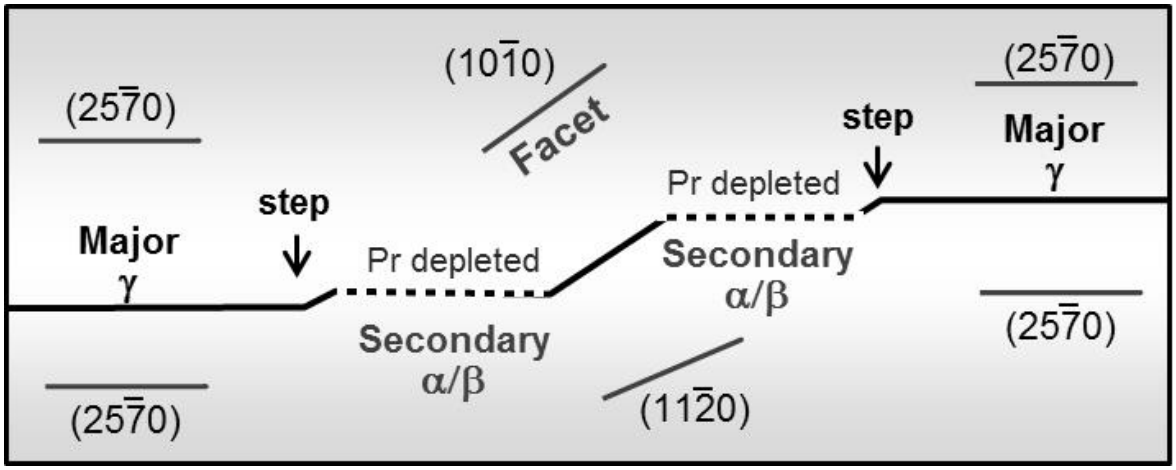

Figure 5-11. Relationship among the atomic structures, Pr concentration, and different grain boundary morphology in the 27.8° tilt grain boundary.

5.4. Conclusion

Extensive STEM observations were carried out for a larger area in Pr-doped ZnO [0001] 27.8° (Σ13) tilt grain boundary in quantitative manner. Relation among atomistic structure, segregation behavior of Pr, and morphology has been studied.

I. The boundary is comprised by several local segments; the major, the secondary, and facet structures. The boundary is decomposed by symmetric $\{25\bar{7}0\}$ and facets that are almost parallel to $\{10\bar{1}0\}$ and $\{11\bar{2}0\}$ of the adjacent crystals.
II. Small fraction of the secondary structure forms near facet corners with depleted Pr concentration.
III. Atomic configuration of the secondary structure is similar to that of undoped grain boundary. Lowered Pr concentration at facet corner may induce formation of secondary structure that is close to the undoped case.

5.5. Reference

[1] Y. Sato, J. –Y. Roh, and Y. Ikuhara, *Phys. Rev. B*, 87, 140101-1-4 (R) (2013)

[2] A.T. Paxton and M.W. Finnis, eds., *J. Mater. Sci*., **40**, 3045-3321 (2005)

[3] T. Sakuma, L. Shepard, and Y. Ikuhara, eds., *Ceram. Trans*., **118**, 427-444 (2000)

[4] C. Elsässer, A. H. Heuer, M. Rühle, and S. M. Wiederhorn, eds., *J. Am. Ceram. Soc.*, **86**, 533-700 (2003)

[5] Y. Ikuhara, *J. Ceram. Soc. Jpn*., **109**, S110-120 (2001)

[6] J. P. Buban, K. Matsunaga, J. Chen, N. Shibata, W.Y. Ching, T. Yamamoto, and Y. Ikuhara, *Science*, **313**, 212-215 (2006)

[7] Z. Zhang, W. Sigle, and M. Rühle, *Phys. Rev. B.*, **66**, 094108-1-8 (2002)

[8] N.D. Browning, J. P. Buban, P. D. Nellist, D.P. Norton, M.F. Chisholm, and S.J. Pennycook, *Physica C*, **294**, 183-193 (1998)

[9] U. Wolf, F.Ernst, T. Muschik, M.W. Finnis, and H.F. Fischmeister, *Phil. Mag. A*, 66, 991-1016 (1992)

[10] A.P. Sutton, and V.Vitek, *Phil. Trans. R. Soc. Lond. A*, **309**, 37-54 (1983)

[11] H. Yang, H.S. Lee, M.C. Sarahan, Y. Sato, M. Chi, P. Moeck, Y. Ikuhara, and N.D. Browning, *Phil. Mag*,.93, 1219-1229 (2013)

[12] S. Nufer, A.G. Marinopoulos, T. Gemming, C. Elsasser, W. Kurtz, S. Kostlmeier, and M. Ruhle, Phys. Rev. Lettl, **86**, 5066 (2001)

[13] S. Azuma, N. Shibata, S.D. Findlay, T. Mizoguchi, T. Yamamoto, and Y. Ikuhara, Phil. Mag. Lett., **90**, 539 (2010)

[14] Y. Sato, J. P. Buban, T. Mizoguchi, N. Shibata, M. Yodogawa, T. Yamamoto, and Y. Ikuhara, *Phys. Rev. Lett*., **97**, 106802-1-4 (2006)

[15] Y. Sato, T. Mizoguchi, N. Shibata, T. Yamamoto, T. Hirayama, and Y. Ikuhara, *Phys. Rev. B*, **80**, 094114 -1-7 (2009)

[16] P. Ruterana, M. Abouzaid, A. Bere, and J. Chen, J. Appl. Phys., **103**, 033501-1 (2008)

[17] J.-Y. Roh , Y. Sato, and Y. Ikuhara, J. Am. Ceram. Soc., **97**, 617 (2013)

[18] A. Kiselev, F. Sarrazit, E. Stepantsov, E. Olsson, T. Claeson, V. Bondarenko, R. Pond and N. Kiselev, Phil. Mag. A, **76,** 633 (1997)

[19] F. Sarrazit, R. Pond, and N. Kiselev, Phil. Mag. Lett., **77**, 191 (1998)

[20] V. Potin, P. Ruterana, G. Nouet, R.C. Pond, and H. Morkoç, Phys. Rev. B, **61**, 5587 (2000)

[21] V. Vitek, Y. Minonishi, and G. J. Wang, J. Phys. Colloques, **46**, 171 (1985)

[22] P. E. Blöchl, Phys. Rev. B, **50**, 17593 (1994)

Chapter 6. Relationship between structure unit and 2θ

Atomistic arrangements for the Pr-doped ZnO grain boundaries with 2θ = 16.4° (Σ49)[1], 21.8° (Σ7)[9], 27.8° (Σ13)[10], 30.0°, 32.2° (Σ13) have been in detail studied. From these results, it is possible to get an idea about relation between the structure (SU) and 2θ in Pr-doped ZnO [0001] symmetric tilt grain boundaries. Grain boundaries with 2θ = 16.4° (Σ49) and 21.8° (Σ7) are described by SUs α and/or β, while the grain boundaries with 2θ = 27.8° (Σ13), 30.0°, and 32.2° (Σ13) are described by SU γ. Further grain boundaries have been fabricated with 2θ =25.8°, 38.2° (Σ7), and 43.6° (Σ49) to reveal 2θ dependent atomic arrangements. Observation result revealed that SU transforms into γ when 2θ is close to 30.0°. Also, SUs coexist in the boundary, whose 2θ is at structure transition state. Prediction of atomic arrangement and Pr-segregation in the Pr-doped ZnO [0001] symmetric tilt grain boundaries in the overall 2θ range ($0° \leq 2\theta \leq 60°$) can be suggested.

6.1. Introduction

It has been emphasized many times that understanding grain boundary structure is essential in order to reveal structure – material property relations. However, it is practically impossible to observe all those grain boundaries in polycrystalline material since there is huge number of grain boundaries with different orientations. Thus, we need to approach to the general grain boundaries in more realistic way, for example, fix the geometric parameters and controls only one or two of them, such as, tilt angle (2θ). For examples, Oba *et al*.[11] fabricated fiber-textured thin film of ZnO on the quartz-glass substrates so that many of the grain boundaries have near [0001] tilt type. Similarly, Potin *et al.* [12] and Chen *et al.* [13],[14] have conducted an extensive HRTEM study of [0001] grain boundaries in GaN films, and systematically discussed the atomic structure in comparison with that of edge dislocations. Shibata *et al.* [15] carried out an extensive HRTEM experiments in conjunction with energy calculation. Limited number of SU described 2θ series of [110] symmetric tilt grain boundaries in yttria-stabilized cubic zirconia. Also, dependency of grain boundary energy on 2θ in the case of a number of f.c.c. metals had been previously studied [16]~[20].

In this regard, grain boundary structures of a series of Pr-doped ZnO [0001] tilt grain boundaries as a function of tilt angle (2θ) is inspected in this chapter. Control only 2θ may give an idea for understanding the Pr-doped ZnO [0001] tilt grain boundary system, which is a part of general Pr-doped ZnO grain boundaries.

So far, Atomistic arrangements for the grain boundaries with 2θ = 16.4° (Σ49) [1], 21.8° (Σ7) [9], 27.8° (Σ13) [10], 30.0°(~Σ97), 32.2° (Σ13) grain boundaries have been studied. The HAADF-STEM images of major structure in those grain boundaries are shown in **Figure 6-1**. Most of the grain boundaries are CSL boundaries where periodic repetition of certain SUs can be observed. In detail, grain boundaries with 2θ = 16.4° (Σ49) and 21.8° (Σ7) are described by SUs α and/or β, and 2θ = 27.8° (Σ13), 30.0°, and 32.2° (Σ13) are described by SU γ. It is therefore indicated that SU transforms into γ when 2θ is close to 30.0°[10]. Also, the atomic structure of the grain boundary is highly dependent on 2θ change. For extend our understanding over wider 2θ, ZnO grain boundaries with further higher 2θ = 38.2° (Σ7) and 43.6° (Σ49) were fabricated, and their atomic structures were characterized using HAADF-STEM. Moreover, non-low ΣCSL boundary; 25.8° (Σ79) tilt grain boundary is also studied whose 2θ is at the structure transition state.

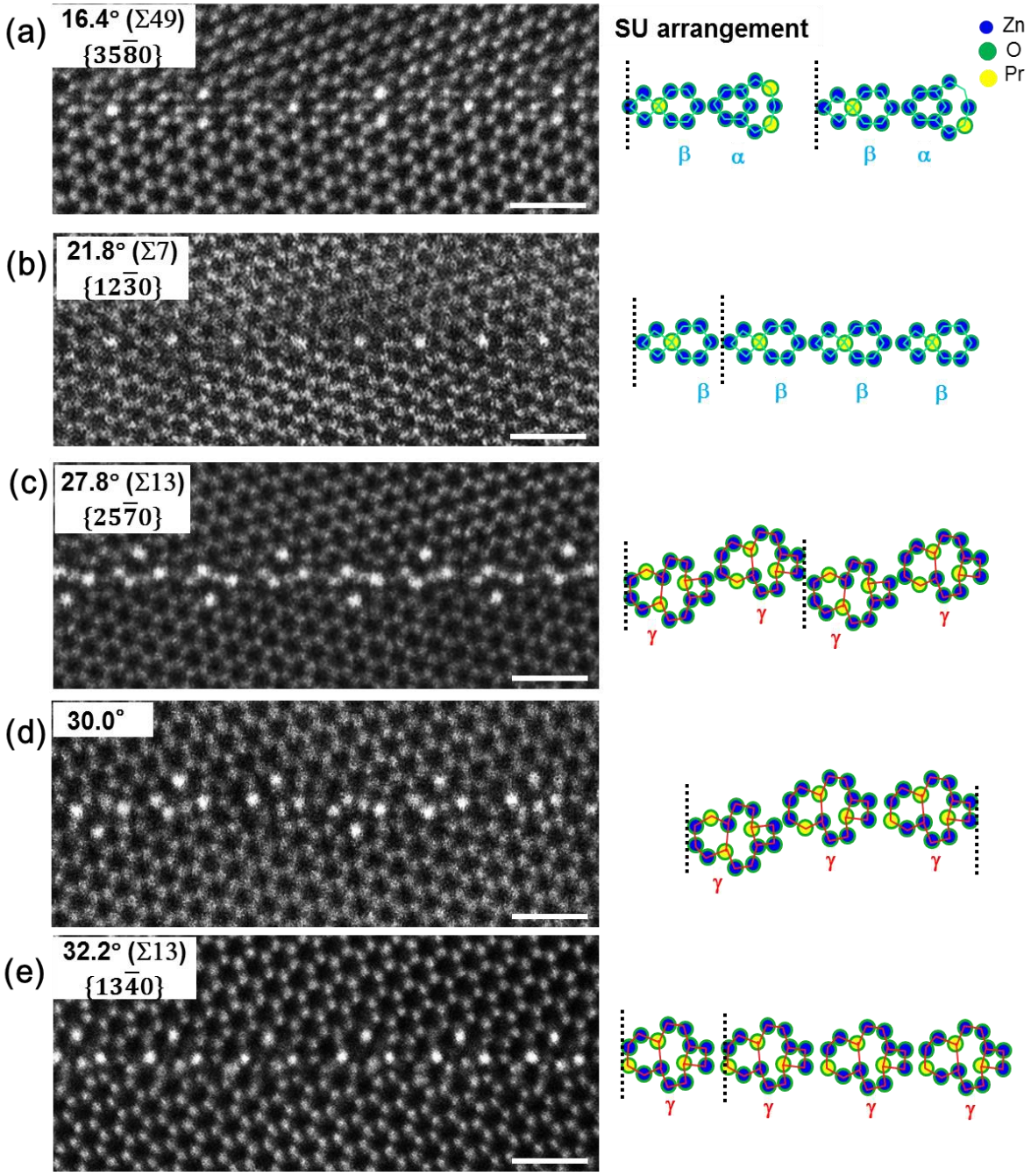

Figure 6-1. HAADF-STEM images of the Pr-doped ZnO [0001] symmetric tilt grain boundaries with 2θ = (a) 16.4°[1], (b) 21.8°[9], (c) 27.8°[10], (d) 30.0°, and (e) 32.2° (scale bar=1nm). SU arrangements of the grain boundaries are shown on the right side. Grain boundary period is indicated within the dotted lines.

6.2. Method

Specimen fabrication, atomic structure observation and theoretic calculations were carried out in similar ways to those in the previous chapter 4. Orientation of the crystals were set to be 2θ = 38.2°, and 43.6° , and 25.8° in order to obtain Pr-doped ZnO [0001] Σ7{14$\bar{5}$0}, Σ49{211$\bar{3}$0}, and Σ79{37$\bar{1}$00}symmetric tilt grain boundaries (**Fig.6-2(a)-(c)**).

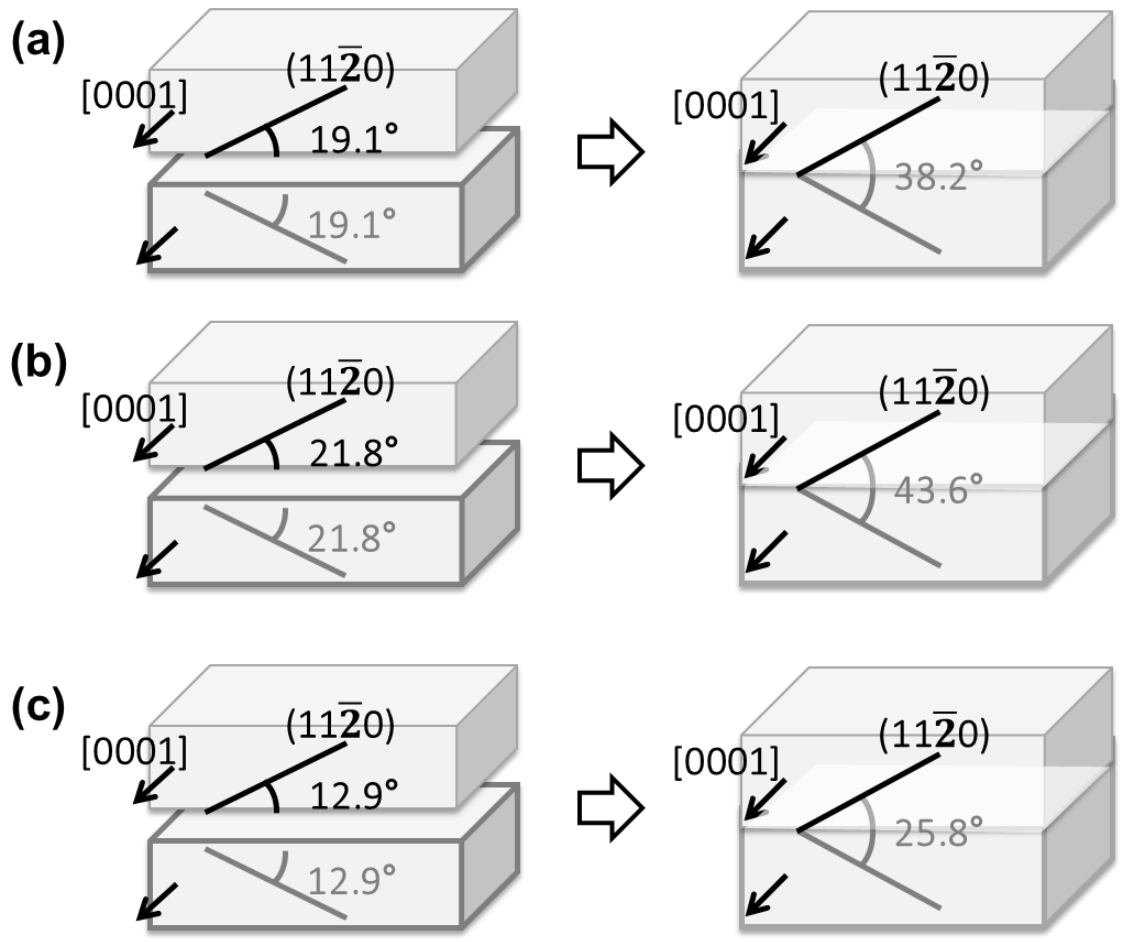

Figure 6-2. Schematic of ZnO bicrystals studied the current chapter. The 2θ is intended to be about 38.2°, 43.6° for obtain of the adjacent crystals in order to obtain Σ13 symmetric tilt grain boundary.

6.3. Results and discussion

6.3.1. Atomic arrangement of Pr-doped ZnO 38.2° (Σ7) and 43.6° (Σ49) tilt grain boundaries.

Atomic structures of grain boundaries were observed by STEM (**Figure 6-3**) First, the boundary plane of 38.2° (Σ7) tilt grain boundary is flat and parallel to $(14\bar{5}0)$ of the adjacent crystals. Its atomic arrangement was described by two kinds of major structures that consist of SU γ in straight array (**Figure 6-3(a)**), and SU α in zig-zag array **(Figure 6-3(b))**. Those structures were observed with the similar frequency; thus, both SU γ and α are considered as the major structures for this grain boundary. The straight array of SU γ is very similar to that of 32.2° (Σ13) grain boundary as it was shown in Chapter 4.3.1. Intervals between SU γ in the 38.2° (Σ7) grain boundary are longer with presence of bulk-like configuration. Next, atomic arrangement of 43.6° (Σ49) grain boundary is characterized. The boundary plane was not so flat and locally facetted probably due to low density (long period) of CSL in the Σ49 grain boundary case. Only the straight boundary region is characterized in this chapter for comparison of atomic structures in the series of symmetric tilt grain boundaries. The boundary plane in the straight area is found to be parallel to $(211\overline{13}0)$ of the adjacent crystals. The atomic arrangement of the grain boundary was described by zig-zag array of SU α (**Figure 6-3(c)**), which is similar to that of previous 38.2° tilt grain boundary (**Figure 6-3(b))**. The intervals between the SUs in 43.6° (Σ49) tilt grain boundary are longer than that of 38.2° (Σ7) tilt grain boundary. According to the observation results, it is again found that SU transformation occurs from SU γ to SU α when *2θ* is greater than 32.2°. In this time, SU α align zig-zag.

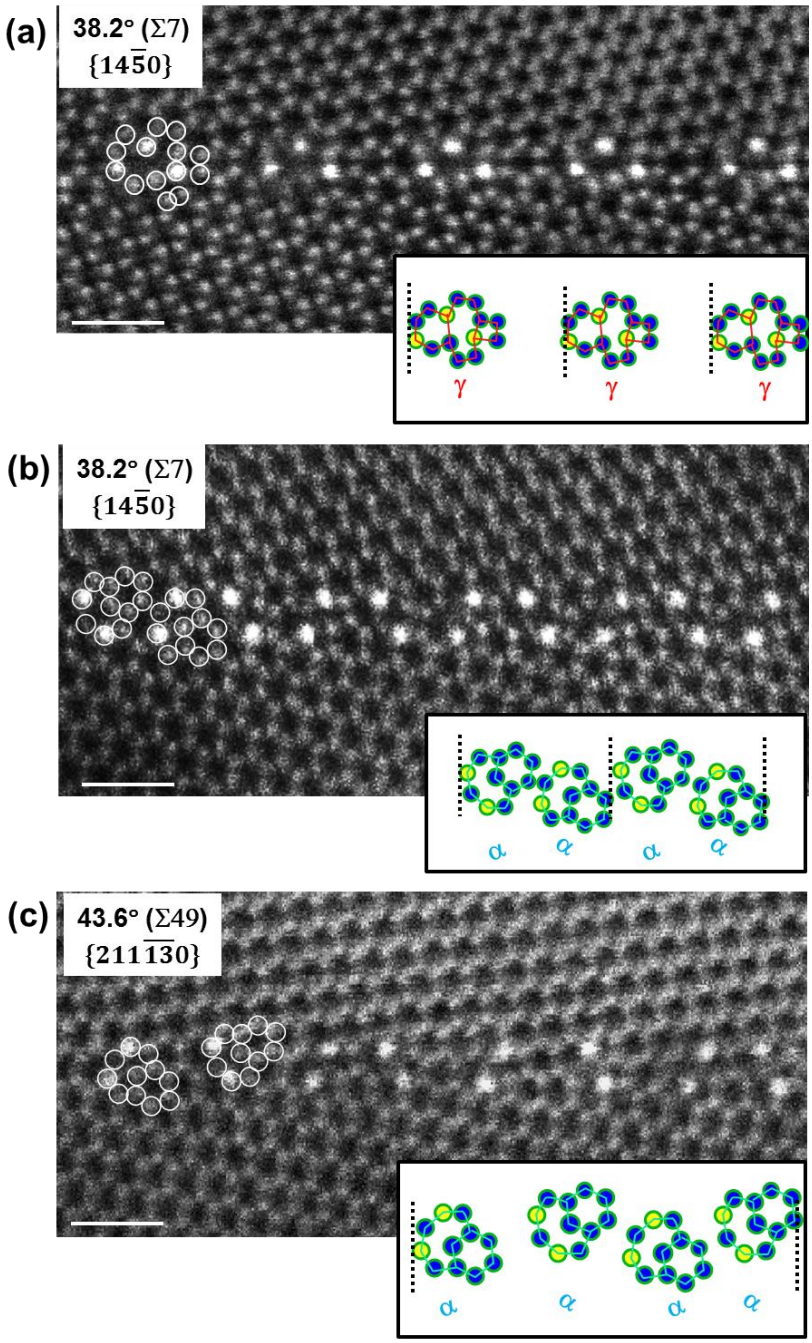

Figure 6-3. HAADF-STEM images of the Pr-doped ZnO symmetric tilt grain boundaries with (a), (b) 2θ = 38.2° and (c) 2θ = 43.6° (scale bar=1nm). In the 38.2° tilt grain boundary case, two kinds of structure were found which are described by SU γ, and zig-zag SU α. Adjacent crystals are parallel to the (14$\bar{5}$0) and (211$\bar{3}$0), for 38.2° and 43.6° tilt grain boundary, respectively. SU arrangements are schematically shown at the insets. Grain boundary period is indicated within the dotted lines.

6.3.2. Atomic arrangement of Pr-doped ZnO 25.8° (Σ79) tilt grain boundary

Atomic structure of non-low Σ CSL boundary-25.8° tilt grain boundary is observed. Although the tilt angle is very close to the Σ79 (26.0°) CSL condition, however, the atomic arrangement in the boundary is very disordered, and columns are not be clearly distinguished due to presence of irregular atomic arrangements along the c-axis. On the other hand, the boundary structure can be divided into two region; (1) straight arrangement of SU α and β, and (2) zig-zag arrangement of SU γ (**Figure 6-4**). Those two regions alternatively observed in the boundary within 10nm. It is considered that periodic arrangement of Σ79 is less stable than decomposed into the (1) and (2) region. The relationship between the SUs in the 25.8° (~Σ79) tilt grain boundary and SUs in the neighbored low- Σ-CSL boundaries will be discussed later.

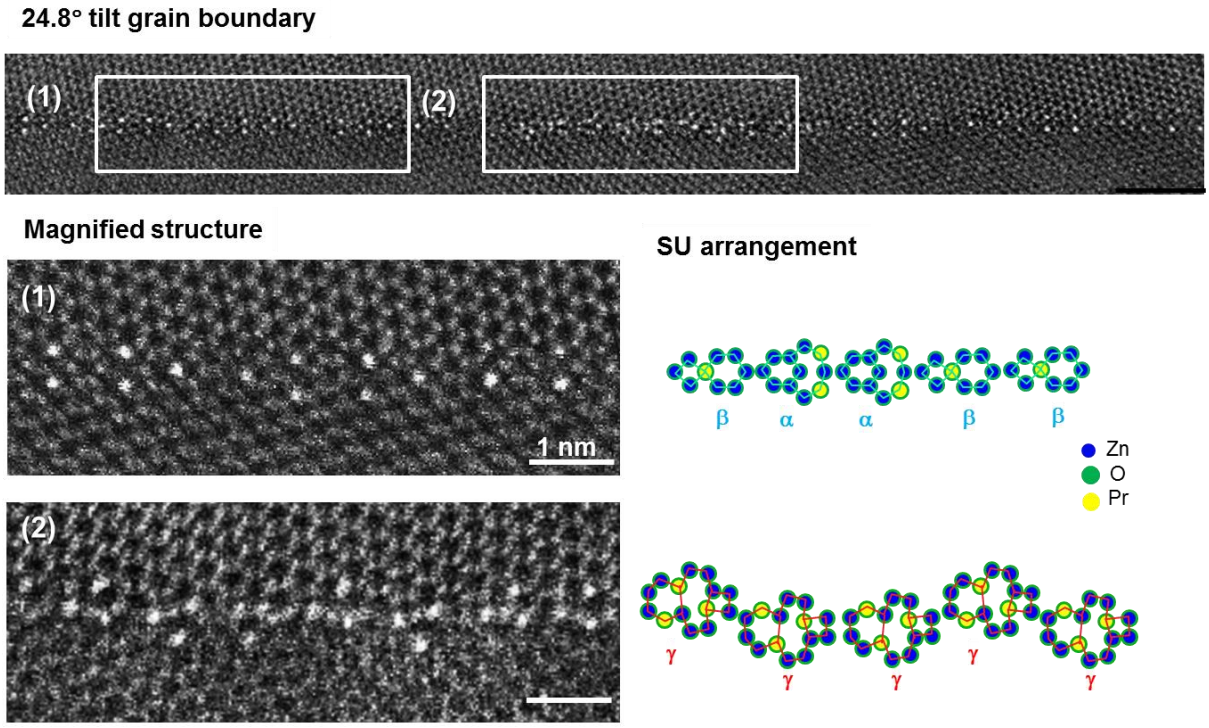

Figure 6-4. HAADF-STEM images of the Pr-doped ZnO 25.8° symmetric tilt grain boundary. Atomic arrangement is irregular without short periodicity. Two types of structure coexist; the first one is described by SU α/β as shown in (1) region, and the second one is described by SU γ, shown in (2).

6.3.3. Prediction of atomic structure of Pr-doped ZnO [0001] symmetric tilt grain boundaries

Table 6-1 shows features of SUs in several Pr-doped ZnO [0001] symmetric tilt grain boundaries, arranged as a function of *2θ* that range from 0° to 60°. Details are explained as below.

First, it was found that the SU transforms from α and/or β to γ near *2θ* ~ 25.8°, and γ to α near *2θ* ~38.2°, again. Some SUs for two *2θ* within 0°~27.8° range are characterized as SU α and/or β. In fact, the configurations of the four- and eight-membered ring in the respective SU α and SU β are very close during the glide of the dislocation in the grain boundary plane; the eight- membered ring is converted into the four-membered ring by connecting the dangling bond in the eight-membered ring toward another to form the four-membered ring [14]. In addition, their formation energies were resulted to be the same ($1.54 Jm^{-2}$) as demonstrated in the undoped ZnO Σ7 grain boundary study [11]. Obviously, atomic configuration of SU γ is largely reconstructed type. Therefore, it is said that SUs transforms between SU α (and/or) β and SU γ, but not the case between SU α and β.

Next, SUs can be expressed as inter-mixed configuration with a certain fraction by those of neighbored CSL boundaries. Two types of SU inter-mixing were found as short range and long range. As described in the chapter. 4.3.3, periodic arrangement of 30.0° (~Σ97) tilt grain boundary is consisting mixed SU configuration that is taken from the SU of the Σ13 (27.8° / 32.2°) grain boundaries one by one. This is the short range intermixing, which is described as

|γγ| –> |γγ・*γ| <– |*γ| (**Table 6-1**).

On the other hand, 38.2°(Σ7) case consists of two separated SUs, α and γ. The arrangements of SUs are similar to those of neighbored 32.2° (Σ13) and 43.6° (Σ49) grain boundaries. However, SU α and γ were found from separated boundary area. That is, the SU α is continuously found from for tens of nanometers boundary area, and at the sudden point SU changes into continuous arrangement of SU γ. Thus, it shows rather long range intermixing of SUs and described as |*γ| –> |γ**||γ**||γ**|.....|αα||αα||αα| <– |α*α*αα| (**Table 6-1**).

Since boundary translation for SU α and SU γ are different, coexist of the SU α and SU γ may require rearrangement of boundary plane, such as step formation. In fact, the step was found between the two SU arrangements (**Figure 6-5**). The height of the step between the SU arrangements has been revealed to be one interplanar spacing of the boundary plane, $d(14\bar{5}0)$ (**Figure 6-6**). Thus, it is considered that different type of SU, α and γ hardly form within one period, but exist separately in the 38.2° (Σ7) tilt grain boundary.

Also, SUs coexist in a metastable grain boundary (non-low Σ CSL boundary), e.g. 24.8° tilt grain boundary (**Figure 6-4**). The boundary structure was very irregular, however, coexistence of SU α (and/or) β and SU γ were found. Thus, it also suggests SUs in the grain boundary have mixed SUs configuration that are taken from neighbored grain boundaries. This will be called the random mix of SUs, hereafter. On the other hand, the SUs are dislocation-like units, and the interval between SUs (number of bulk configuration, *) gradually extends in the low angle boundary region. Thus, SU arrangement in the low angle boundary region can be speculated as ones shown in the **Table 6-1**.

Table 6-1. 2θ dependent SU arrangements in Pr-doped ZnO [0001] symmetric tilt grain boundaries. Grain boundary is expressed by periodic arrangement of SU and the bulk-configuration (*). Zig-zag configuration of the SU is indicated by $(^{+})(^{-})$. SU arrangement for low angle grain boundaries are speculated based on the structural multiplicity.

2θ (°)	**Σ**	**Boundary plane**	**SU, |period|**	**remarks**
0	1	$\{11\bar{2}0\}$	**********	
Low angle			|α(and/or)β****||α(and/or)β)****|	Speculated
16.4	49	$\{35\bar{8}0\}$	|αβ*||αβ*||αβ*||αβ*||αβ*||αβ*|	[1]
21.8	7	$\{12\bar{3}0\}$	|β||β||β||β||β||β||β||β||β||β||β||β||β||β||β|	[9]
25.8			..αββαααγγγγγααββαβαγγγγγ..	
27.8	13	$\{25\bar{7}0\}$	|γγ||γγ||γγ||γγ||γγ||γγ||γγ||γγ||γγ||γγ||βαα|	[10]
30.0	~97	$\{38\bar{1}\bar{1}0\}$	|γγ*γ||γγ*γ||γγ*γ||γγ*γ||γγ*γ||γγ*γ||γγ*γ|	
32.2	13	$\{13\bar{4}0\}$	|γ*||γ*||γ*||γ*||γ*||γ*||γ*||γ*||γ*|	
38.2	7	$\{14\bar{5}0\}$	|γ**||γ**||γ**||γ**||α⁺α⁻||α⁺α⁻||α⁺α⁻||α⁺α⁻||α⁺α⁻|	
43.6	49	$\{211\bar{3}0\}$	|α⁺*α⁻*α⁺α⁻||α⁺*α⁻*α⁺α⁻||α⁺*α⁻*α⁺α⁻|	
Low angle			|α⁺α⁻******||α⁺α⁻******||α⁺α⁻*******|	Speculated
60	1	$\{10\bar{1}0\}$	**********	

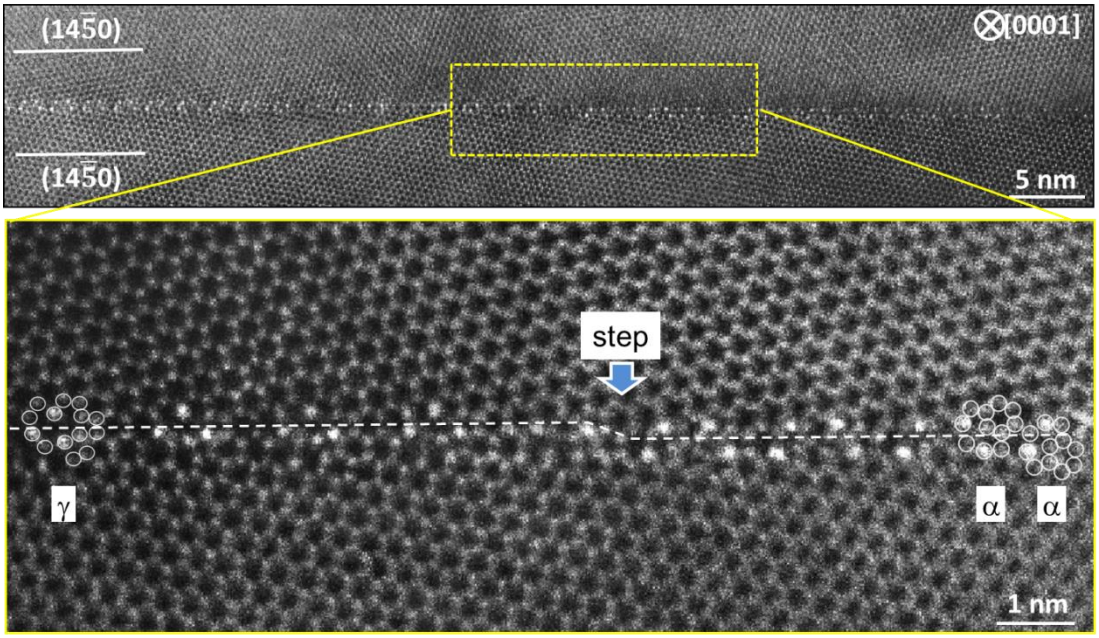

Fig.6-5. HAADF-STEM image showing step between two SU arrays (left – straight arrangement of SU γ, right – zig-zag arrangement of SU α) in the Pr-doped ZnO 38.2° symmetric tilt grain boundary.

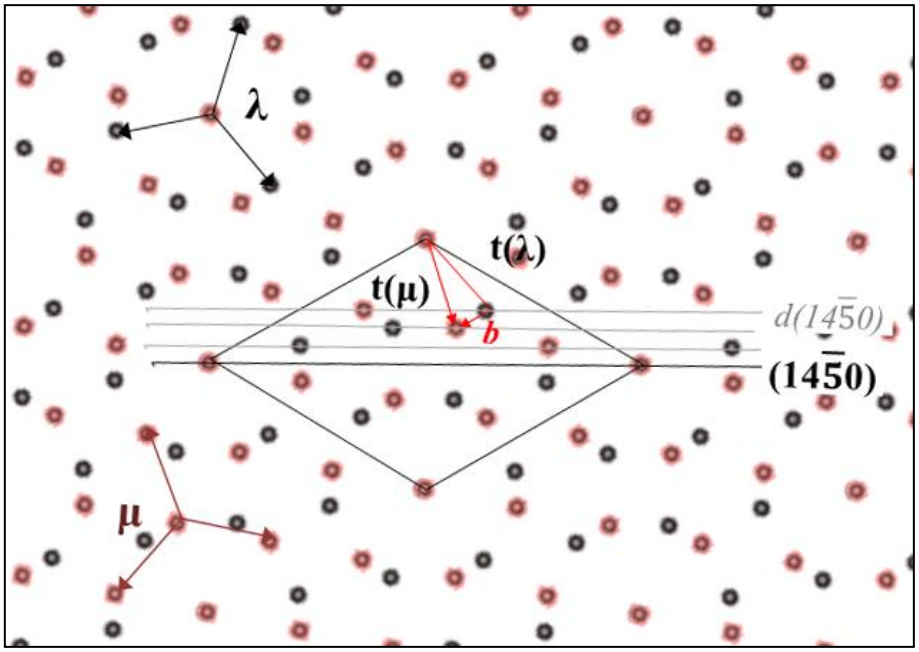

Fig.6-6. Dichromatic complex of Σ7 (38.2°) grain boundary for characterization of the step element, shown in **Fig. 6-3**. Translation between both upper and lower crystals (t(λ), t(μ)) results Burgers vector ***b***. The height of this step is estimated to be one inter planar spacing of (14$\bar{5}$0), *d(14$\bar{5}$0)*

Again, SU arrangements in the Pr-doped ZnO [0001] symmetric tilt grain boundaries are schematically expressed in **Figure 6-7**, according to the experimental results. Frequency of SU was roughly estimated from respective grain boundary. First, in low angle boundary region (*2θ* < 15°, and *2θ* > 45°), SUs act like isolated dislocation cores. Intervals between SUs are reversely proportional to the *2θ*, that is, frequency of SU gradually increases as *2θ* increases.

Next in the high angle region (15° < 2θ < 45°), the intervals between SUs are almost zero, and SUs interact eachother and they transform (SU α and/or β ~ SU γ ~ SU α)). Fraction between SU α(β) and γ is estimated when those SUs coexist (*2θ* =21.8°, 25.8°, and 27.8°). In the similar way, fraction between SU γ and SU α is estimated at *2θ* =38.2°. The estimated results can describe three parabolas that roughly show the frequency of SU and the type of SU as a function of *2θ* (**Figure 6-7**). It should be also noticed that arrangements of SU transforms from straight to the zig-zag near *2θ* =30.0°. It is because the burgers vector of SU α and/or β are perpendicular to the boundary plane at 0° < 2θ < 30° region, while those are inclined 30.0° toward $(11\bar{2}0)$ of adjacent crystals in 2θ > 30° region.

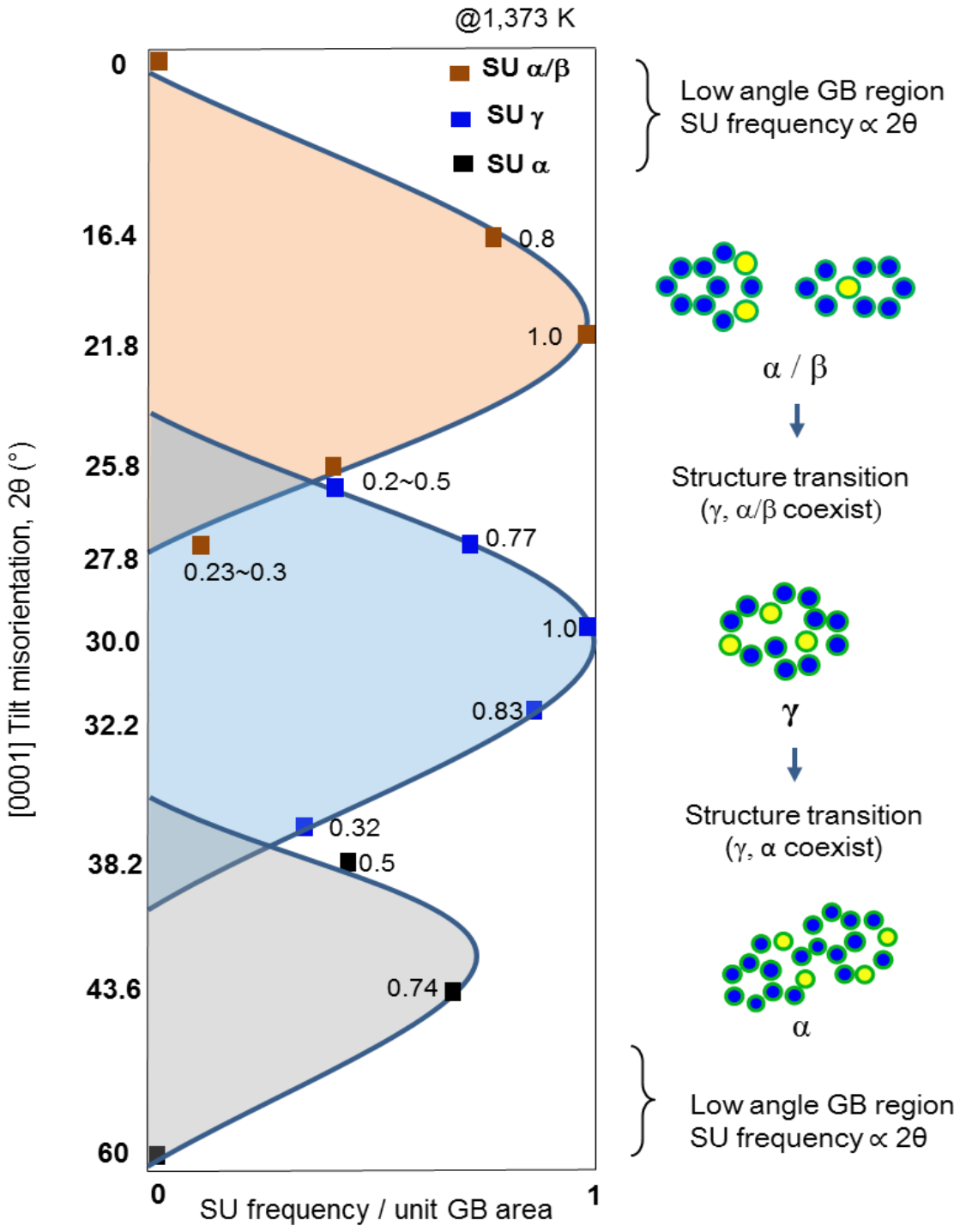

Figure 6-7. Relationship among SU, frequency, and misorientation angle (*2θ*) based on the experimental results. Graph roughly suggests the transition of SU, and the frequency of SU per unit boundary area as a function of *2θ*.

So far, atomic arrangements of Pr-doped ZnO [0001] symmetric tilt grain boundaries were described using SU. As it has been demonstrated, Pr was found from the same sites within the same SU. That is, Pr locates at two shoulder sites in seven membered ring of SU α, centered sites between four- and six-membered ring of SU β, and three triangle-like sites in the SU γ (**Figure 6-8(a)**). Density of Pr per unit grain boundary area is estimated suppose the Pr columns have same occupancy. First, the number of Pr in periodic grain boundary volume is measured and it is converted into the number of Pr per unit grain boundary volume, $1nm^3$. Calculated Pr concentration is shown in **Figure 6-8(b)**. Pr concentration shows a gaussian distribution as a function of *2θ*. It is implied that the concentration of Pr is dependent on misfit angle between two adjacent crystals, since large misfit allows Pr to segregate. As introduced, Sato *et al*. [1] had reported role of Pr segregation that promotes the formation of native defect, most likely Zn vacancies. The Zn vacancy was found to form acceptor state in the boundary, which derives from the two nearest oxygen atoms. Thus, higher Pr concentration would facilitate deeper acceptor state at the grain boundary.

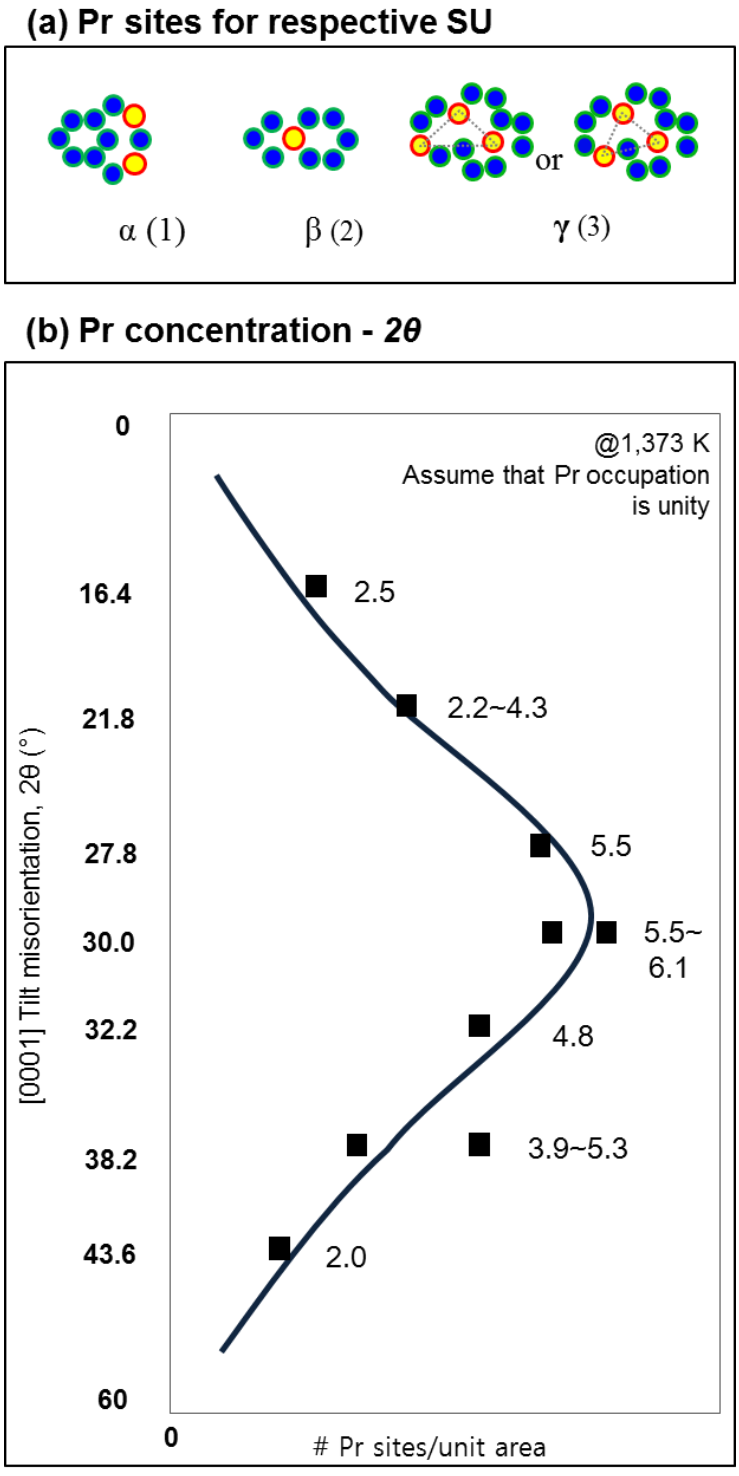

Figure 6-8. (a) Number of Pr sites for respective SU (two sites for the SU α, one site for the SU β, and three sites for the SU γ). (b) Relationship between Pr concentrations - *2θ*. Pr occupation is assumed to be unity for all columns. Number of Pr sites was calculated using SU models.

6.4. Conclusion

Relationship between atomic arrangement of Pr-doped ZnO [0001] symmetric tilt grain boundaries and 2θ is studied in this chapter.

I. Atomic arrangements of Pr-doped ZnO [0001] symmetric tilt grain boundaries are described by limited SU models; α, β, and γ.

II. SU transforms from α, β into γ, and from γ into zig-zag α again when 2θ is close to 30.0°.

III. SUs can be expressed as inter-mixed configuration by SUs of neighbored grain boundaries that is called SU inter-mixing. (Long range (38.2° tilt case), short range (30°-tilt case), and random type (25.8° tilt case).

IV. Each type of SU has specific number of Pr sites within it. Thus, concentration of Pr is the highest when 2θ of grain boundary is close to 30°.

6.5. References

[1] A.T. Paxton and M.W. Finnis, eds., J. Mater. Sci., **40**, 3045 (2005)

[2] T. Sakuma, L. Shepard, and Y. Ikuhara, eds., Ceram. Trans., **118**, 427 (2000)

[3] C. Elsässer, A.H. Heuer, M. Rühle, and S.M. Wiederhorn, eds., J. Am. Ceram. Soc., **86**, 533 (2003)

[4] Y. Ikuhara, J. Ceram. Soc. Jpn., **109**, S110 (2001)

[5] J.P. Buban, K. Matsunaga, J. Chen, N. Shibata, W.Y. Ching, T. Yamamoto, and Y. Ikuhara, Science, **313**, 212 (2006)

[6] Z. Zhang, W. Sigle, and M. Rühle, Phys. Rev. B, **66**, 094108-1 (2002)

[7] N.D. Browning, J.P. Buban, P.D. Nellist, D.P. Norton, M.F. Chisholm, and S.J. Pennycook, Physica C, **294**, 183 (1998)

[8] Y. Sato, J. P. Buban, T. Mizoguchi, N. Shibata, M. Yodogawa, T. Yamamoto, and Y. Ikuhara, Phys. Rev. Lett., **97**, 106802-1-4 (2006)

[9] Y. Sato, T. Mizoguchi, N. Shibata, T. Yamamoto, T. Hirayama, and Y. Ikuhara, Phys. Rev. B, **80**, 094114 -1-7 (2009)

[10] Y. Sato, J. –Y. Roh, and Y. Ikuhara, Phys. Rev. B, **87**, 140101-1-4 (R) (2013)

[11] F. Oba, H. Ohta, Y. Sato, H. Hosono, T. Yamamoto, and Y. Ikuhara, Phys. Rev. B. **70**, 125415-1 (2004)

[12] V. Potin, P. Ruterana, G. Nouet, R.C. Pond, and H. Morkoç, Phys. Rev. B, **61**, 55 87 (2000)

[13] J. Chen, P. Ruterana, and G. Nouet, Phys. Rev. B 67, 205210 (2003).

[14] J. Chen, P. Ruterana, and G. Nouet, Phys. stat. sol. (a) **203,** 247 (2006)

[15] N. Shibata, F. Oba, T. Yamamoto, and Y. Ikuhara, Phil. Mag., **11**, 2381 (2004)

[16] G.-J. Wang, and V. Vitek, Acta metal, **34**, 951 (1986)

[17] K.T. Aust, Trans. Am. Inst. Min. Engrs., **206**, 1026 (1956)

[18] N.A. Gjostein and F.N. Rhines, Acta metal., **7**, 319 (1959)

[19] G.C. Hasson and C. Goux, Scripta metal., **5**, 889 (1971)

[20] G. Hasson, J.-Y. Boos, I. Herbeuval, M. Biscondi and C. Goux, Surf. Sci., **31**, 115 (1972)

Summary

Potential impact of presence of grain boundaries and segregations on the polycrystalline material has challenged a number of researchers so far. However, the detailed mechanisms are not widely understood mainly because of a huge number of grain boundaries in the material. As a model for studying the ambiguous grain boundary phenomena, ZnO, which is an electroceramic material where the grain boundaries control the electrical properties, such as nonlinear current-voltage characteristics, has been focused.

As a way to investigate detailed grain boundary structure, boundary conditions are specified into a series of [0001] ZnO wurtzite tilt grain boundaries based on the CSL theory. Complex atomic arrangements in the high-angle tilt grain boundaries were described by several low-energy configurations, which is often designated by SU. As demonstrated from the topological analysis, the atomic arrangement of the undoped ZnO tilt boundaries could be built up by a SU, and it was found that SU behaves like an edge dislocation. According to a special boundary case for the ZnO Σ13 (32.2°) grain boundary, it was found that the arrangement of SUs changes from straight to zig-zag as 2θ increases. Understanding the structural trend over 2θ range provides an insight of ZnO [0001] tilt grain boundaries with the SU description.

The motivation of the study moved to the dopant-introduced grain boundary case. Segregation of large metal ions at the ZnO grain boundary enhances voltage gradient. Segregation behavior as well as grain boundary atomic structure has to be studied in detail. Pr is chosen that is known as one of famous varistor former. From the simulation of stable atomic structure from first principles calculation, it was revealed that Pr seeks Zn sites of locally highest tension. The variation of strain distribution in the different grain boundaries would be a reason for differentiating the Pr segregation sites.

The boundary inclination sometimes occurs toward stable facet plane. And structural minorities may coexist. This is the case for the Pr-doped ZnO 27.8° tilt grain boundary. Different boundary morphology such as steps and facets were found. Those may induce local fluctuation of Pr concentration, by changing the local atomic arrangements. Thus, the result implies an importance of revealing the relationship among atomistic structure, composition, and the boundary morphology.

As a realistic step to get an idea for grain boundary in general, atomic arrangement and Pr segregation in a series of Pr-doped ZnO CSL grain boundaries were investigated. 2θ dependent structural trend has been found. The Pr-doped ZnO [0001] symmetric tilt grain boundaries consist of limited atomic configuration. The type of SU transforms when 2θ is close to 30.0°. SUs in a certain grain boundary can be expressed as inter-mixed configuration by the SUs of neighbored CSL boundaries. 2θ dependency of Pr concentration is also suggested. Each type of SU has specific number of Pr sites within it. Since the SU phase transition and frequency are predictable, concentration of Pr can be roughly explained as a function of 2θ, assume that the Pr occupancy is unity.

In this thesis, ZnO grain boundaries for its undoped and Pr-doped cases are studied. Atomic arrangement and Pr segregation of several CSL grain boundaries were first determined, and other non-low Σ CSL grain boundaries were predicted. Structural minorities including secondary defects were also covered. 2θ dependency of atomic arrangements and Pr concentration are suggested. Those findings are expected to give an insight for designing polycrystalline ZnO based devices.

Research Activity

Publications with peer review

1. J.-Y. Roh, Y. Sato, and Y. Ikuhara, "Atomic structure of ZnO Σ13 [0001]/{13$\bar{4}$0} symmetric tilt grain boundary", J. Am. Ceram. Soc., **97**, 617 (2014)
2. J.-Y. Roh, Y. Sato, and Y. Ikuhara, "Atomistic structure and segregation behavior in seco ndary structure and facet of Pr-doped ZnO Σ13 27.8° [0001] tilt grain boundary", J. Ceram. Soc. Jpn.,**122**, 1 (2014)
3. Y. Sato, J.-Y. Roh, and Y. Ikuhara, "Grain-boundary structural transformation induced by geometry and chemistry", Phys. Rev. B, 87, 140101-1 (R) (2013)

Proceedings

4. J.-Y. Roh, Y. Sato, and Y. Ikuhara, "Structural Multiplicity in Pr-doped ZnO [0001] 27.8° and 30.0° Tilt Grain Boundaries", AMTC Letter, **4**, 26 (2014)
5. J.-Y. Roh, Y. Sato, and Y. Ikuhara, "Atomic Structure Characterization of ZnO Σ13 (13$\bar{4}$0) Symmetric Tilt Grain Boundaries", AMTC Letter, **3**, 48 (2012)

Awards

第33回エレクトロセラミックス研究討論会ポスター発表賞,(Oct. 25th, 2013, Tsukuba, Japan)

Acknowledgements

I am thankful to everyone who has in any way contributed in the completion of this thesis.
First of all, I want to express my respect and appreciation to Professor Yuichi Ikuhara, who first gave an opportunity to join his research group, and continuously motivated me to continue research activities.
I appreciate to Prof. Ikuhara for precious guidance and helpful comments during my whole university life in Japan.

I wish to thank to Prof. Naoya Shibata, Prof. Takahisa Yamamoto, Prof. Eiji Abe, Prof. Masato Yoshiya, and Prof. Junya Inoue for their helpful suggestions and insigts during the defense of this thesis. For all their guidance, I wish to express my sincerest appreciation. Especially Prof. Naoya Shibata always gave me valuable advice and kindness.

I also acknowledge all the staffs and members who are or were in crystal interface laboratory Interface laboratory of the University of Tokyo. I want to give my special gratitude to Dr. Yukio Sato for his contribution in my research with a great deal of discussions, teachings, and experimental and theoretical supports.

And I express my gratitude to Prof. Teruyasu Mizoguchi, Dr. Tetsuya Tohei, Dr. Tsubasa Nakagawa, Dr. Ryo Ishikawa, Dr. Eita Tochigi, Dr. Akihito Kumamoto who are great teachers with the excellent experimental and theoretical backgrounds.

I thank to Ms. Naomi Inoue, Ms. Kazue Sugawara, and Ms. Natsumi Saito female member of the laboratory. I appreciate for their friendship, kindness, as well as lots of supports in school life.

I appreciate Mr. Nayuki Keiichiro in JEOL. Ltd. who is my good friend and a mentor. Also, I want to thank Ms. Sun Rong, Mr. Bin Feng and Mr. Akiho Nakamura as my good friends and same Ph.D. candidates. I appreciate for academic discussions, lots of experiences at the conferences that we shared together. Also I want to give my thanks to Dr. Nobuaki Takahashi, and Dr. Teng-Yuan Chang for their friendship, and helpful advices.

I want to thank to my Korean colleagues. First I express my respects and appreciation to Prof. Do-Yeon Kim who is a distinguished Professor in the University of Tokyo. Seniors of crystal interface laboratory, Dr. Hak-Sung Lee, and Dr. Si-Young Choi gave me valuable advice and support from the time that I was planning to come to Japan. Dr. Kyu-bong Jung, Mr. Woojin Song, and Mr. Sanghoon Shin are my senior members from Hanyang University, Korea. They helped me to enter the University of Tokyo, and kept in good relationship during the life in Japan. I thank to Ms. Hyo-Jin Kim who is my good adviser and my good friend. I will never forget those memories and acknowledgements given from those many people.

I send special thanks my beloved parents who always want the best for their children. In particular, my

father continuously encouraged me to step forward, care my people, and care myself. My mother is my best mentor guided me be commonplace and modest. Also I thank to my older sister and younger brother who always supported family members.

Finally, I gratefully acknowledge that this research is supported by the International Graduate Program in Mechanical, Electrical and Materials Engineering (MEM) program in the University of Tokyo, and the Japanese Government's Monbu-kagakusho (MEXT; The Ministry of Education, Culture, Sports, Science and Technology).